FILE COPY
DO NOT TAKE

NIST-GCR-98-744

CORRELATIONS FOR FIRE PLUMES

J.G. Quintiere and B.S. Grove

University of Maryland
Department of Fire Protection Engineering
College Park, MD 20742

United States Department of Commerce
Technology Administration
National Institute of Standards and Technology

NIST-GCR-98-744

CORRELATIONS FOR FIRE PLUMES

Prepared for
U.S. Department of Commerce
Building and Fire Research Laboratory
National Institute of Standards and Technology
Gaithersburg, MD 20899

By
J.G. Quintiere and B.S. Grove
University of Maryland
Department of Fire Protection Engineering
College Park, MD 20742

February 1998

Notice

This report was prepared for the Building and Fire Research Laboratory of the National Institute of Standards and Technology under grant number 60NANB6D0073. The statement and conclusions contained in this report are those of the authors and do not necessarily reflect the views of the National Institute of Standards and Technology or the Building and Fire Research Laboratory.

CORRELATIONS FOR FIRE PLUMES

J. G. Quintiere and B. S. Grove
Department of Fire Protection Engineering
University of Maryland
College Park, MD 20742

FINAL REPORT

February 1998

Prepared for:

U. S. Department of Commerce
National Institute of Standards and Technology
Laboratory of Building and Fire Research
Washington, D. C. 20234

ABSTRACT

This study began as a review of data and correlations for line plumes. In its attempt to develop a consistent set of correlations for that data set, it developed an analysis to account for the base geometry of the fuel source. An integral model was used for the plume to address the flame zone (near field) and the noncombusting plume (far field). Although point source models were used, the diameter or rectangular source dimensions were included in improved solutions for flame height and entrainment rate. The analysis also explicitly includes the effect of flame radiation by a loss fraction, X_r, and the parameter,

$$\Psi = \frac{(1 - X_r)(\Delta H_c / s)}{c_p T_o}.$$

Although radiation data are not usually recorded, estimates allowed correlations to be computed with radiation considerations. The entrainment coefficients determined for Gaussian velocity and temperature profiles and for constant density were found to be 0.098 and 0.091 for the axisymmetric and line far field values, respectively. The entrainment coefficients in the near field were found to be 0.22 and 0.59 for the axisymmetric and line cases, respectively. Theoretically developed equations for near field entrainment and flame height with empirical lead coefficients were found to fit a wide range of data including fuel base diameters of up to 0.5 m. The same lead coefficient is used for the line and the axisymmetric cases as suggested by theory. The entrainment and the flame height correlations are directly related by the ratio of air entrained to stoichiometric air required, n, which is found to be 9.6 for both geometries. The entrainment rate is given in the form,

$$\frac{\dot{m}_e}{\rho_o g^{1/2} D^{5/2}} = C_e \left(\frac{z}{D}\right)^{1/2} \left[1 + 2C_1 \left(\frac{z}{D}\right)\right]^2$$

which does not depend on the energy release rate except to determine the position z where the near field equation no longer applies. This result is consist with a recent correlation of Delichatsios and an old concept originally put forth by Thomas. Yet the near field, flame zone, entrainment rate given by Heskestad in the SFPE Handbook (2nd ed.) depends on z and Z_f, the flame height or in other words, the energy release rate. The figure that follows gives the essence of this near field result and shows how our present analytical result follows the Delichatsios correlations which also agree well with available data.

Results are also presented for rectangular fires, and the theoretical basis for the correlation developed unifies data over a wide range of base dimensions ranging from a square to a line.

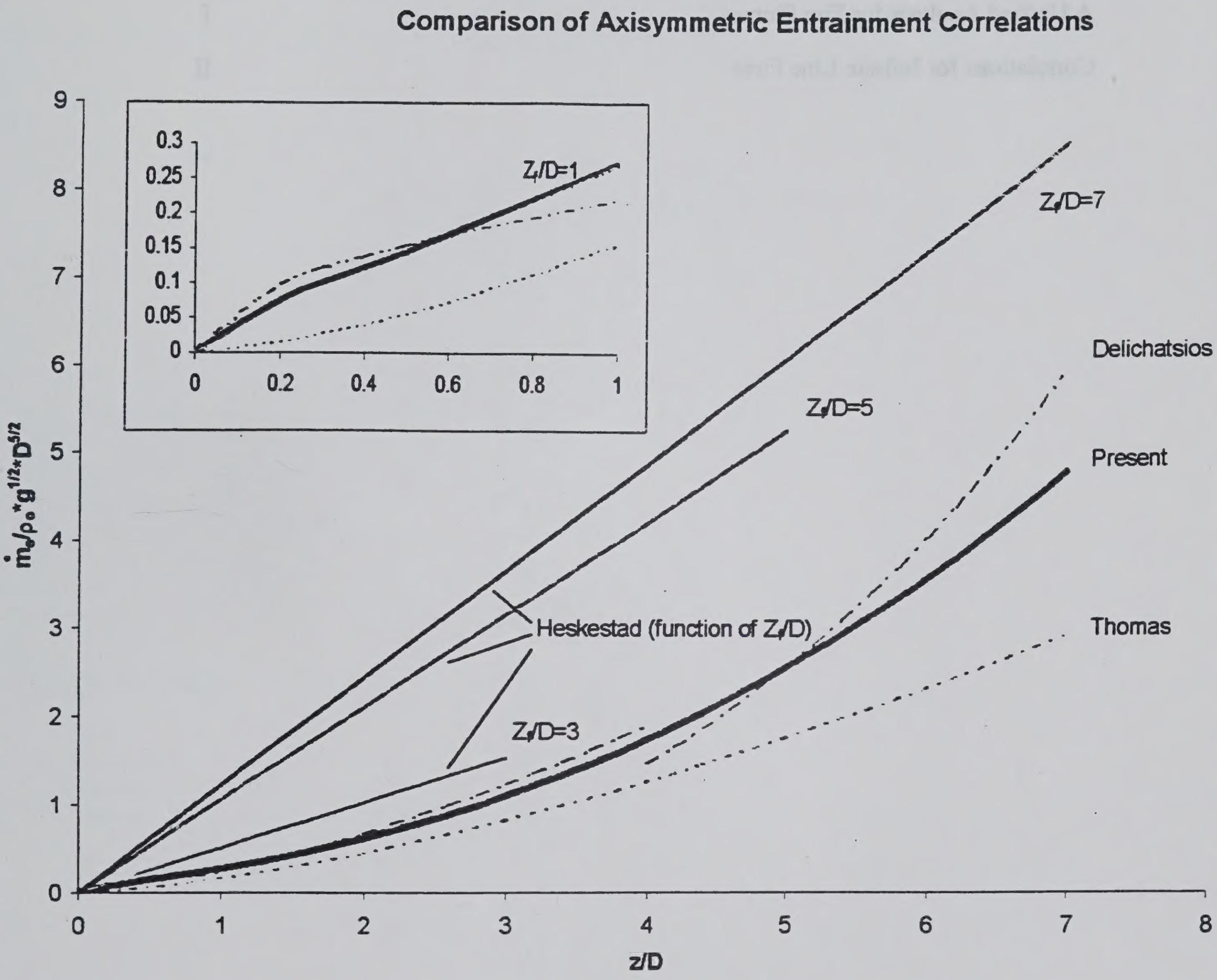

Comparison of Axisymmetric Entrainment Correlations

TABLE OF CONTENTS

Page

Abstract iv

A Unified Analysis for Fire Plumes I

Correlations for Infinite Line Fires II

A Unified Analysis for Fire Plumes

TABLE OF CONTENTS

Page

Abstract iv

A Unified Analysis for The Proton 1

Conditions for Infinite Lim Feed 11

A UNIFIED ANALYSIS FOR FIRE PLUMES

J. G. Quintiere* and B. S. Grove

Department of Fire Protection Engineering
0151 Engineering Building
University of Maryland
College Park, MD 20742-3031
USA

***Corresponding author**
Department of Fire Protection Engineering
0151 Engineering Building
University of Maryland
College Park, MD 20742-3031
USA
Tel. (301) 405 3993
Fax. (301) 405 9383
email: jimq@eng.umd.edu

Word Count:

Text:	2700
Equations:	300
Figures:	1400
Tables:	1000
TOTAL:	5400

Submitted for consideration in the 27th Int. Symp. On Combustion, The Comb. Inst., Aug 1998

A UNIFIED ANALYSIS FOR FIRE PLUMES

J. G. Quintiere* and B. S. Grove

Department of Fire Protection Engineering
0151 Engineering Building
University of Maryland
College Park, MD 20742-3031
USA

ABSTRACT

A unified analysis based on an integral approach is presented for fire plumes involving finite axisymmetric and rectangular sources. The analysis, using Gaussian profiles, obtains the best fits to experimental data found in the literature. Phenomenological constants in the theory are found to give consistent results in that coefficients expected to be numerically similar by theory are found similar among the various data sets. Thorough reviews of the literature data for line and rectangular sources are presented and yield consensus correlations, accordingly. The effect of flame radiation is explicitly included by a radiation fraction which proves to be a significant variable, previously overlooked in experiments. Effective entrainment coefficients for the far field noncombusting plume are found to be 0.09 to 0.10, and for the flame region about 0.22 for the axisymmetric and rectangle cases as long as $D/L > 0.1$. For $D/L < 0.1$, the infinite line gives nearly double the flame entrainment. Generalized results are presented for entrainment rate and flame height in terms of single algebraic equations which span a wide range of Q^* or energy release rate values. For low Q^* fires, the effect of diameter and line width are important and expressed by the theory but not enough to address dependence involving Grashof and possibly Froude number effects near the origin. Laminar results are also addressed.

Introduction

Many have studied fire plumes, with most attention on axisymmetric rather than line or other geometric plume sources [1-15]. Theoretical analyses are principally couched in terms of assumed similarity velocity and temperature distributions with Gaussian profiles proving adequate for the noncombusting region (e.g. Rouse [2]). Turbulent mixing is taken into account by an entrainment rule based on the axial plume velocity or its momentum to account for density effects. Often, idealized point source solutions (e.g. [3,8]) for noncombusting plumes are used to describe the results for combusting plumes using an origin offset, virtual source, to adjust the data (e.g. [7]). Steward [10, 11] developed integral solutions to both finite line and axisymmetric fire plumes which lead to rather complex algebraic results which might have discouraged their use. Thomas et al. [16] show that the flame geometry has a significant influence on the power law behavior for flame height. Delichatsios [17] used these flame geometry characteristics to derive entrainment and flame height results for axisymmetric fires which are consistent with data, thereby showing the intimacy of entrainment and flame height. One of the earliest and most comprehensive studies of plume from small fire sources was done by Yokoi [1]. He was first to point out that the axial velocity, w_m, the axial temperature rise, $T-T_o$, and position, z, are related by the constancy of $w_m^2/[(T-T_o)/T_o gz]$. We will show that this constant differs slightly in the flame and noncombusting regions.

This study will demonstrate how a theory can unify experimental correlations for fire plumes -- dissecting them into two regions: the "near field" combustion zone and the "far field", having a point source character. An integral analysis will be used for each plume geometry and a second order correction will be applied in the near field solution to determine better results for flame height and flame entrainment. All numerical coefficients of the theoretical results will be determined from the available ensemble of data. We shall address finite axisymmetric, line and rectangular fire sources of width D and (longer) length L. Turbulent analyses will be considered, but we will draw on the laminar results of Roper et al. [18,19] to fully describe the data in the literature.

This work was motivated by the need to synthesize the literature results for line plumes into a presentation comparable to the level of engineering comfort currently associated with axisymmetric plume formulas. Yuan and Cox [14] recently reviewed the line plume literature and presented some new data. We examined the available data in the literature to establish overall correlations with our theory. In many cases we have only plotted representative data due to the tedious nature of extracting data points from literature graphs.

Model Formulation

A point (or infinite line) source model is used for both the near and far field domains. For these cases, the base dimensions, D and D/L become zero. We make the following assumptions in the spirit of deriving dimensions relationships consistent with the commonly measured plumes variables.

1. Use the Bousinnesq assumption, density constant except in the buoyancy term; and all other properties are constant. A correction factor in terms of T_f/T_o could be included, but we regard the flame temperature factor as nearly constant.
2. Gaussian profiles are used for w/w_m and $(T-T_o)/(T_m-T_o)$ in both regions for consistency in this presentation, although we have no justification for using it in the near field. For example,

$$\frac{T-T_o}{T_m-T_o} = \exp\left[-\beta\left(\frac{r}{b}\right)^2\right] \tag{1}$$

where β is selected as 1 for the near field and the rectangular source amalysis.

3. Entrainment is based on a constant entrainment, α, which is the ratio of the entrainment to axial velocity. Without any loss in generality for the correlations, we do not represent the entrainment coefficient as a momentum ratio which would introduce $(\rho/\rho_o)^{1/2}$.

4. The energy release rate is assumed to be uniformly distributed in the combustion zone and

directly determined from the entrainment rate by the quantity, $\Delta H_c/sn$ where ΔH_c is the heat of combustion, s is the stoichiometric air to fuel ratio, and n is the ratio of air entrained to air involved in combustion. The last term, n, is solely a fluid dynamic factor characteristic of the mixing in the plume. $\Delta H_c/s$ taken as a constant for computations as 2.91 kJ/g, corresponding to methane.

5. Flame radiation is accounted for by a constant fraction, X_r.

6. Mass, momentum and energy flow rates of the supplied fuel are small and ignored for these buoyancy dominated plumes.

7. The plume is fully turbulent.

Combusting Plume Structure: Axial Temperature and Velocity

The details of the integral solutions are common in the literature (e.g.[3,8,10]) and the specifics for our results are found in the thesis by Grove[20]. Dimensionless variables are introduced as follows:

$$\Phi=\frac{T-T_o}{T_o},\ W=\frac{w_m}{(gZ_c)^{1/2}},\ B=\frac{b}{Z_c},\ \text{and}\ \zeta=\frac{z}{Z_c} \tag{2}$$

where the characteristic plume dimension, Z_c, is given as

$$Z^*=\left(\frac{\dot{Q}}{\rho_o c_p T_o g^{1/2}}\right)^{2/5}\ \text{and}\ Z^{**}=\left(\frac{\dot{Q}'}{\rho_o c_p T_o g^{1/2}}\right)^{2/3} \tag{3}$$

for the axisymmetric and line plumes, respectively. The solutions can be expressed in power relationships as

$$B=C_l\zeta^m,\ W=C_V\zeta^n,\ \text{and}\ \Phi=C_T\zeta^p \tag{4}$$

The theoretical solutions and the experimentally determined coefficients are given in Tables 1 and 2. Using the data of Yokoi[ ] for the axisymmetric far field, we determined the coefficients using a representative value of $X_r = 0.2$. Consequently, we find a value for α of 0.098 while Zukoski [21] reports 0.11 for no radiation loss. β is found to be 0.913, independent of X_r. The temperature and velocity data for the infinite line source are shown in Fig. 1 and 2 for the array of data found in the literature [1,2,8,12,14,15,22]. Here we assign a value of $X_r = 0.3$ as representative of these data and derive the empirical coefficients accordingly. We find $C_T = 2.6$, the same as Yuan and Cox [14] and most others reported by them. In the combusting zone, the parameter

$$\Psi = \frac{\left(1 - X_r\right)\left(\Delta H_c / s\right)}{c_p T_o} \tag{5}$$

occurs in the solution. Except for X_r this is a constant for all of these data. The empirical coefficients shown in Table 2 are nearly identical for velocity and differ somewhat for temperature. The C_T value here depends on the accuracy of the temperature measurement. For the axisymmetric case, we have used the results of McCaffrey who reported ΔT of about 800 °C[4], but Cox and Chitty [23] found the flame temperature for natural gas in square burners to be 960 to 980 °C for corrected themocouple measurements. Using the latter, increases the axi-C_T from 0.347Ψ to 0.427Ψ, closer to the line value, 0.450Ψ. Indeed, for large pool fires where smoke blockage causes X_r to become zero, the maximum temperature rise is indicated to be roughly 1000 to 1250 °C corresponding to our coefficients: $C_T = 0.347$ to 0.427. These temperatures are consistent with data presented by Baum and McCaffrey [24] for D ranging from 6 to 30 m. The velocity fit is shown in Figure 2, and the scatter in the data and the effect of X_r should be noted.

Finally, we note the constancy of the parameter, $W^2/\Phi\zeta$, being approximately 1.6 and 1.4

in the far and near fields, respectively for both geometries. Also the α values only vary from approximately 0.09 to 0.1 in the far fields, but differ significantly for the near fields. The near field results come from the respective flame height analysis which will be discussed below.

Entrainment

The entrainment rates from the integral solutions follow from:

$$\frac{d\dot{m}_e}{dz} = 2\pi\rho_o \frac{d}{dz}\int_0^\infty rw\,dr \quad \text{or} \quad \dot{m}_e = \pi\rho_o w_m b^2 \tag{6a}$$

and

$$\frac{d\dot{m}_e'}{dz} = 2\rho_{o} \frac{d}{dz}\int_0^\infty w\,dy \quad \text{or} \quad \dot{m}_e' = \pi^{1/2}\rho_o w_m b. \tag{6b}$$

The far field results follow in Table 3 using the coefficients listed in Table 1. Yuan and Cox [ ] find for their far field line plume data, $C_e = 0.51$ while we find 0.54.

In the near field we seek to find a solution that now accounts for the finite fuel source. Thomas [9] was first to argue that flame perimeter is key to determining entrainment into the flame, and Zukoski [25] needed this argument to explain his entrainment data within the continuous flame zone for burners of D = 0.19 and 0.50 m. We account for this fuel geometry effect by expressing the next order solution to b as

$$B = \frac{D}{2Z_c} + C_1\zeta. \tag{7}$$

Substituting Eq. (7) into Eq. (6), along with w_m and C_1 from Table 2, gives the entrainment results in Table 4 for the near field flame region. The form of the result is

$$\frac{\dot{m}_e}{\rho_o g^{1/2} D^{5/2}} = C_e\left(\frac{z}{D}\right)^{1/2}\left[1 + 2C_1\left(\frac{z}{D}\right)\right]^2 \tag{8}$$

for the axisymmetric case and similarly for the line case as shown in Table 4.

The best fit for C_1 comes from the following flame height results, and leads to the α values listed in Table 2. These entrainment coefficients are just modeling constants used to account for mixing and could be adjusted for density differences; however, they may be inadequate to address pressure contributions to entrainment near the base of the plume as described by Smith et al. [26]. We speculate that the distinctly larger value of α for the line plume in the flame region is due the narrow strip flame enhancing mixing from distinct "fire whirl" flame structures which tend to occur near its base. As the plume rises, the line or rectangular plume tends to approach the axisymmetric case and we would expect these coefficients to become similar in the far field as shown in Table 1.

The C_e for the axisymmetric case comes from the best fit of the Zukoski data [25] shown in Fig. 3. It should be pointed out that this is the first unified single-equation correlation of such entrainment data. No comparable flame entrainment data exist for the line plume so we are stymied on a direct data fit for this C_e. However, we note from the theory, that these coefficients are nearly equal (and not dependent on entrainment), i.e. $\pi/(2\sqrt{3}) \approx \pi^{1/2}/2$. Therefore, we select the same C_e for the infinite line as in the axisymmetric case, $C_e = 0.0565\Psi^{1/2}$. Alternatively, an attempt to use the lowest entrainment data point of Yuan and Cox [14], that may have been at the flame tip, produced a C_e nearly double the value in Table 4.

Flame Height

The deduction of flame height comes from Assumption 4 giving:

$$\dot{Q} = \dot{m}_e(Z_f)\frac{\Delta H_c}{ns}, \text{ or } Q_D^* = \left(\frac{\dot{m}_e}{\rho_o g^{1/2} D^{5/2}}\right)\frac{\Psi}{n(1-X_r)} \tag{9}$$

and similarly for the line case. By making this connection between Eq. (9) and Table 4 we easily obtain Table 5. The lead coefficient, C_f, for the axisymmetric case was determined from the data shown in Figure 4 as presented by Zukoski [6]. The Heskestad [7] correlation is also shown for comparison. We selected the same value of C_f for the line flames based on their approximate equality as given by theory. The C_l values for each of the geometries were found by the best fits to their respective flame height data and are given in Tables 4 and 5 accordingly. The fit to the line flame height data is shown in Figure 5 where we plot all of the (representative) data [8-11,13,14]. Again we see the distinct effect of D for low Q_D^{**} (or $Z^{**}/D)^{3/2}$ which changes the slope of the correlation. An experimental value of n can be deduced, independent of the theoretical profile effects, from Eq. (9) which gives $C_f = C_e\,[\Delta H_c/(n s c_p T_o)]$. Using the empirical coefficients from Tables 4 and 5 we obtain n = 9.6 for both plumes consistent with results by Taminini [28] and general literature estimates which tend to range from 5 to 15.

Some of the difficulties for the correlations to match all of the data may be due to laminar flow effects. Yuan and Cox [14] have assigned their data below $Z^{**}/D = 7$ as laminar. Our correlation for the line case gives $Z_f/D \sim Z^{**}/D$ for Z^{**}/D large, and $Z_f/D \sim (Z^{**}/D)^3$ for Z^{**}/D small: a profound D effect. However, this D effect is not sufficient to account for all of the data. We suspect that both Grashof ($Gr = gD^3/\nu^2$) and Froude ($Fr = w(0)/(gD)^{1/2}$) numbers are important factors for both laminar and turbulent domains. From the work of Roper et al. [18,19], we can express solutions to laminar flames as

$$\text{Axisymmetric:} \quad \frac{Z_f}{D} \sim \left(\frac{1-X_r}{\Psi}\right) Q_D^{*}\, Gr^{1/2}\ , \text{ and}$$

$$\text{Line or slot (buoyancy controlled):} \qquad (10)$$

$$\frac{Z_f}{D} \sim \left[\left(\frac{1-X_r}{\Psi}\right) Q_D^{**}\, Gr^{1/4}\right]^{4/3} .$$

The 4/3 power result for the line case does fit the laminar data given by Yuan and Cox [14], but the data listed by McCaffrey [27] of Becker and Liang (shown in Fig. 4) follow a 2 power behavior, not 1 as indicated in the laminar solution of Roper above. More significantly, the low Q_D^* region needs more attention, especially when it is realized that natural fires tend to fall between Q_D^* values of 0.05 and 5 [27].

Rectangular Fire Sources

Yokoi [1] and recently Hasemi and Nishihata [12] investigated rectangular burner fire plumes, with the latter study addressing larger propane fires (D = 0.1-1.0 m up to 150 kW). Our analysis is extended to these finite sources by the following specifications:

1. Gaussian profiles, $\beta = 1$, i. e. $\exp\left\{-\left[\left(\frac{x}{a}\right)^2 + \left(\frac{y}{b}\right)^2\right]\right\}$.

2. $W^2/\Phi\zeta = C^2$, a constant, which we found to be nearly identical for the line and axisymmetric cases with a C of about 1.5, varying for the far and near fields.

3. Geometrical effects are addressed by representing: $a = L/2 + C_1 z$, and $b = D/2 + C_1 z$ as done in Eq. (7), but we apply this now for both the near and far field regions.

In the far field the energy equation yields

$$\dot{Q}(1 - X_r) = 4\int_0^\infty\int_0^\infty \rho_o c_p w(T - T_o)\, dx\, dy. \tag{11}$$

By applying the conditions 1-3, we can solve for the temperature:

$$Q^*_{mod}(1 - X_r) = \frac{\pi}{8} C \Phi^{3/2} \left(\frac{z}{D}\right)^{1/2} \left[1 + 2C_1\left(\frac{z}{D}\right)\right]\left[1 + 2C_1\left(\frac{D}{L}\right)\left(\frac{z}{D}\right)\right]$$

$$Q^*_{mod} = \frac{\dot{Q}}{\rho_o c_p T_o g^{1/2} D^{3/2} L} \tag{12}$$

Explicitly,

$$\Phi = C_T \zeta_{\mathrm{mod}}^{-1}, \quad \zeta_{\mathrm{mod}} = \left[\frac{\left(\frac{z}{D}\right)^{1/2} \left[1 + 2C_1\left(\frac{z}{D}\right)\right]\left[1 + 2C_1\left(\frac{D}{L}\right)\left(\frac{z}{D}\right)\right]}{Q^*_{\mathrm{mod}}} \right]^{2/3} . \tag{13}$$

We have chosen $C_1 = (6/5)\alpha = 0.132$ which corresponds to the axisymmetric far field α of 0.11 for $\beta = 1$ given by Zukoski [21]. Our fit to the data of Hasemi et al. [12], is shown in Fig. 6. We find $C_T = 2.3$ or $2.9\,(1\text{-}X_r)^{2/3}$ for $X_r = 0.3$ corresponding to propane. This C_T is related to the previous far field values of the infinite line and (point) axisymmetric sources, but we have not tried to unify these results further. The above solution does converge to the correct limiting geometric behavior.

In the combusting region, we simply fit the rectangular data as $\Phi = 0.421\Psi$ which corresponds to the limiting values of 0.35Ψ and 0.45Ψ of Table 3.

W can be computed from the application of condition 2 with the selection of the constant C as 1.5. The entrainment equation can be written as

$$\dot{m}_e = 4 \int_0^\infty \int_0^\infty \rho_o w \, dx \, dy = \pi \rho_o w_m a \, b. \tag{14}$$

Accordingly the entrainment expressions can be determined for each plume region. By Eq. (9) or (12) where Φ is constant, the flame height can be determined from the expression,

$$Q^*_{\mathrm{mod}} = C_f \left(\frac{Z_f}{D}\right)^{1/2} \left[1 + 2C_1\left(\frac{Z_f}{D}\right)\right]\left[1 + 2C_1\left(\frac{D}{L}\right)\left(\frac{Z_f}{D}\right)\right]$$
$$\text{with } C_f = 0.00590\left(\frac{\Psi^{2/3}}{1 - X_r}\right) \text{ and } C_1 = 0.199. \tag{15}$$

We have retained the same C_f used in both the axisymmetric and line cases as given in Table 5. The C_l value for the rectangular data fit is slightly higher than the axisymmetric flame region result. At some point, for D/L small enough (roughly < 0.1), C_l must increase to the larger infinite line value of Table 5. A refinement might include an inclusion of a D/L effect on C_l for the rectangular case.

Conclusions

We have formulated a unified analysis that expresses the behavior of finite axisymmetric and rectangular fire plumes. The analysis gives the correct power relationships and consistent results for the phenomenlogical constants. It appears that for line plumes where $D/L < 0.1$, the entrainment coefficient in the combusting region is greater than that for the axisymmetric case; and both are greater than their noncombusting plume counterparts in the far field having a value of 0.09 to 0.10. A systematic incorporation of flame radiation loss, X_r, shows that this parameter is a significant factor that permeates the analysis and consequently it is recommended that future experimental studies report X_r. Low Q^* values show distinctive dependence on D and fire source geometric effects which suggest the influence of Gr effects in addition to the D dependence given by the theory presented herein.

Nomenclature

a	half-length variable
b	half-width or radius of plume
B	dimensionless length variable, Eq. (2)
c_p	specific heat (1.01 kJ/kg(K)
C_i	generic constants used in equations
D	diameter or line width
g	gravity (9.81 m/s^2)
L	length of rectangular fuel source

m	mass
n	fraction of stoichiometric air entrained
Q	energy release
r	radius in polar coordinates
s	stoichiometric air to fuel mass ratio
T	Temperature (T_o=293 K)
v	horizontal velocity
w	vertical velocity
W	dimensionless velocity (Eq. (2))
x	horizontal coordinate parallel to length
X_r	radiation loss fraction
y	horizontal coordinate parallel to width
z	vertical coordinate
Z_c	characteristic plume length scale (Eq. (3))

Greek Symbols

α	dimensionless entrainment coefficient
β	Gaussian profile constant
$\Delta H_c/s$	heat of combustion per unit mass of air (2.91 kJ/g)
ρ	density (ρ_o=1.21 kg/m^3)
Φ	dimensionless temperature, Eq. (2)
ζ	dimensionless height ratio, Eq. (2)
Ψ	dimensionless parameter, Eq. (5)

Subscripts

e	entrained air
f	flame
m	maximum or center-line value
o	ambient conditions

Superscripts

()	signifies rate of change
()’	single prime (per unit length)
()’’	double prime (per unit area)
()’’’	triple prime (per unit volume)

Acknowledgement

The authors are grateful to the support for this study from NIST/BFRL and Dr. David Evans .

References

1. Yokoi, S., "Study on the Prevention of Fire Spread Caused by Hot Upward Current," Building Research Report 34, Japanese Ministry of Construction, 1960

2. Rouse, H., Yih, C. S. and Humphries, H. W., *Tellus* 4:202 -210 (1952)

3. Morton, B. R., Sir Geoffrey Taylor and Turner, F.R.S. and J. S., *Proc. of the Royal Soc. of London* 234. A. 1956, pp 1-23.

4. McCaffrey, B. J., "Purely buoyant diffusion flames: Some experimental results," National Bureau of Standards Report No. NSBIR 79-1910, 1979

5. Cox, G. and Chitty, R., *Combust. Flame* 39:191-209 (1980)

6. Zukoski, E. E., *First Symposium (International) on Fire Safety Science*, 1985, pp 1-11.

7. Heskestad, G., *Combustion and Flame* 83:293-301 (1991)

8. Lee, S. L. and Emmons, H. W., *J. of Fluid Mech.*, 11:353-368 (1961)

9. Thomas P. H., *Ninth Symposium (International) on Combustion*, Academic Press, New York, 1963, pp 844-859.

10. Steward, F. R., *Combust. Flame* 8:171 -178 (1964)

11. Steward, F. R., *Combust. Sci. Tech.* 2:203-212 (1970)

12. Hasemi, Y. and Nishita, M., *Second Symposium (International) on Fire Safety Science*, Hemisphere, New York, 1988, pp 275-284.

13. Sugawa, O., Yasushi, O. and Satoh, H., *Third Symposium International on Fire Safety Science*, 1991, pp 435-444.

14. Yuan, L. and Cox, G., *Fire Safety J.* 27:123- 139 (1996)

15. Sugawa, O., Yasushi, O. & Hirofumi, H., "Fire induced flow in a clean room with downward vertical laminar flow," NSBIR 88-3753, 1987

16. Thomas, P. H., Webster, C. T. and Raftery, M. M., *Combustion and Flame* 5:359-367 (1961)

17. Delichatsios, M. A., *Combust. Flame* 70:33-46 (1987)

18. Roper, F. G., *Combust. Flame* 91:226 -238 (1992)

19. Roper, F. G., Smith, C. and Cunningham, A. C., *Combust Flame* 29:227-234 (1977)

20. Grove, B. S., "Correlations for Infinite Line Fires," MS Thesis, Dept. of Fire Prot. Eng.,University of Maryland, College Park, MD

21. Zukoski, E. E., "Properties of Fire Plumes," *Combustion Fundamentals of Fire*, Ed. G. Cox, Academic Press, London, 1995

22. Brodowicz, K. and Kierkus, K. T., *Int. J. Heat Mass Transfer* 9:81-94 (1966)

23. Cox, G. and Chitty, R., *Combust. Flame* 60:219-232 (1985)

24. Baum, H. R. and McCaffrey, B. J., *Second Symposium (International) on Fire Safety Science*, 1988 pp 129-148.

25. Zukoski, E. E., *Fourth Symposium (International) on Fire Safety Science*, 1994 pp 137-147

26. Smith, R. K. and Morton, B. R., *J. of Fluid Mech.* 68/1:1-19 (1975)

27. McCaffrey, B., "Flame Heights," *SFPE Handbook of Fire Protection Engineering* (2nd ed.) National Fire Protection Assoc., Quincy, MA, 1995

28. Taminini F., *Comb. and Flame* 30:85-101 (1977)

Table 1: Far Field Correlations: Coefficients = Theory, Experiment

Dimensionless Variable	Axisymmetric ($\chi_r = 0.20$ for data)	Infinite Line ($\chi_r = 0.30$ for data)
B	$C_l\zeta$ $C_l = \frac{6}{5}\alpha$, 0.118	$C_l\zeta$ $C_l = \frac{2}{\sqrt{\pi}}\alpha$, 0.103
W	$C_v\zeta^{-1/3}$ $C_v = \left[\left(\frac{25}{24\pi}\right)\left(\frac{\beta+1}{\beta}\right)\alpha^{-2}(1-\chi_r)\right]^{1/3}$ $C_v = 4.17(1-\chi_r)^{1/3}$	$C_v\zeta^0$ $C_v = \left[\left(\frac{\beta+1}{2\beta}\right)^{1/6}\alpha^{-1/3}(1-\chi_r)^{1/3}\right]$ $C_v = 2.3(1-\chi_r)^{1/3}$
Φ	$C_T\zeta^{-5/3}$ $C_T = \left[\frac{2}{3}\left(\frac{25}{24\pi}\right)^{2/3}\frac{(\beta+1)^{2/3}}{\beta^{-1/3}\alpha^{4/3}}(1-\chi_r)^{2/3}\right]$ $C_T = 10.58(1-\chi_r)^{2/3}$	$C_T\zeta^{-1}$ $C_T = \left[\frac{(\beta+1)^{1/3}}{2^{5/6}\beta^{-1/6}}\alpha^{-2/3}(1-\chi_r)^{2/3}\right]$ $C_T = 3.3(1-\chi_r)^{2/3}$
$\frac{W^2}{\Phi\zeta}$	$\frac{3}{2}\beta$, 1.64	$\sqrt{\frac{2}{\beta}}$, 1.54
α	0.098	0.091
β	0.913	0.845

Table 2: Near Field Correlations: Coefficients = Theory, Experiment

Dimensionless Variable	Axisymmetric ($\chi_r = 0.20$ for data)	Infinite Line ($\chi_r = 0.30$ for data)
B	$C_l\zeta$ $C_l = \frac{4}{5}\alpha$, 0.176	$C_l\zeta$ $C_l = \frac{4\alpha}{3\sqrt{\pi}}$, 0.272
W	$C_v\zeta^{1/2}$ $C_v = \sqrt{\frac{4}{3}\frac{\Psi}{n}}$, 2.02 or $0.720\sqrt{\Psi}$	$C_v\zeta^{1/2}$ $C_v = \sqrt{\frac{\Psi}{n}}$, 2.3 or $0.877\sqrt{\Psi}$
Φ	$C_T\zeta^0$ $C_T = 2\frac{\Psi}{n}$, 2.73 or 0.347Ψ	$C_T\zeta^0$ $C_T = \sqrt{2}\frac{\Psi}{n}$, 3.1 or 0.450Ψ
$\frac{W^2}{\Phi\zeta}$	$\frac{3}{2}\beta$, 1.49	$\sqrt{\frac{2}{\beta}}$, 1.42
α	0.22	0.590
β	1	1

Table 3: Far Field Entrainment Correlations: Coefficients = Theory, Experiment

Axisymmetric ($\chi_r = 0.20$ for data)	Infinite Line ($\chi_r = 0.30$ for data)
$\frac{\dot{m}_e}{\rho_o\sqrt{gz}z^2} = C_e\zeta^{-5/6}$ $C_e = \pi C_v C_l^2$, 0.169	$\frac{\dot{m}'_e}{\rho_o\sqrt{gz}z} = C_e\zeta^{-1/2}$ $C_e = \sqrt{\pi}C_v C_l$, 0.647

Table 4: Near Field Entrainment Correlations: Coefficients = Theory, Experiment

Axisymmetric ($\chi_r = 0.30$ for data)	Infinite Line ($\chi_r = 0.30$ for data)
$\frac{\dot{m}_e}{\rho_o\sqrt{gD}D^2} = C_e\left(\frac{z}{D}\right)^{1/2}\left(1+2C_l\left(\frac{z}{D}\right)\right)^2$ $C_e = \frac{\pi}{2\sqrt{3}}\sqrt{\frac{\Psi}{n}}$, 0.148 or $0.0565\sqrt{\Psi}$ $C_l = \frac{4}{5}\alpha$, 0.179	$\frac{\dot{m}'_e}{\rho_o\sqrt{gD}D} = C_e\left(\frac{z}{D}\right)^{1/2}\left(1+2C_l\left(\frac{z}{D}\right)\right)$ $C_e = \frac{\sqrt{\pi}}{2}\sqrt{\frac{\Psi}{n}}$, 0.148 or $0.0565\sqrt{\Psi}$ $C_l = \frac{4\alpha}{3\sqrt{\pi}}$, 0.444

Table 5: Flame Height Correlations: Coefficients = Theory, Experiment

Axisymmetric ($\chi_r = 0.30$ for data)	Infinite Line ($\chi_r = 0.30$ for data)
$Q_D^* = \left(\frac{Z^*}{D}\right)^{5/2} = C_f\left(\frac{Z_f}{D}\right)^{1/2}\left(1+2C_l\left(\frac{Z_f}{D}\right)\right)^2$ $C_f = \frac{\pi}{2\sqrt{3}}\frac{(\Psi/n)^{3/2}}{(1-\chi_r)}$, 0.152 or $0.00590\frac{\Psi^{3/2}}{(1-\chi_r)}$ $C_l = \frac{4}{5}\alpha$, 0.179	$Q_D^{**} = \left(\frac{Z^{**}}{D}\right)^{3/2} = C_f\left(\frac{Z_f}{D}\right)^{1/2}\left(1+2C_l\left(\frac{Z_f}{D}\right)\right)$ $C_f = \frac{\sqrt{\pi}}{2}\frac{(\Psi/n)^{3/2}}{(1-\chi_r)}$, 0.152 or $0.00590\frac{\Psi^{3/2}}{(1-\chi_r)}$ $C_l = \frac{4\alpha}{3\sqrt{\pi}}$, 0.444

Figure 1: Dimensionless Temperature vs. Height for the Infinite Line

$X_r = 30\ \%$

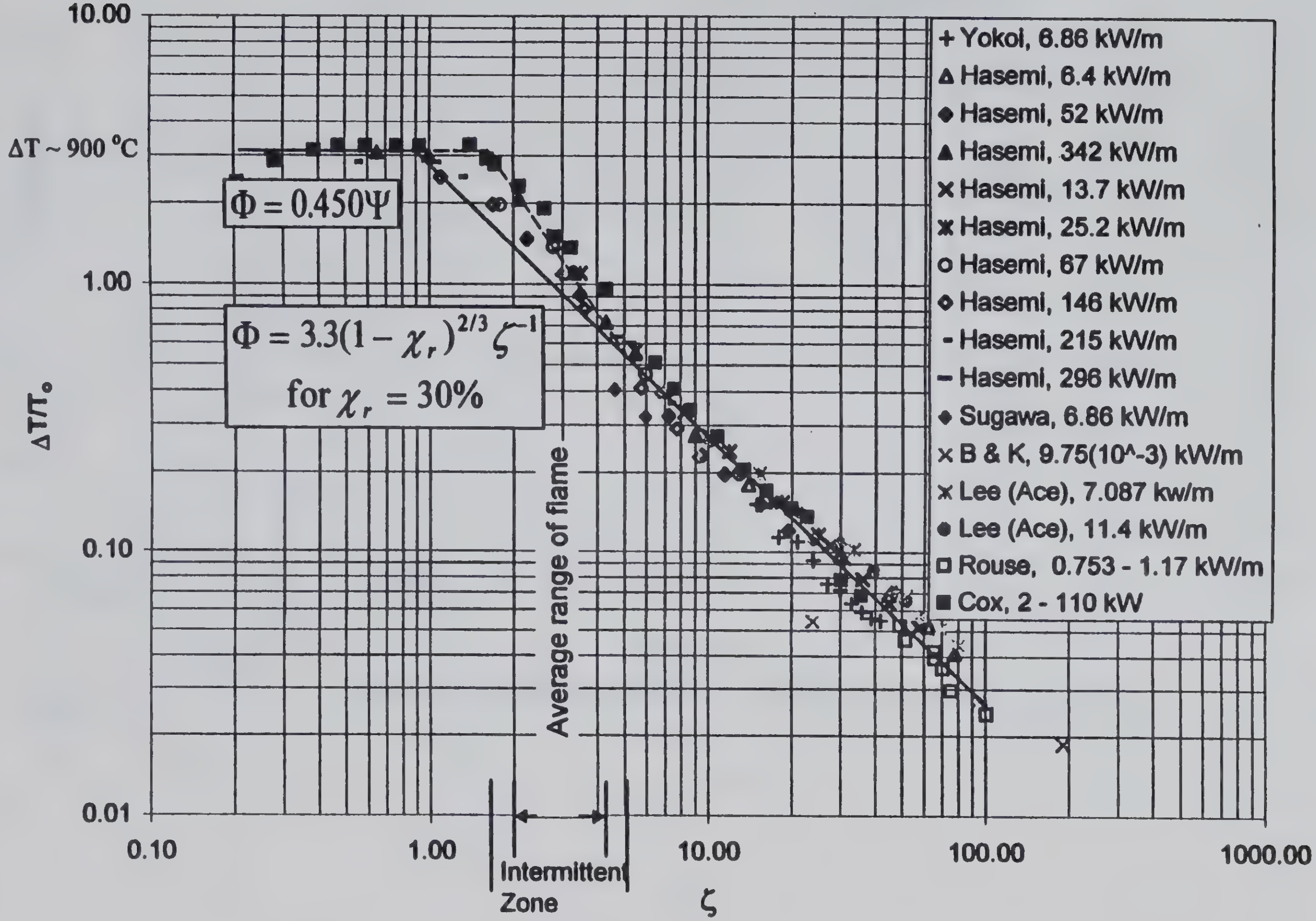

Figure 2: Velocity Radiation Curves for the Infinite Line
Initial X_r = 30 %

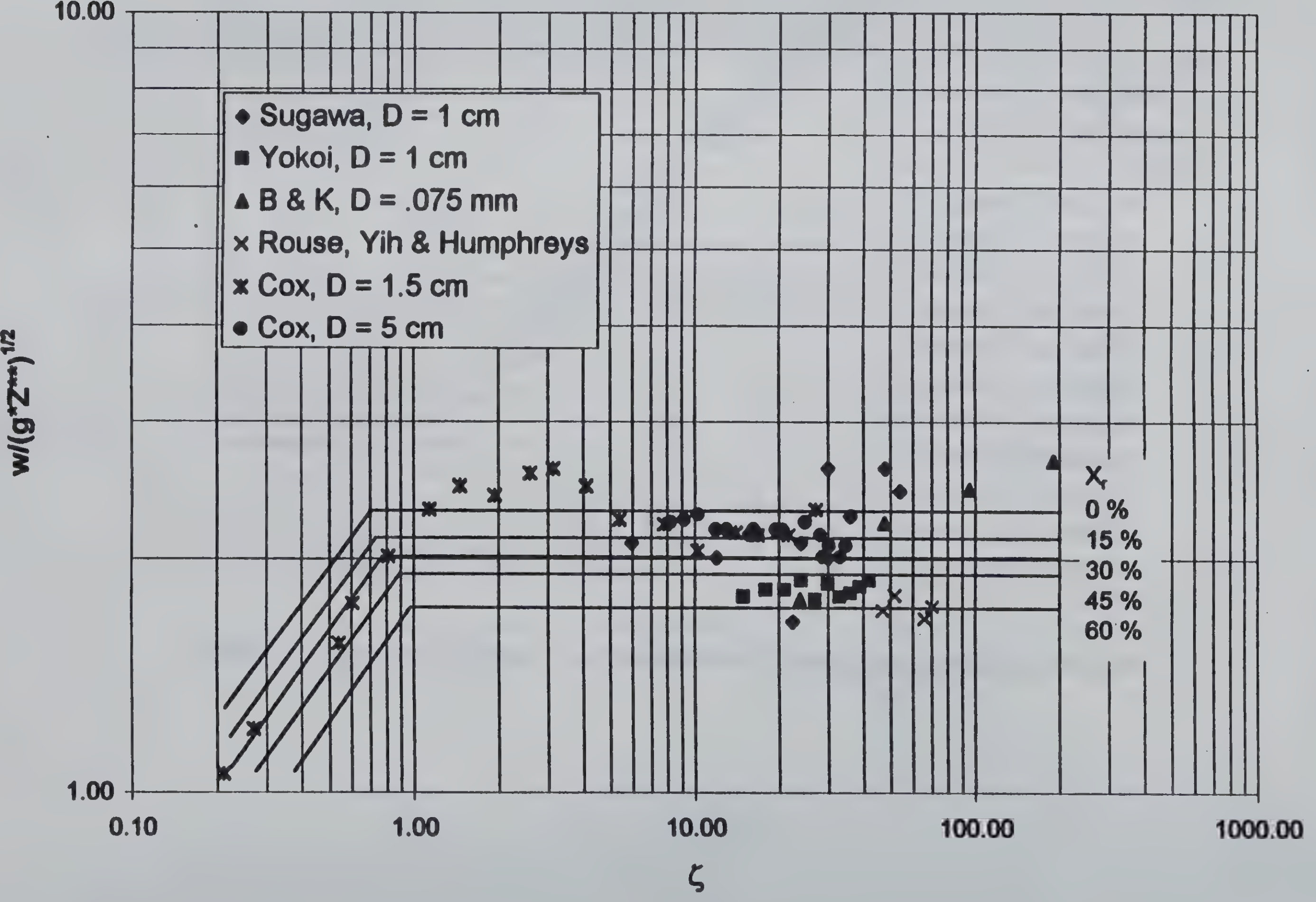

Figure 3: Near Field Axisymmetric Dimensionless Entrainment vs. Height (plotted for $X_r = 0.3$)

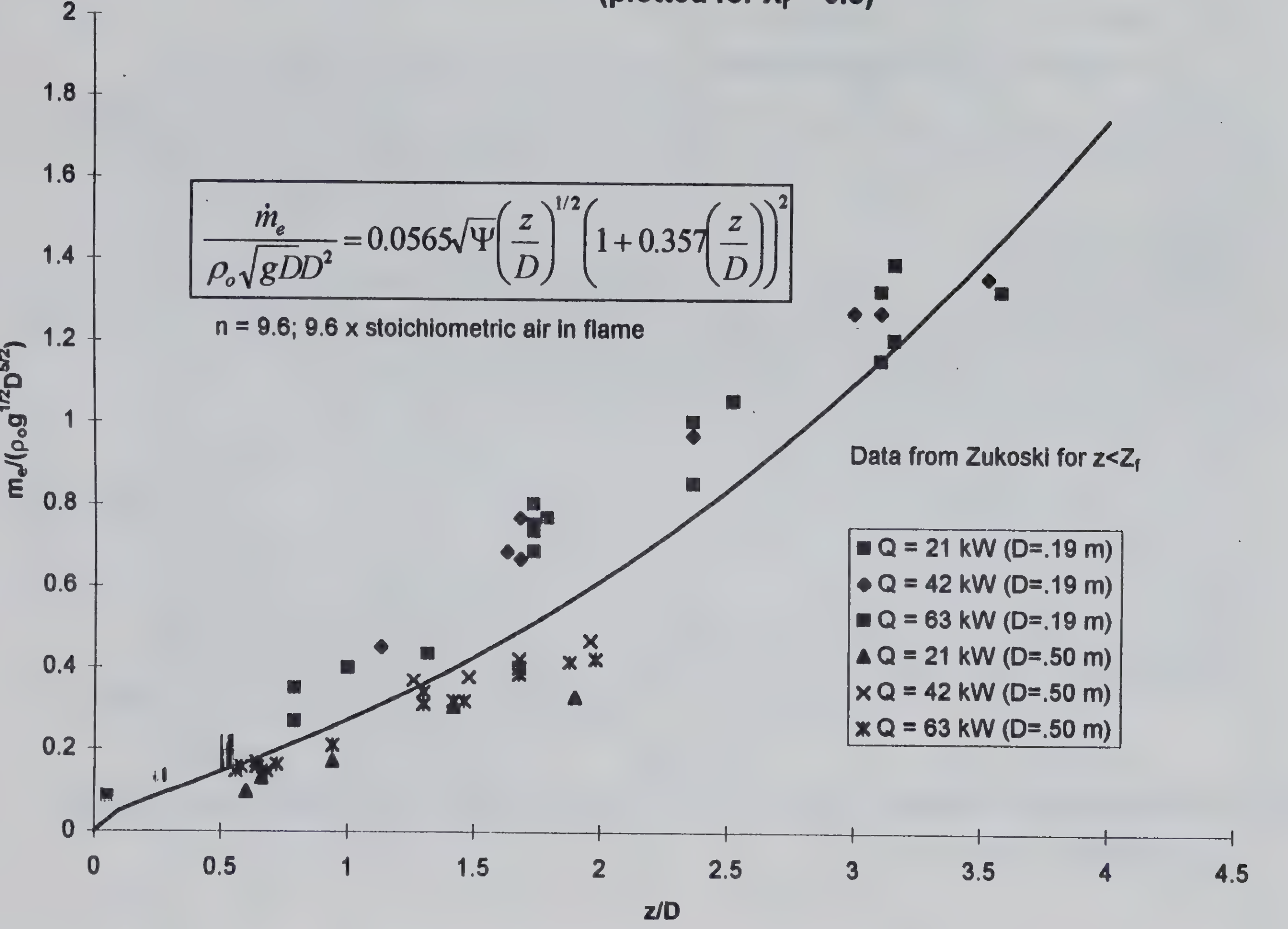

Figure 4: Axisymmetric Smooth Fit of Dimensionless Flame Height, Z_f/D, vs. Energy Release Rate, Q_D^*

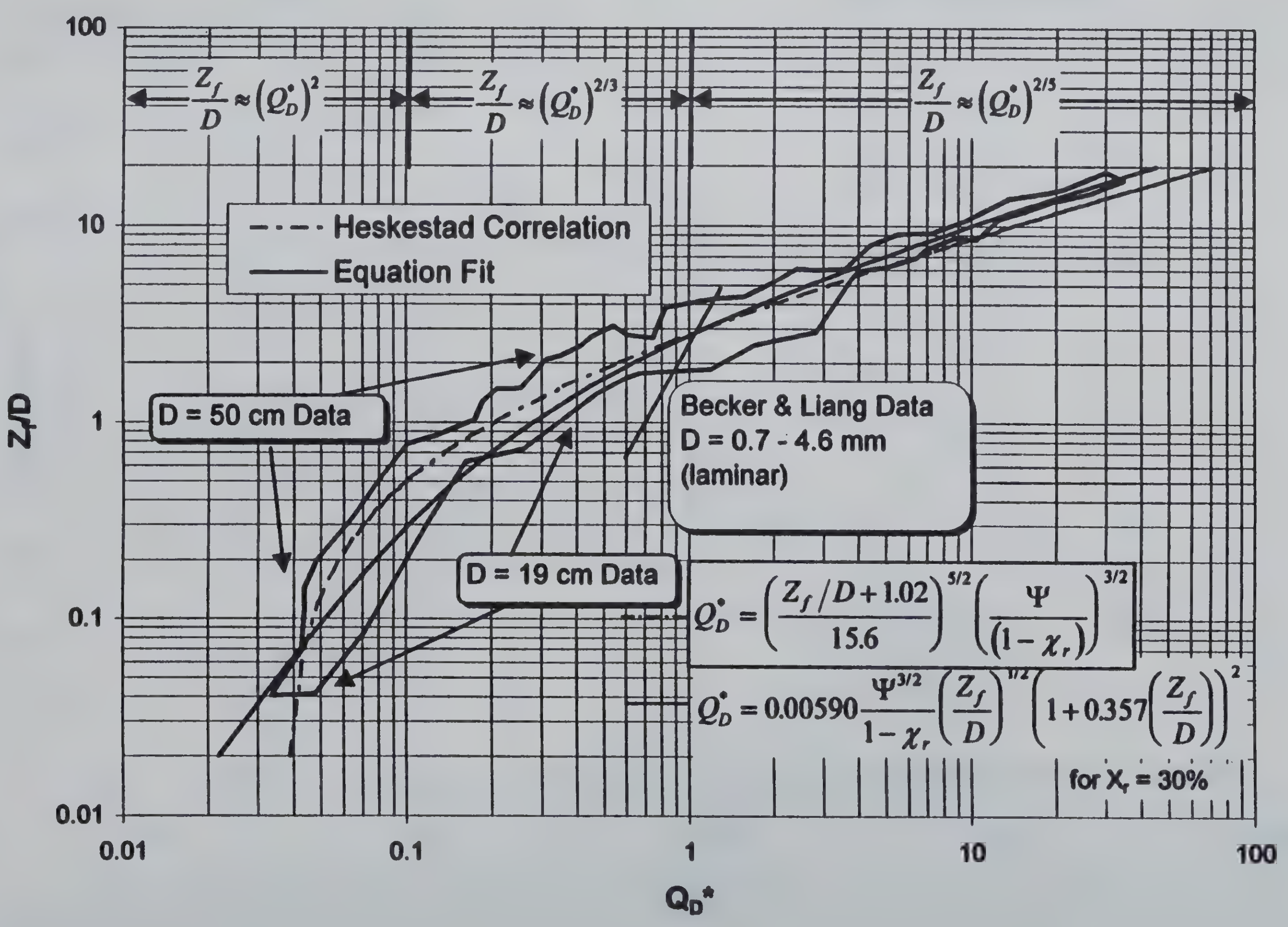

Figure 5: Dimensionless Flame Height Equation for the Infinite Line

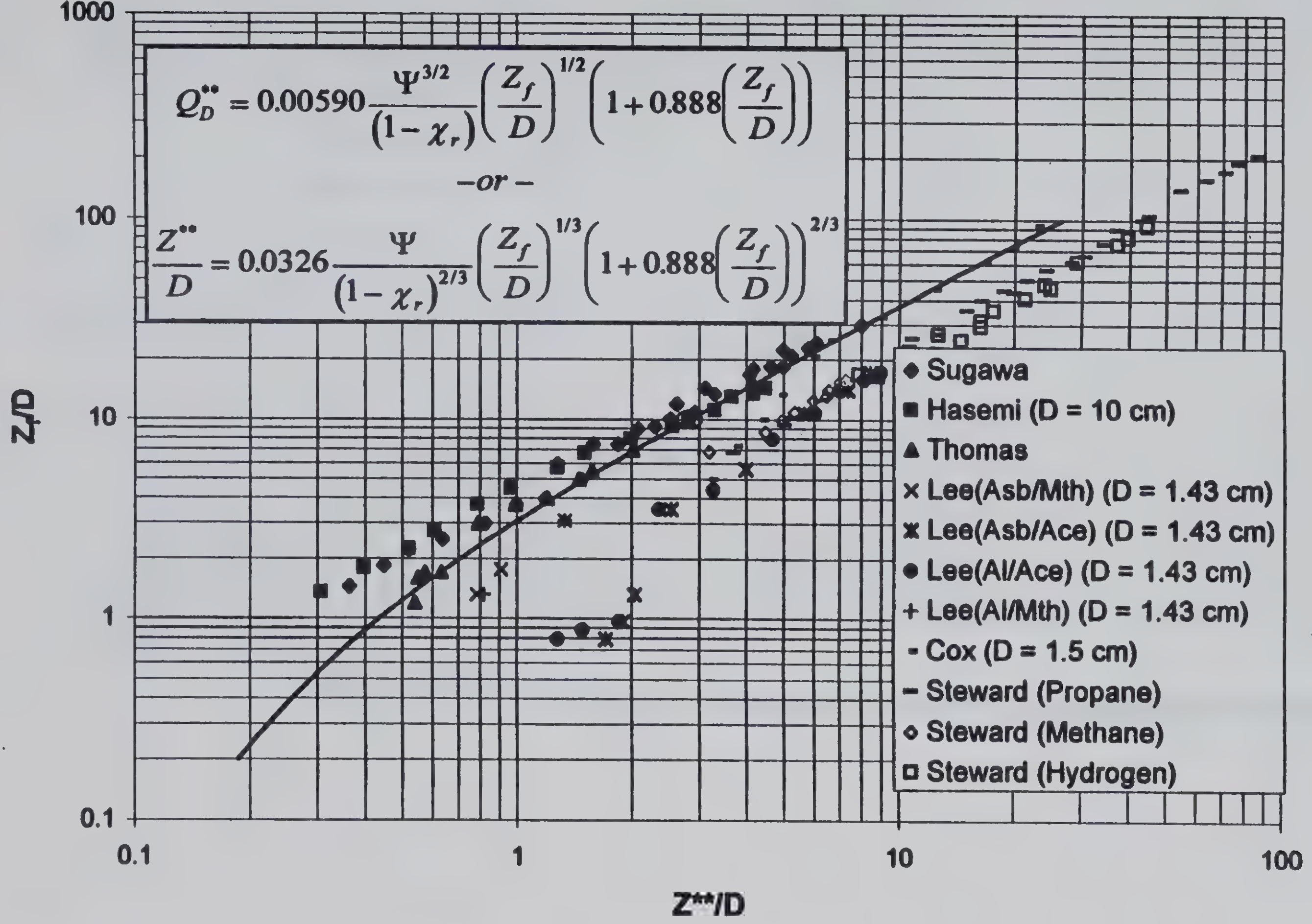

Figure 6: Dimensionless Temperature vs. Height for a Rectangular Source

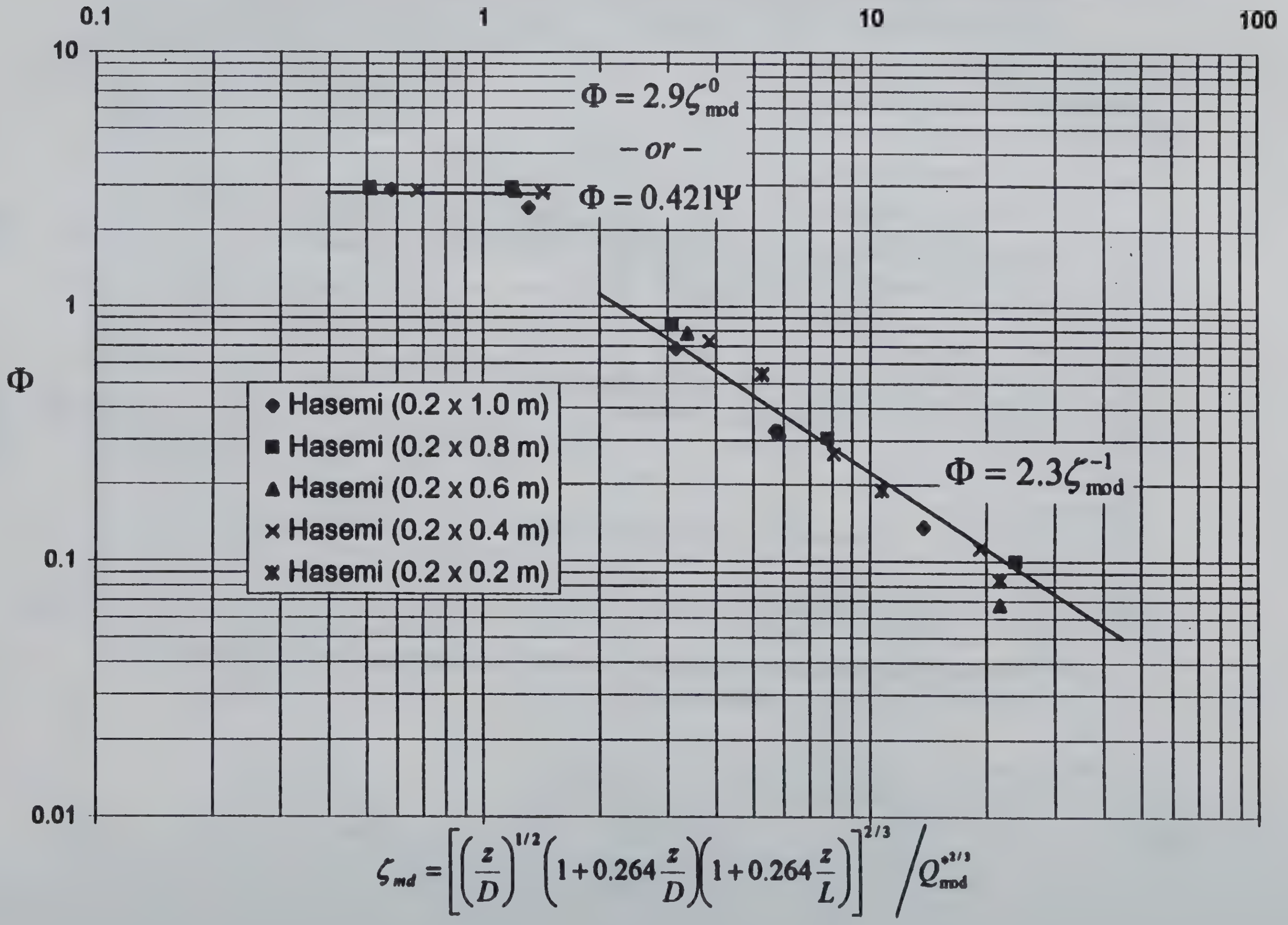

Correlations for Infinite Line Fires

II

CORRELATIONS FOR INFINITE LINE FIRES

by

Brian S. Grove

Thesis submitted to the Faculty of the Graduate School of the
University of Maryland in partial fulfillment
of the requirements for the degree of
Master of Science
1997

Advisory Committee:

Dr. James G. Quintiere, Chair/Advisor
Dr. Marino di Marzo
Dr. Jose Torero

ABSTRACT

Title of Thesis: CORRELATIONS FOR INFINITE LINE FIRES

Degree Candidate: Brian S. Grove

Degree and Year: Master of Science, 1997

Thesis directed by: Professor James G. Quintiere
Department of Fire Protection Engineering

Empirical correlations are developed for both buoyancy dominated axisymmetric fires and infinite line fires, or fire sources having one side substantially larger than the other. New theory has been developed for the combustion zone or near field of the fire plume and the smoke plume or far field of the fire plume. Solutions were found for temperature, velocity, and plume width in both predescribed zones of the plume. Also considered were flame height and entrainment in both parts of the plume. Representative data from select authors was utilized to determine empirical constants to these solutions. After developing empirical correlations for the two extreme cases, axisymmetric sources and infinite line sources, theory was modified for rectangular cases and applied to available temperature and flame height data.

Keywords: buoyant plume, aspect ratio, line fire,

CORRELATIONS FOR INFINITE LINE FIRES

by

Brian S. Grove

Thesis submitted to the Faculty of the Graduate School of the
University of Maryland in partial fulfillment
of the requirements for the degree of
Master of Science
1997

Advisory Committee:

Dr. James G. Quintiere, Chair/Advisor
Dr. Marino di Marzo
Dr. Jose Torero

Dedication

To my grandfather Arnold J. P. Rausenberger who I always loved very much but often never appreciated. I never realized the man he was until I became the man I am.

Acknowledgement

I would like to express my deepest gratitude to Dr. James G. Quintiere for his leadership, patience, and understanding. Following in his footsteps was truly an enlightening and humbling experience. After loosing his linear-log interpolator; breaking an experimental apparatus; and erasing the hard drive on one of his computers he never let me fall from his graces. Thank you.

Special thanks to Dr. Jose Torero who gave me excellent advice for my presentation at ICFRE2 and thesis defense.

The financial support provided by the National Institute of Standards and Technology and the use of their excellent library system was essential to the completion of this work.

TABLE OF CONTENTS

List of Tables v

List of Figures vi

Nomenclature vii

Chapter 1 Introduction

- 1.1 Background 1
- 1.2 Definition of Line Fires 3
- 1.3 Physical Examples of Line Fires 3

Chapter 2 Overview of Thesis

- 2.1 Introduction 4
- 2.2 Methodology 5
- 2.3 Outline 6
- 2.4 Author Review 7

Chapter 3 Theory

- 3.1 Introduction 12
- 3.2 Assumptions 13
- 3.3 Conservation Equations 14
  - 3.3.1 Infinite Line Source 15
  - 3.3.2 Axisymmetric Source 16
- 3.4 Far Field Theory for the Infinite Line Source (Temperature, Velocity, Plume Width) 16
  - 3.4.1 Entrainment 20
- 3.5 Far Field Theory for the Axisymmetric Source (Temperature, Velocity, Plume Width) 21
  - 3.5.1 Entrainment 25
- 3.6 Summary of Far Field Results 26
- 3.7 Near Field Theory, (Combusting Plume Region) (Temperature, Velocity, Plume Width) 27
  - 3.7.1 Infinite Line Source 27
  - 3.7.2 Axisymmetric Source 32
- 3.8 Summary of Near Field Results 37
- 3.9 Entrainment in the Combustion Zone 37
  - 3.9.1 Infinite Line Source 38
  - 3.9.2 Axisymmetric Source 39
- 3.10 Flame Height 40
  - 3.10.1 Infinite Line Source 40
  - 3.10.2 Axisymmetric Source 41

Chapter 4 Empirical Constants

4.1 Introduction 43
4.2 Infinite Line Temperature Data 43
4.3 Infinite Line Velocity Data 46
4.4 Infinite Line Far Field Correlations 46
4.5 Infinite Line Near Field Correlations 48
    4.5.1 Temperature 48
    4.5.2 Velocity 49
4.6 Infinite Line Radiation Effects 50
    4.6.1 Temperature 50
    4.6.2 Velocity 51
4.7 Introduction to Near Field Entrainment and Flame Height 56
4.8 Axisymmetric Flame Height Correlations 57
    4.8.1 Radiation Effects 61
4.9 Axisymmetric Entrainment Correlations 64
4.10 Infinite Line Flame Height Correlations 69
4.11 Infinite Line Entrainment Correlations 75

Chapter 5 Comparison of Empirical Correlations (Infinite Line vs. Axisymmetric) 80

Chapter 6 Rectangular Theory

6.1 Introduction 84
6.2 Assumptions 84
6.3 Far Field Non-Combusting Plume Temperature 85
6.4 Far Field Entrainment 90
6.5 Flame Height 90

Chapter 7 Conclusion 95

References 96

LIST OF TABLES

1 Summary of Data and Author Review 10, 11

2 Far Field Summary 26

3 Near Field Summary 37

4 Axisymmetric Flame Height Data Fit Points 60

5 Infinite Line Flame Height Data Fit Point 75

6 Far Field Correlations 80

7 Near Field Correlations 81

8 Far Field Entrainment Correlations 82

9 Flame Height Correlations 82

10 Near Field Entrainment Correlations 83

11 Rectangular Flame Height Data Fit Point 92

LIST OF FIGURES

A1 Aspect ratio 3

1 Dimensionless Temperature vs. Height for the Infinite Line 44

2 Axisymmetric Dimensionless Velocity vs. Height 47

3 Temperature Radiation Curves for the Infinite Line 52

4 Velocity Radiation Curves for the Infinite Line ($\chi_r = 15\ \%$) 54

5 Velocity Radiation Curves for the Infinite Line ($\chi_r = 30\ \%$) 55

6 Axisymmetric Smooth Fit of Flame Height vs. Energy Release Rate 59

7 Axisymmetric Smooth Fit Radiation Curves of Z_f/D vs. Q_D^* 62

8 Near Field Axisymmetric Dimensionless Entrainment vs. Height 65

9 Axisymmetric Far and Near Field Entrainment 67

10 Dimensionless Flame Height for the Infinite Line 70

11 Dimensionless Flame Height Equation for the Infinite Line 73

12 Near Field Entrainment Equations for the Infinite Line 76

13 Qualitative Presentation of Plume Width in Far and Near Fields 81

14 Dimensionless Temperature vs. Height for a Rectangular Source 88

15 Dimensionless Flame Height for Rectangular Sources 94

NOMENCLATURE

a	width of plume
A	width of rectangular fuel source
b	length of plume
B	length of rectangular fuel source
c_p	specific heat (kj/kg·K)
C	generic constant used in power series
D	axisymmetric diameter or line width
g	gravity (9.81 m/s^2)
$\dot{m}$	mass flow rate
n	multiplication factor for stoichiometric oxygen
$\dot{q}''$	heat transfer rate per unit area
$\dot{q}'''$	energy release rate per unit volume
$\dot{Q}$	energy release rate (kW)
r	horizontal direction in polar coordinates
s	stoichiometric air to fuel
T	Temperature
v	horizontal velocity
w	vertical velocity
x	horizontal direction parallel to length
y	horizontal direction parallel to width
z	vertical direction
Z*	characteristic axisymmetric height (m)
Z**	characteristic infinite line height (m)

Greek Symbols

α	dimensionless entrainment coefficient
β	gaussian profile constant
χ_r	radiation loss fraction
ΔH_c	heat of combustion (kj/kg)
ΔH_a	heat of combustion of air (kj/kg)
ΔT	change in temperature (K)
ρ	density
Φ	dimensionless temperature
τ	shear stress
ζ	dimensionless height ratio; either z/Z* or z/Z**

Subscripts

e	entrained air
f	fuel
l	width of plume
m	maximum or center-line value

o	ambient conditions
T	temperature
v	velocity

Superscripts

$\dot{X}$	signifies rate of change
X'	single prime (per unit length)
X''	double prime (per unit area)
X'''	triple prime (per unit volume)

Chapter 1 INTRODUCTION

1.1 Background

Modeling of fire and smoke movement in buildings requires accurate knowledge of the structure itself including the building's materials and construction method in conjunction with the potential hazard, or more specifically fuel load and orientation. We are addressing only one piece of this complicated matrix; the fire source characteristics inherent to the burning of the fuel load. Here fire source characteristics include flame height, entrainment, temperature and velocity both in the fire plume and its ascending smoke plume. Also of substantial importance is flame radiation which can have a dramatic effect on all of the above fire source characteristics as will be shown later.

The study of fire is a fairly new field. When its earliest pioneers first studied and tried to quantify the behavior of a fire plume it was easiest and logical to use an axisymmetric source. As the study of fire progressed, although still in its infantile stages, scientists discovered innate differences between flat 2-D fuel sources, such as chemical pool fires, and 3-D sources such as wood cribs or sofas. However, studies were not performed to clearly show the effects that fuel geometry can have on fire plume source characteristics.

As a result, numerous studies, experiments, and correlations have been performed or respectively developed for the above fire source characteristics for axisymmetric fire plumes. All pertinent information has been well documented and agreed upon in the fire protection community. Unfortunately, two-dimensional fire sources, or in this case line fires, have not received the same level of detail as their axisymmetric counterparts.

Indeed, upon performing my literature review I came across a plethora of axisymmetric source papers that overwhelmed available information on line fires. In addition, a quick examination of the SFPE Handbook of Fire Protection Engineering addresses only the axisymmetric fire source regarding the prementioned fire source characteristics: McCaffrey (Flame Height) [14], Heskestad (Fire Plumes) [15], Delichatsios (Air Entrainment…) [16]. This is not to say that a significant amount of work has not been invested in the study of line plumes, merely that until recently little effort has been placed on comparing their correlations and thus arriving at a consensus for using them. Within the past few years, Gupta [25] [26] has compared the theories and analyses of some of these authors along with their empirical constants for the infinite line. More recently, Cox et al. [9] took detailed measurements of all of the prementioned fire source characteristics throughout the entire plume for various size line sources. He then compared his empirical constants to those of more historical works [1] [2] [3] [4].

The objective of the present research is to bring the understanding of line fires to the same level of credibility as their axisymmetric counterparts through quantitative equations. This paper seeks to enhance the knowledge of two dimensional sources through a new theory combined with empirical constants taken from representative data of pertinent experiments that has been assimilated onto single variable graphs. Similar to the studies performed by Gupta [25] [26] and Cox et al [9] validation of previous works is also an objective. However, rather than examining and comparing the correlation constants of previous works on an individual basis the validity of these separate works will be illustrated through the consistency of data on single variable plots.

Definition

Aspect ratio is defined as the fire source's width divided by length, (D/L). Theoretically, line fires have infinitely small aspect ratios, whereas axisymmetric fires have aspect ratios equal to one. Aspect ratios for our line data range from 0.1 to 0.007 with 0.01 being the norm. In other words on the average, length is 100 times greater than the width.

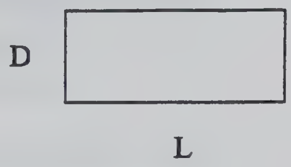

Figure A1: Aspect Ratio

Physical Examples of Line Fires

The importance of studying line fires and thus quantifying their behavior revolves around the fact that they can be used as idealized representations of situations of much greater complexity [9]. Physical examples that correlations developed from line fires could be used to model include:

- Row of townhouses
- Long sofa
- Advancing front of forest fire
- Balcony spill plume
- Flame spread over flammable wall linings [9]

2.1 Introduction

It has been shown by Cox et al [9] that a fire plume can be broken into as many as four separate and distinct regimes:

- Continuous
- Intermittent
- Transition
- Smoke/Buoyant plume

Where these regimes are explained by a combination of definitions from both McCaffrey [31] and Morton, Taylor, and Tuner [22].

(i) The *continuous* zone contains a persistent turbulent diffusion flame yielding an accelerating flow of burning gases that are strongly buoyant.

(ii) In the *intermittent* region temperature remains quite high, though there is a negligible occurrence of chemical reaction, but the gases are still strongly buoyant in flow.

(iii) The *transition* region occurs where the velocity decays to a different level from that in the intermittent flame region accompanied by a corresponding steeper temperature decay before settling to the expected linear temperature decay in the buoyant plume[9].

(iv) The *buoyant plume* is characterized by decreasing velocity and temperature with height, where the temperature has fallen to a value at which the strongly buoyant plume reverts to a weak buoyant plume.

We seek to simplify the problem by dividing the plume into two regimes:

- Continuous
- Smoke Plume

Some authors [31] [3] have performed correlations for three regimes by inserting an intermittent region between the continuous and smoke plume regime. However, we chose to only correlate two regimes for two reasons. (1) Data can be inaccurate and hard to interpret in the intermittent region. (2) Individual researchers define the boundaries of the intermittent zone differently.

2.2 Methodology

Solutions were developed through a simplified version of Steward's [6] theory. His analysis was diluted by incorporating point source theory; thus ignoring initial conditions at the fuel source including temperature, velocity, and source geometry. As a result of this assumption, we obtained simplified solutions that were much easier to use than his complicated solution. When determining plume characteristics in the far field this assumption proved valid as all of the characteristics fit well to available data. The same was true when correlating temperature and velocity in the near field. However, the point source assumption proved suspect when correlating flame height and entrainment in the near field.

Thomas, Webster and Raftery referenced by Zukoski [20], were the first researchers to recognize the importance of source geometry, especially for large sources, when developing correlations for both near field entrainment and flame height. Therefore, through an iterative process the effects of fuel diameter were addressed in both of these instances where they would be the most dramatic. First, as stated above, the equations were developed incorporating the point source assumption. Source geometry effects were then added to these "point source" equations. The new equations fit the data much better and have a similar form to Zukoski's [20] corresponding correlations.

The initial effects of velocity and plume width at $z = 0$ proved negligible in all cases. Although, Steward's equations are more physically correct than ours the accuracy he gained by incorporating all of the above initial conditions is negligible.

2.3 Outline

The thesis can be thought of as being split into three main parts, I, II, and III. Part I details solutions for temperature, velocity and plume width for both axisymmetric and infinite line sources and in both parts of the plume; continuous, (near field), and smoke plume, (far field). Part II focuses on solutions for flame height and entrainment in both parts of the plume. However, empirical correlations were only developed for the near field. Part III is an extension of parts I and II and presents correlations for rectanglular sources normalized between their axisymmetric and infinite line boundaries for temperature and flame height. In general, solutions were developed for the axisymmetric source first as a means of verifying the new theory because more data is available for this source than the line. In many instances verification was more practical for flame height and entrainment, but nonetheless for consistency was carried over to the first part of the paper.

More specifically, empirical solutions for temperature, velocity, and plume width are developed in both regimes for the axisymmetric source using data from Yokoi [3] in the far field and McCaffrey [17] in the near field. For the line source, the same sets of data [1] [2] [3] [4] [9] [11] [12] were used in both regimes. The solutions to these characteristics are simply a constant times dimensionless height to a power.

$$\begin{aligned} Temperature(\Phi) &= C_T \zeta^m \\ Velocity(W) &= C_v \zeta^n \\ Plume\ Width(B) &= C_l \zeta^p \end{aligned}$$

In part II, empirical correlations are developed for both flame height and entrainment. Multiple sources were used for the infinite line including Hasemi [1], Cox [9], Steward [6] and others [2] [5] [13]. Although much more data is available for axisymmetric sources than for line sources only Zukoski's [20] data were used to develop axisymmetric empirical correlations for flame height, because we had faith in its accuracy and it contained a wide range of burner sizes. Zukoski's [20] data was also used to develop correlations for axisymmetric near field entrainment correlations. Unfortunately, no data could be found in the near field for the line so a mock point was invented through Yuan and Cox's recent publication [9]. Unlike the correlations found in part I, flame height and entrainment solutions are much more complicated and overall more difficult to correlate. However, there is a strong inter-dependence between infinite line and axisymmetric correlations that was not exhibited for temperature, velocity, and plume width correlations. This inter-dependence is exploited when determining empirical correlations for the infinite line.

2.4 Author Review

Although the papers used in creating our dimensionless graphs originate from the same narrow field of study, with relatively few exceptions, the motivation for their study was quite different in many cases. Some authors set out to study fire plume characteristics explicitly [1] [2] [5] [6] [9] [13]. Others, such as Yokoi[3] and Sugawa [11] used line fires implicitly to model or solve new fire protection problems. Yokoi used an infinite line heat source in a preliminary study for obtaining the temperature distribution of hot currents rising from burning wooden houses in the crowded post World War II cities of Japan. Sugawa used line fires to study the effect downward vertical flow, issuing from an air conditioning system for example, would have on detection times of a weakly buoyant plume. Another application of line fires outside the field of fire science was utilized by Rouse et al [4] to enable meteorologists to evaluate the role of the basic convective process in the more complex movements of the atmosphere.

The experimental apparatus, not to mention procedures, also very extensively from paper to paper. Most authors used liquid fuels supplied to long metal burners through an externally controlled feed as their heat source. However, in many cases this is where the similarity ends. Burners were placed in different size rooms, with different ambient conditions resulting in different external wind disturbances. Some authors such as Lee and Emmons [2] and Yokoi [3] were careful to minimize these external disturbances, others were not. In addition, some burners were placed between parallel walls, some were set in the center of a room, and yet others were placed several feet off of the floor. All of these factors were noted when selecting appropriate data. When possible data was neglected if variances from the “norm” were severe. Other experimental apparatus used included long wooden strips by Thomas [5] and a heated wire by Brodowicz and Kierkus [12]. Note that although the data by Brodowicz and Kierkus ware included on both temperature and velocity graphs it was not used in developing fire correlations.

The following chart summarizes the data used in creating our dimensionless graphs. Included on the chart are the papers used; type of data recorded; type and amount of fuel used; and width and aspect ratio of burners. A more detailed explanation of the experimental apparatus and procedures used to take data is presented in Appendix A.

Table 1: Summary of Data and Author Review

Author/Paper	Data Recorded	(Q) Fuel	Width (w)	Aspect Ratio (w/l)	Comments
Shao-Lin Lee Natural Convection Above a Line Fire	• Temperature • Flame Height	2.79 - 52.17 kW/m methyl alcohol and acetone	.564 " (1.43 cm)	.007	The burner was 78" long by .564" wide and .282" deep.
(Sugawa, Satoh, & Oka) Flame Height from Rectangular Fire Sources Considering Mixing Factor	• Flame Height	Not available Propane	Possibly 1 - 2 cm Not clear	Possibly .025 - .017	No exact burner dimensions were given for the test of interest, however, later tests included burner dimensions of 1 cm X 40 cm, 1 cm X 60 cm, 2 cm X 60 cm & 2 cm X 120 cm. Vessel constructed of stainless steel which contained fine sand as a diffuser.
(Sugawa, Oka, Hotta) Fire Induced Flow in a Clean Room with Downward Vertical Laminar Flow	• Temperature • Velocity	5.83 kW/m Methanol	1 cm	.012	All of the experiments were performed in a "clean room" with a 22 cm/sec downward vertical flow.
(Hasemi, Nishihata) Fuel Shape Effect on the Deterministic Properties of Turbulent Diffusion Flames	• Temperature • Flame Height	6.4 - 342 kW/m Propane	10 cm	.1 - 1	The burner was filled with ceramic beads of approximately 5 mm in diameter.

Continuation of Table

(Yokoi) Report of the Building Research Institute "Study on Prevention of Fire Spread Caused by Hot Upward Current"	• Temperature • Velocity	6.86 kW/m Alcohol	1 cm	.01	The burner was made out of tin. Q/l calculated from Sugawa's "Fire Induced Flow in a Clean Room..."
(F. R. Steward) Linear Flame Heights for Various Fuels	• Flame Height	Hygrogen Propane Methane	Not given	Not given	Steward did not take take his own data
(Lin-Ming Yuan, G. Cox) An Experimental Study of Some Line Fires	• Temperature • Velocity • Flame Height	2 - 110 kW Natural Gas (94% Methane)	15 mm 50 mm	.03, .075, 0.1	Two 15 mm porous refractory burners were used in addition to a sandbox burner.
(Rouse, Yih, Humphreys) Gravitational Convection from a Boundary Source)	• Temperature • Velocity	.753 - 1.17 kW/m "recessed gas burners yielding low, blue flames..."	Not given	Not given	Flow was confined between two parallel walls. Burner appears to be 8 feet long based upn the length of these confining walls.
(P. H. Thomas) The Size of Flames from Natural Fires	• Flame Height	Unknown Wood	Not given	Not given	"wood fires on effectively infinite strips of width D..." were used for the fuel.
(Brodowicz, Kierkus) Experimental Investigation of Laminar Free-Convection Flow in Air Above Horizontal Wire with Constant Heat Flux	• Temperature • Velocity	9.75×10^{-3} kW/m Heated wire	0.075 mm O.D.	.0003	A wire 0.075 mm O.D. and 250 mm long was stretched horizontally and heated by a direct electric current passing through it.

Chapter 3 THEORY

3.1 Introduction

The objective of this analysis is to provide useful analytical relationships for fire plumes, concentrating on fires originating from infinite line and rectilinear sources. Since extensive data exist for axisymmetric fire plumes, applicability of the developed theoretical approach will be verified for this geometry as a justification for its use in infinite line and rectilinear fire plumes where supporting data may be lacking. Turbulent plumes shall be considered although we believe that some data exhibit laminar fire characteristics.

The approach taken is based on the point source model of Morton, Taylor and Turner [22], and the extended analysis by Steward [6] for finite axisymmetric and infinite line fire sources. Other theoretical analyses by Yokoi [3], Zukoski [20], and Lee and Emmons [2] are also similar based on a constant entrainment coefficient. We shall adopt the combustion assumptions of Steward, but will ignore the finite source effects to allow for a direct analytical result. However, we shall, in the spirit of an iterate solution include the initial condition of a finite source diameter or width, but ignore any fuel mass or momentum source effects. It will be shown that the results produced in this fashion can correlate much of the combustion region effects for finite sources. Its implementation will also show a consistency between flame length and entrainment rates in the combustion zone. More specifically, entraiment rates in the flame zone can be predicted with knowledge of flame height. This analysis is similar in some ways to Delichatsios[16] and Thomas et al.[35] whose derivation is based more on flame geometry characteristics. Due to laminar or more specifically viscous effects, the theoretical results may not show all of the source geometry effects.

In many cases a detailed examination of the solutions is only presented for the case of the infinite line. The interested or confused reader should find this presentation helpful in determining the method of solution for the axisymmetric or rectangular source geometries. In addition there are numerous sources available which document such a solution [22] [24] [25].

3.2 Assumptions

Because our methodology follows the framework laid out by Steward [6], we will use all but one of his assumptions. Steward neglected radiation from the flame because, "its inclusion would make an analytical solution impossible." He concludes that, "neglecting radiation is probably the worst assumption of all, ...because high temperature cases, such as in a flame, will give up a considerable fraction of their thermal energy by this method of heat transfer." We, however, have included radiation and devoted a considerable amount of time to studying its effects on our correlations both in and out of the flame.

Assumptions used in developing the theory or limitations of the theory were adapted directly from Steward[6] and are as follows:

(1) Turbulent flow fully developed.
(2) Transverse forces small compared with those in the vertical direction.
(3) Mixing in the vertical direction neglected.
(4) No horizontal pressure variation.
(5) Ambient fluid is of uniform density.

(6) The heat capacities of the ambient air, plume and fuel are equal and independent of temperature. The molecular weight of the air, plume, and fuel are equal and the plume and air are perfect gases.

(7) Normalized density and velocity profiles are independent of height.

(8) The rate of entrainment is proportional to the centerline value of the plume velocity.

(9) In the far field, assume an ideal point source plume where all the heat is released at the origin. Whereas analysis of the fire plume assumes that entrained air mixes with fuel and burns to stoichiometric completion instantaneously.

A detailed explanation of the limitations and benefits inherent to each assumption can also be found in the same paper.

In our analysis, we simplified Steward's approach by utilizing the Boussinesq or small density approximation, which assumes that $\rho = \rho_o$ everywhere except in the buoyancy term. It can be shown that ρ is principally a function of temperature, T. As a result, the assumption $\frac{\rho_o - \rho}{\rho_o} = \frac{T - T_o}{T_o}$ is developed.

3.3 Conservation Equations

The conservation equations for continuity, momentum and energy were developed through a conservation of mass, force and energy in a control volume. That is, we define a differential control volume; identify the relevant mass, energy and force transfer processes; and introduce the appropriate physical equations [30]. Because changes in the vertical direction are generally much smaller than changes in the horizontal r or y directions, for the axisymmetric and infinite line sources respectively, terms containing $\partial/\partial z$ are ignored compared to those containing $\delta/\partial r$ or $\delta/\partial y$. This is a consequence of the far field assumption that plume height is generally much greater than plume width. In addition, changes in the x direction are ignored for the infinite line because this direction is more or less diminished by the assumption that the length is infinitely longer than the width. (The x-axis is taken along the length of the source and the y-axis is taken across the width.) A similar assumption is often used in heat transfer problems where the temperature is assumed constant along the axis of a "long" cylinder in a heat conduction problem. Thus a 3-D problem can be simplified to a 2-D problem.

As a result of integrating the equations with respect to y or r, the laminar and turbulent stress terms and heat conduction flux terms drop out of the problem. The turbulent nature of the flow is embodied only in the entrainment term of the integrated mass and energy equations.

3.3.1 Line Source

The conservation equations for an infinite line buoyant plume are as follows:

Continuity:

$$\frac{\partial w}{\partial z}+\frac{\partial v}{\partial y}=0$$

Momentum:

$$\rho_0\left(v\frac{\partial w}{\partial y}+w\frac{\partial w}{\partial z}\right)=g\rho_o\left(\frac{T-T_o}{T_o}\right)+\frac{\partial \tau}{\partial y}$$

Energy:

$$\frac{\dot{Q}'(1-\chi_r)}{2}=\int_0^\infty \rho_o c_p w (T-T_o)dy$$

or

$$\rho_o c_p\left(v\frac{\partial T}{\partial y}+w\frac{\partial T}{\partial z}\right)=\dot{q}'''(1-X_r)-\frac{\partial \dot{q}''_y}{\partial y} \text{ (for combusting region)}$$

where $\dot{Q}'=\dot{m}'_f\Delta H_c$

with:
χ_r = The fraction of combustion energy radiated away
$\dot{m}'_f$ = The rate of fuel mass supply per unit length
ΔH_c = The effective heat of combustion

3.3.2 Axisymmetric Source

The conservation equations for an axisymmetric buoyant plume are as follows:

Continuity:
$$\frac{1}{r}\frac{\partial}{\partial r}(rv)+\frac{\partial w}{\partial z}=0$$

Momentum:
$$\rho_0\left(v\frac{\partial w}{\partial r}+w\frac{\partial w}{\partial z}\right)=g\rho_o\left(\frac{T-T_o}{T_o}\right)+\frac{1}{r}\frac{\partial(r\tau_{rz})}{\partial r}$$

Energy:
$$\frac{\dot{Q}(1-\chi_r)}{2\pi}=\int_0^\infty \rho_o c_p r w(T-T_o)dr$$

or

$$\rho_o c_p\left(v\frac{\partial T}{\partial r}+w\frac{\partial T}{\partial z}\right)=\dot{q}'''(1-\mathrm{X}_r)-\frac{1}{r}\frac{\partial(r\dot{q}''_r)}{\partial r}\quad\text{(for combusting region)}$$

where $\dot{Q}=\dot{m}_f\Delta H_c$
with
χ_r = The fraction of combustion energy radiated away
$\dot{m}_f$ = The rate of fuel mass supply
ΔH_c = The effective heat of combustion

3.4 Far Field Theory for the Infinite Line, $z>z_{fl}$ (Temperature, Velocity, Plume Width)

The above equations can be written in an integral form by integrating the continuity and momentum equations over y from 0 to ∞. Where 0 corresponds to the centerline of the plume and ∞ physically represents the end of the domain of the plume or its outer radius. Upon performing these integrations, the stress term drops out of the momentum equation. At the plume center-line, y = 0, the stress term drops out because the velocity gradient equals zero, $\frac{\partial w}{\partial y} = 0$. The stress term also equals zero at the plume boundary, y = ∞, because the ambient fluid has no shear effects on the plume in the vertical direction as velocity, w, equals zero. Thus the equations have been reduced from partial differential equations to ordinary differential equations.

Continuity:
$$2\frac{d}{dz}\int_0^\infty \rho_o w dy = \frac{d\dot{m}'_e}{dz} = -2\rho_o \lim_{y\to\infty}(v) \qquad (1)$$

Momentum:
$$\frac{d}{dz}\int_0^\infty w^2 dy = \frac{g}{T_o}\int_0^\infty (T - T_o)dy \qquad (2)$$

Energy:
$$\frac{\dot{Q}'(1-\chi_r)}{2} = \rho_o c_p \int_o^\infty w(T - T_o)dy \qquad (3)$$

We assume Gaussian profiles for temperature difference, ΔT, and vertical velocity, w, in the y- direction:

$$\frac{w(y,z)}{w_m(z)} = \exp\left[-\left(\frac{y^2}{b^2}\right)\right] \qquad (4)$$

$$\frac{T - T_o}{T_m - T_o} = \exp\left[-\beta\left(\frac{y^2}{b^2}\right)\right] \qquad (5)$$

The entrainment assumption follows that proposed by Morton, Taylor, and Turner [22].

$$\lim(-v)_{y\to\infty} = \alpha w_m \qquad (6)$$

Where α is an empirical constant.

Using our Gaussian profiles, (4) and (5), in conjunction with the relationship $\int_0^\infty e^{-x^2}dx = \frac{\sqrt{\pi}}{2}$ and the substitution x = y/b the integrals in the above differential equations, (1), (2), (3), can be solved as follows:

(a)
$$\int_o^\infty w\,dy = \int_0^\infty w_m e^{-y^2/b^2} dy = b\int_0^\infty w_m e^{-x^2} dx = \frac{\sqrt{\pi}}{2} w_m b$$

(b)
$$\int_o^\infty w^2 dy = w_m^2 \int_o^\infty e^{-2\left(y^2/b^2\right)} dy = b w_m^2 \int_o^\infty e^{-2x^2} dx = \frac{\sqrt{\pi}}{2\sqrt{2}} w_m^2 b$$

(c)
$$\int_o^\infty w(T - T_o)dy = w_m(T_m - T_o)\int_o^\infty e^{-(1+\beta)y^2/b^2} dy \frac{\sqrt{1+\beta}}{b}\cdot\frac{b}{\sqrt{1+\beta}}$$
$$= \frac{\sqrt{\pi}}{2\sqrt{1+\beta}} w_m(T_m - T_o)b$$

(d)
$$\int_o^\infty (T - T_o)dy = (T_m - T_o)\int_0^\infty e^{-\beta\left(y^2/b^2\right)} dy \frac{\sqrt{\beta}}{b}\cdot\frac{b}{\sqrt{\beta}}$$
$$= \frac{(T_m - T_o)b\sqrt{\pi}}{2\sqrt{\beta}}$$

Substituting the solutions of these integrals back into their respective differential equations yields:

$$\frac{d}{dz}(w_m b) = \frac{2}{\sqrt{\pi}} \alpha w_m$$
$$\frac{d}{dz}\left(w_m{}^2 b\right) = \frac{2\sqrt{2}}{\sqrt{\cancel{\pi}}}\cdot\frac{g}{T_o}\cdot\frac{\sqrt{\cancel{\pi}}}{2\sqrt{\beta}}\cdot(T_m - T_o)b = \sqrt{\frac{2}{\beta}}\frac{g(T_m - T_o)b}{T_o}$$
$$\frac{\dot{Q}'(1-\chi_r)}{2} = \rho_o c_p \frac{\sqrt{\pi}}{2\sqrt{1+\beta}} w_m (T_m - T_o)b$$

Next make the equations dimensionless through the following terms:

$$
\begin{aligned}
\Phi &= \frac{T_m - T_o}{T_o} \\
B &= \frac{b}{Z^{**}} \\
\zeta &= \frac{z}{Z^{**}} \\
W &= \frac{w_m}{\sqrt{gZ^{**}}} \\
Z^{**} &= \left(\frac{\dot{Q}'}{\rho_o T_o c_p \sqrt{g}} \right)^{2/3}
\end{aligned}
\qquad (7)
$$

(Note- The derivation of Z** follows as the equations are made dimensionless and a "natural length" scale is sought since none exists for the point or line source.)

$$
\begin{gathered}
\frac{d}{d\zeta}(WB) = \frac{2\alpha}{\sqrt{\pi}} W \\
(gl_o)\frac{d}{d\zeta}\left(W^2 B\right) = \sqrt{\frac{2}{\beta}}(gl_o)\Phi B \\
\dot{Q}'(1-\chi_r) = \rho_o c_p \sqrt{\frac{\pi}{\beta+1}}\sqrt{gl_o}\, W\Phi T_o B l_o \\
or \\
\frac{\dot{Q}'(1-\chi_r)}{\rho_o c_p T_o \sqrt{g} l_o^{3/2}} = \sqrt{\frac{\pi}{\beta+1}} W\Phi B
\end{gathered}
$$

Let the LHS = 1 = $\dfrac{\dot{Q}'}{\rho_o c_p T_o \sqrt{g} l_o^{3/2}}$ in order to select the most useful value to l_o. Set l_o

equal to Z** through the following relation: $l_o = Z^{**} = \left(\dfrac{\dot{Q}'}{\rho_o c_p T_o \sqrt{g}} \right)^{2/3}$

Solve the following simplified equations a by power series:

$$\frac{d}{d\zeta}(WB)=\frac{2\alpha}{\sqrt{\pi}}W \tag{8}$$

$$\frac{d}{d\zeta}\left(W^2B\right)=\frac{\sqrt{2}}{\sqrt{\beta}}\Phi B \tag{9}$$

$$(1-\chi_r)=\sqrt{\frac{\pi}{\beta+1}}W\Phi B \tag{10}$$

Using the following assignments:

$$\begin{aligned} B &= C_l\zeta^n \\ W &= C_v\zeta^m \\ \Phi &= C_T\zeta^P \end{aligned} \tag{11}$$

After solving for the constants and powers the equations can be written:

$$B=\left(\frac{2\alpha}{\sqrt{\pi}}\right)\zeta \tag{12}$$

$$W=\left(\frac{\beta+1}{2\beta}\right)^{1/6}\alpha^{-1/3}(1-\chi_r)^{1/3} \tag{13}$$

$$\Phi=\left[\frac{(\beta+1)^{1/3}\beta^{1/6}(1-\chi_r)^{2/3}}{2^{5/6}\alpha^{2/3}}\right]\zeta^{-1} \tag{14}$$

These constants will be determined empirically along with α and β in section 4.4 using two experimental inputs for temperature and velocity respectively.

3.4.1 Entrainment

Entrainment in the smoke plume can be computed from equation (1):

$$2\rho_o\frac{d}{dz}\int_0^\infty w\,dy=\frac{d\dot{m}'_e}{dz}$$

Recall that solution of the integral, (a) on page 8, yields:

$$\int_0^\infty w\,dy=\frac{\sqrt{\pi}}{2}w_m b$$

Substituting:

$$\sqrt{\pi}\,\rho_o \frac{d}{dz}\left(w_m b\right) = \frac{d\dot{m}'_e}{dz}$$

Integrating:

$$\sqrt{\pi}\,\rho_o w_m b = \dot{m}'_e \tag{15}$$

Insert dimensionless terms, (7):

$$\begin{aligned}\dot{m}'_e &= \sqrt{\pi}\,\rho_o w_m b\\ &= \sqrt{\pi}\,\rho_o W \sqrt{gZ^{**}}\,BZ^{**}\\ &= \sqrt{\pi}\,\rho_o C_v \sqrt{gZ^{**}}\,C_l \frac{z}{Z^{**}} Z^{**}\end{aligned}$$

Rearrange terms to make the equation dimensionless:

$$\frac{\dot{m}'_e}{\rho_o\sqrt{gz}\,z} = \sqrt{\pi}\,C_v C_l \left(\frac{Z^{**}}{z}\right)^{1/2}$$

$$-\,or\,-$$

$$\frac{\dot{m}'_e}{\rho_o\sqrt{gz}\,z} = \sqrt{\pi}\,C_v C_l \left(Q_z^{**}\right)^{1/3} \tag{16}$$

$$Where\ Q_z^{**} = \left(\frac{Z^{**}}{z}\right)^{3/2} = \left(\frac{\dot{Q}'}{\rho_o c_p T_o \sqrt{gz}}\right)^{3/2}$$

Empirical correlations have not been developed for equation (16) because we found no entrainment data other than that of Cox [9].

3.5 Far Field Theory for the Axisymmetric Source, $z>z_{fl}$ (Temperature, Velocity, Plume Width)

The conservation equations for an axisymmetric buoyant plume can be written in an integral form by multiplying each equation by r and integrating over r from 0 to ∞.

Continuity: $$2\pi\rho_o \frac{d}{dz}\int_0^\infty rw\,dr = \frac{d\dot{m}_e}{dz} = -2\pi\rho_o \lim_{r\to\infty}(rv) \tag{17}$$

Momentum: $$\frac{d}{dz}\int_0^\infty rw^2 dr = \frac{g}{T_o}\int_0^\infty r(T-T_o)dr \tag{18}$$

Energy: $$\frac{\dot{Q}(1-\chi_r)}{2\pi} = \rho_o c_p \int_0^\infty rw(T-T_o)dr \tag{19}$$

Gaussian profiles for vertical velocity, w, and temperature difference, ΔT, in the r - direction are as follows:

$$\frac{w(r,z)}{w_m(z)} = \exp\left[-\left(\frac{r^2}{b^2}\right)\right] \tag{20}$$

$$\frac{T-T_o}{T_m-T_o} = \exp\left[-\beta\left(\frac{r^2}{b^2}\right)\right] \tag{21}$$

The entrainment coefficient, α, is defined by:

$$-\lim_{r\to\infty}(rv) = \alpha w_m b \tag{22}$$

Using our Gaussian profiles, (20) and (21), in conjunction with the relationship $\int_0^\infty xe^{-x^2}dx = \frac{1}{2}$ and the substitution x = r/b the integrals in the above differential equations, (17), (18), (19), can be solved as follows:

(e) $$\int_o^\infty rw\,dr = w_m b^2 \int_0^\infty xe^{-x^2}dx = \frac{1}{2}w_m b^2$$

(f) $$\int_o^{\infty} r w^2 dr = b^2 w_m^2 \int_o^{\infty} x e^{-2x^2} dx = \frac{w_m^2 b^2}{4}$$

(g) $$\int_o^{\infty} r (T - T_o) dr = b^2 (T_m - T_o) \int_o^{\infty} x e^{-\beta x^2} dx = \frac{(T_m - T_o) b^2}{2\beta}$$

(h) $$\int_o^{\infty} r w (T - T_o) dr = (T_m - T_o) w_m b^2 \int_0^{\infty} x e^{-(\beta+1)x^2} dx = \frac{(T_m - T_o) w_m b^2}{2(\beta + 1)}$$

Substitute the solutions of these integrals back into their respective differential equations:

$$\frac{d}{dz}\left(w_m b^2\right) = 2\alpha w_m b$$

$$\frac{d}{dz}\left(w_m^2 b^2\right) = \frac{2}{\beta} \frac{g (T_m - T_o) b^2}{T_o}$$

$$\frac{(T_m - T_o) w_m b^2}{(\beta + 1)} = \frac{\dot{Q}(1 - \chi_r)}{\pi \rho_o c_p}$$

Next make the equations dimensionless through the following terms:

$$\Phi = \frac{T_m - T_o}{T_o}$$

$$B = \frac{b}{Z^*}$$

$$\zeta = \frac{z}{Z^*} \qquad (23)$$

$$W = \frac{w_m}{\sqrt{g Z^*}}$$

$$Z^* = \left(\frac{\dot{Q}}{\rho_o T_o c_p \sqrt{g}} \right)^{2/5}$$

Inserting these dimensionless terms into the above equations and simplifying yields:

$$\frac{d}{d\zeta}\left(WB^2\right)=2\alpha WB \tag{24}$$

$$\frac{d}{d\zeta}\left(W^2B^2\right)=\frac{2}{\beta}\Phi B \tag{25}$$

$$\left(1-\chi_r\right)=\frac{\pi}{\beta+1}W\Phi B^2 \tag{26}$$

Solving these dimensionless equations with the same assignments, (11), from section 3.4.1 yields:

$$B=\left(\frac{6}{5}\alpha\right)\zeta \tag{27}$$

$$W=\left[\left(\frac{25}{24\pi}\right)^{1/3}\left(\frac{\beta+1}{\beta}\right)^{1/3}\alpha^{-2/3}\left(1-\chi_r\right)^{1/3}\right]\zeta^{-1/3} \tag{28}$$

$$\Phi=\left[\frac{2}{3}\left(\frac{25}{26\pi}\right)^{2/3}\beta^{1/3}\left(\beta+1\right)^{2/3}\alpha^{-4/3}\left(1-\chi_r\right)^{2/3}\right]\zeta^{-5/3} \tag{29}$$

Due to the large amounts of axisymmetric data and relative acceptance of previous correlations, comparisons of our correlations in equations (27) – (29) have not been made against any of these data. We rely on the data of Yokoi [3]. It can be shown that $\frac{W^2}{\Phi\zeta}=\frac{(3/2)}{\beta}$, is constant throughout the plume. First, $C_T = 9.115$ and $C_v = 3.87$ from Yokoi [3]. β, α and C_l are then determined through a similar process presented for the infinite line in section 4.4.

α = 0.098
β =0.913
C_l =0.118

Zukoski details a better explanation of the operation in "Properties of Fire Plumes" pgs. (119-121) [10]. However, our values for α and C_l differ slightly from his because we incorporated a 20 % radiation loss into the equations to correct for losses from his alcohol data, whereas he did not.

3.5.1 Entrainment

Entrainment in the smoke plume can be calculated from equation (17).

$$2\pi\rho_o \frac{d}{dz}\int_0^\infty rwdr = \frac{d\dot{m}_e}{dz}$$

Solving the integral yields:

$$\int_0^\infty rwdr = \frac{1}{2}w_m b^2$$

Substituting:

$$\pi\rho_o \frac{d}{dz}\left(w_m b^2\right) = \frac{d\dot{m}_e}{dz}$$

Elimination of derivatives gives:

$$\pi\rho_o w_m b^2 = \dot{m}_e \qquad (30)$$

Insert dimensionless terms:

$$\begin{aligned}\dot{m}_e &= \pi\rho_o w_m b^2 \\ &= \pi\rho_o W\sqrt{gZ^*}B^2 Z^{*2} \\ &= \pi\rho_o C_v \zeta^{-1/3}\sqrt{gZ^*}C_l^2\zeta^2 Z^{*2} \\ &= \pi\rho_o C_v C_l^2\sqrt{gz}\zeta^{-5/6}z^2\end{aligned}$$

Make the equation dimensionless:

$$\frac{\dot{m}_e}{\rho_o\sqrt{gz}z^2} = \pi C_v C_l^2 \zeta^{-5/6}$$

$$-or-$$

$$\frac{\dot{m}_e}{\rho_o\sqrt{gz}z^2} = \pi C_v C_l^2 Q_z^{*1/3} \qquad (31)$$

$$Where\ Q_z^* = \zeta^{-5/2} = \left(\frac{Z^*}{z}\right)^{5/2} = \left(\frac{\dot{Q}}{\rho_o c_p T_o \sqrt{g}z}\right)^{5/2}$$

Zukoski [20] found $\pi C_v C_l^2 = 0.21$; we found a slightly lower value due to the addition of a 20 % radiation loss.

3.6 Far Field Summary

The following table serves as both a summary and comparison of the theoretical correlations developed for the infinite line and the axisymmetric source.

Table 2: Far Field Summary

Dimensionless Variable	Axisymmetric	Infinite Line
B	$\left(\frac{6}{5}\alpha\right)\zeta$	$\left(\frac{2}{\sqrt{\pi}}\alpha\right)\zeta$
W	$\left[\left(\frac{25}{24\pi}\right)\left(\frac{\beta+1}{\beta}\right)\alpha^{-2}(1-\chi_r)\right]^{1/3}\zeta^{-1/3}$	$\left[\left(\frac{\beta+1}{2\beta}\right)^{1/6}\alpha^{-1/3}(1-\chi_r)^{1/3}\right]$
Φ	$\left[\frac{2}{3}\left(\frac{25}{24\pi}\right)^{2/3}\frac{(\beta+1)^{2/3}}{\beta^{-1/3}\alpha^{4/3}}(1-\chi_r)^{2/3}\right]\zeta^{-5/3}$	$\left[\frac{(\beta+1)^{1/3}}{2^{5/6}\beta^{-1/6}}\alpha^{-2/3}(1-\chi_r)^{2/3}\right]\zeta^{-1}$
Z**/Z*	$\left(\frac{\dot{Q}}{\rho_o c_p T_o \sqrt{g}}\right)^{2/5}$	$\left(\frac{\dot{Q}'}{\rho_o c_p T_o \sqrt{g}}\right)^{2/3}$
ζ	$\frac{z}{Z^*}$	$\frac{z}{Z^{**}}$
$\frac{W^2}{\Phi\zeta}$	$\frac{3}{2}\beta$	$\sqrt{\frac{2}{\beta}}$

3.7 Combusting Plume Region, $0 \le z \le z_{fl}$
(Temperature, Velocity, Plume Width)

The analysis of the combusting plume region is analogous to that of the non-combusting plume region presented earlier. The analysis resembles that performed by Steward [6] except fuel mass and momentum effects will be ignored.

It can be shown, for a constant density Boussinesq model, that the mass and momentum equations are identical to (1) and (2) for the infinite line and (17) and (18) for the axisymmetric model. However, the energy equations for both geometries change in this region.

The equations for the far field assume that all of the energy is released at a single point or line at the fire source. Whereas the energy equations in the combustion zone assume that the energy is released evenly throughout this zone and that entrained air mixes with the fuel and burns to stoichiometric completion instantaneously [6].

3.7.1 Infinite Line

Partial differential energy equation:

$$\rho_o c_p\left(v\frac{\partial T}{\partial y}+w\frac{\partial T}{\partial z}\right)=\dot{q}'''(1-X_r)-\frac{\partial \dot{q}''_y}{\partial y}$$

It can also be shown that the energy equation in partial differential format can be changed into an ordinary differential equation in three steps. First, expand the two terms on the LHS of the equation into four terms. Two of the expanded terms then cancel through the continuity of mass equation. Finally, integrate with respect to (y) yielding:

$$\rho_o c_p \frac{d}{dz}\int_0^\infty w(T-T_0)dy=(1-\chi_r)\int_0^\infty \dot{q}'''dy \tag{32}$$

As was the case with the shear force term in the momentum equation, the heat conduction term also drops out after integrating. At the plume boundary, $y \to \infty$, the temperature of the plume has decayed to ambient, thus no heat can transfer. At the plume centerline, y = 0, where temperature is at a maximum, the temperature gradient is zero, $\frac{\partial T}{\partial y} = 0$. Thus, heat transfer through conduction is impossible.

The energy release rate per unit volume integral, $\int_0^\infty \dot{q}'''dy$, can be related to the flux of entrained air through:

$$\int_0^\infty \dot{q}'''dy = \frac{1}{2}\left(\frac{\Delta H_c}{s}\right)\frac{d\dot{m}'_e}{dz} \tag{33}$$

$\dot{m}'_e$ = total rate of entraind air per unit length, l

s = mass of air required to react with a unit mass of fuel

However, due to incomplete mixing, s does not represent the ideal stoichiometric ratio. The actual air to fuel ratio is represented as ns, however temporarily n will not be shown explicitly but will be absorbed into s.

$$n = \frac{\text{actual air entrained}}{\text{mass of air reacted}}$$

Through an overall mass balance $\dot{m}'_e$, found in the energy release rate per unit volume equation, (33), can be related to density, ρ, and vertical center line velocity w.

$$2\cdot\int_{o}^{\infty}\rho w dy = \dot{m}'_e + \dot{m}'_f \tag{34}$$

$$-\,or\,-$$

$$2\cdot\frac{d}{dz}\int_{o}^{\infty}\rho w dy = 2\rho_o \alpha w_m = \frac{d\dot{m}'_e}{dz} + \frac{d\dot{m}'_f}{dz} = \left(1+\frac{1}{s}\right)\frac{d\dot{m}'_e}{dz}$$

$\dot{m}'_f$ = the total rate of fuel flow per unit length l

(Note- the integral in both of the above equations is multiplied by 2 to account for mass flow through the entire width of the plume.)

Next solve for $\frac{d\dot{m}'_e}{dz}$ in the above equation so that it may be substituted into equation (33).

$$\frac{d\dot{m}'_e}{dz} = 2\left(\frac{s}{s+1}\right)\frac{d}{dz}\int_{0}^{\infty}\rho_o w dy = 2\left(\frac{s}{s+1}\right)\rho_o \alpha w_m$$

Since s is usually large s/s+1 ≅1. Therefore substituting into equation (33):

$$\int_{0}^{\infty}\dot{q}''' dy = \frac{1}{2}\left(\frac{\Delta H_c}{ns}\right)2\rho_o \alpha w_m = \frac{\rho_o \alpha(\Delta H_a)}{n} w_m$$

$\frac{\Delta H_c}{s} = \Delta H_a$, the heat of combustion per unit mass of air reacted

$\Delta H_a \approx 13.1\frac{kJ}{g_{O_2}} x0.233\frac{g_{O_2}}{g_{air}} = 3.05\frac{kJ}{g_{air}}$, for most hydrocarbon fuels

The full energy equation (32) can now be written:

$$\frac{d}{dz}\int_0^\infty w(T-T_o)dy = \frac{(1-\chi_r)\Delta H_a}{nc_p\rho_o}\rho_o\alpha w_m$$

$$-or-$$

$$\frac{d}{dz}\int_0^\infty w\left(\frac{T-T_o}{T_o}\right)dy = \frac{(1-\chi_r)\Delta H_a}{nc_pT_o}\alpha w_m = \frac{\Psi}{n}\alpha w_m = \frac{\Psi}{n}\frac{d}{dz}\int_0^\infty wdy \qquad (35)$$

$$\text{Where } \Psi = \frac{(1-\chi_r)\Delta H_a}{c_pT_o}$$

Note, through the continuity equation, (1): $\Psi\alpha w_m = \Psi\frac{d}{dz}\int_0^\infty wdy$

The integral on the LHS of the equation is now solved arbitrarily assuming Gaussian profiles for temperature and velocity. However, in the combusting region, β is assumed equal to one, (β=1), since there is not enough data on the temperature and velocity profiles in this region to justify any other value.

Hence:

$$\frac{w}{w_m} = \frac{T-T_o}{T-T_m} = \exp\left(-y^2/b^2\right) \qquad (36)$$

Substitute the Gaussian profiles:

$$\int_0^\infty w(T-T_o)dy = w_m(T_m-T_o)\int_0^\infty e^{-2y^2/b^2}dy = \frac{\sqrt{\pi}}{2\sqrt{2}}bw_m(T_m-T_o)$$

Note, we have substitued x = y/b and used the relation $\int_0^\infty e^{-2x^2/b^2} = \frac{\sqrt{\pi}}{2\sqrt{2}}$

The integration of, (a), $\int_0^\infty wdy$ was shown to equal $\frac{\sqrt{\pi}}{2}w_mb$ in section 3.4, (Far Field Theory for the Infinite Line), and will not be shown here.

From equation (35):

$$\frac{\sqrt{\pi}}{2\sqrt{2}}\frac{d}{dz}\left[\frac{w_m(T_m-T_o)}{T_o}b\right] = \Psi\alpha w_m = \Psi\frac{d}{dz}\left(\frac{\sqrt{\pi}}{2}w_mb\right)$$

Make the energy equation dimensionless using the same variables presented in section 3.4, (7):

$$\frac{\sqrt{\pi}}{2\sqrt{2}}\sqrt{gZ^{**}}\left(\frac{1}{Z^{**}}\right)\frac{d}{d\zeta}(W\Phi B)Z^{**} = \Psi\alpha\sqrt{gZ^{**}}W = \Psi\frac{\sqrt{\pi}}{2}\sqrt{gZ^{**}}\frac{d}{d\zeta}(WB)$$

$$-or-$$

$$\frac{\sqrt{\pi}}{2\sqrt{2}}\frac{d}{d\zeta}(W\Phi B) = \Psi\alpha W = \Psi\frac{\sqrt{\pi}}{2}\frac{d}{d\zeta}(WB)$$

The energy equation is now in dimensionless format and can be placed with the dimensionless continuity and momentum equations (8) and (9) respectively.

$$\begin{aligned} \frac{d}{d\zeta}(WB) &= \frac{2\alpha}{\sqrt{\pi}}W && \text{(a)} \\ \frac{d}{d\zeta}(W^2B) &= \frac{\sqrt{2}}{1}\Phi B && \text{(b)} \qquad (37) \\ \frac{d}{d\zeta}(W\Phi B) &= \sqrt{2}\Psi\frac{d}{d\zeta}(WB) && \text{(c)} \end{aligned}$$

From 37 (c) integrating with WB = 0 at $\zeta = 0$:

$$W\Phi\mathrm{B} = \sqrt{2}\Psi WB$$

$$-or-$$

$$\Phi = \sqrt{2}\Psi$$

Plume width, B, and velocity, W, are solved for through the continuity and momentum equations by a power series as in the far field region, section 3.4, presented before. The assignments for these two conservation equations remains the same:

$$\begin{aligned} B &= C_l\zeta^n \\ W &= C_v\zeta^m \end{aligned} \qquad (11)$$

After solving for the constants and powers the equations can be written:

$$B = \left(\frac{4\alpha}{3\sqrt{\pi}}\right)\zeta \qquad (38)$$

$$W = \sqrt{\Psi}\zeta^{1/2} \qquad (39)$$

$$\Phi = \sqrt{2}\Psi \qquad (40)$$

Empirically derived coefficients are addressed in section 4.5. The above are theoretical. The constant entrainment coefficient, α, is not justified, but we will see how well it does in fitting the above data.

3.7.2 Axisymmetric Source

Partial differential energy equation:

$$\rho_o c_p\left(v\frac{\partial T}{\partial r} + w\frac{\partial T}{\partial z}\right) = \dot{q}'''(1-\mathrm{X}_r) - \frac{1}{r}\frac{\partial(r\dot{q}''_r)}{\partial r}$$

As was the case with the infinite line, section 3.7.1, the above partial differential energy equation can be converted into an ordinary differential equation.

$$\rho_o c_p \frac{d}{dz}\int_0^\infty rw(T-T_0)dr = (1-\chi_r)\int_0^\infty \dot{q}'''rdr \qquad (41)$$

The energy release rate per unit volume integral, $\int_0^\infty \dot{q}'''rdr$, can be related to the flux of entrained air as:

$$\int_0^\infty \dot{q}'''rdr = \frac{1}{2\pi}\left(\frac{\Delta H_c}{s}\right)\frac{d\dot{m}_e}{dz} \qquad (42)$$

$\dot{m}_e$ = total rate of entrained air

Where s represents only the stoichiometric air to fuel ratio. As before, the actual air to fuel ratio is modeled through sn. Also recall that n is absorbed into s.

Through an overall mass balance, assuming $\dot{m}_f$ is negligible compared to $\dot{m}_e$, it can be shown that the mass rate of entrainment at z is equal to the mass flow rate in the plume at z.

Note- $\dot{m}_f$ could have been shown to be negligible through the $\frac{s}{s+1} \cong 1$ argument presented above.

$$\frac{d\dot{m}_e}{dz} = 2\pi \frac{d}{dz}\int_0^\infty \rho_o wrdr = 2\pi\rho_o \alpha w_m b$$

Recall that $\frac{d}{dz}\int_0^\infty rwdr = \alpha w_m b$ from the continuity of mass equation, (17), found in section 3.5.

Next, substitute $\frac{d\dot{m}_e}{dz}$ into equation (42):

$$\int_0^\infty \dot{q}'''rdr = \frac{1}{2\pi}\left(\frac{\Delta H_c}{s}\right)2\pi\rho_o \alpha w_m b = \rho_o \alpha w_m b \Delta H_a$$

The full energy equation, (41), can now be written:

$$\frac{d}{dz}\int_0^\infty rw(T - T_o)dr = \frac{(1-\chi_r)\Delta H_a}{c_p \rho_o}\rho \alpha w_m b$$

$$-or-$$

$$\frac{d}{dz}\int_0^\infty rw\left(\frac{T - T_o}{T_o}\right)dr = \frac{(1-\chi_r)\Delta H_a}{c_p T_o}\alpha w_m b = \Psi \alpha w_m b = \Psi \frac{d}{dz}\int_0^\infty rwdr \qquad (43)$$

$$where\ \Psi = \frac{(1-\chi_r)\Delta H_a}{c_p T_o}$$

Recalling that $\beta = 1$ in the combustion zone, the Gaussian profiles for temperature and velocity are as follows:

$$\frac{w}{w_m} = \frac{T - T_o}{T - T_m} = \exp\left(-r^2/b^2\right) \qquad (44)$$

Substitute the Gaussian profiles:

$$\int_0^\infty rw(T-T_o)dr = b^2 w_m (T_m - T_o)\int_0^\infty xe^{-2(x^2)}dx = \frac{b^2 w_m (T_m - T_o)}{4}$$

Note- we have substituted x = r/b.

The integration of $\int_0^\infty wrdr$ was shown to equal $\frac{w_m b^2}{2}$ in section 3.5, (Far Field Theory for the Axisymmetric Source), and will not be shown here.

From equation (43):

$$\frac{1}{4}\frac{d}{dz}\left[\frac{w_m (T_m - T_o)b^2}{T_o}\right] = \Psi \alpha w_m b = \Psi \frac{d}{dz}\left(\frac{w_m b^2}{2}\right)$$

Make the energy equation dimensionless using the same variables presented in section 3.5, equation (23):

$$Z^{*2}\frac{1}{4}\sqrt{gZ^*}\left(\frac{1}{Z^*}\right)\frac{d}{d\zeta}\left(W\Phi B^2\right) = \Psi \alpha \sqrt{gZ^*}WBZ^* = \frac{1}{2}\Psi\sqrt{gZ^*}\frac{1}{Z^*}\frac{d}{d\zeta}\left(WB^2\right)Z^{*2}$$

$$-or-$$

$$\frac{d}{d\zeta}\left(W\Phi B^2\right) = 4\Psi \alpha WB = 2\Psi \frac{d}{d\zeta}\left(WB^2\right)$$

The energy equation is now in dimensionless format and can be placed with the dimensionless continuity and momentum equations (24) and (25) respectively.

$$\frac{d}{d\zeta}(WB^2) = 2\alpha W\mathbf{B} \qquad \text{(a)}$$

$$\frac{d}{d\zeta}(W^2B^2) = \frac{2}{\beta}\Phi B \qquad \text{(b)} \qquad (45)$$

$$\frac{d}{d\zeta}(W\Phi B^2) = 2\Psi\frac{d}{d\zeta}(WB^2) \qquad \text{(c)}$$

Temperature,Φ, is solved for by integrating and canceling like terms as in section 3.7.1:

$$W\Phi B^2 = 2\Psi W B^2$$

$$-\,or\,-$$

$$\Phi = 2\Psi$$

The process for finding plume width, B, and velocity, W, was outlined in section 3.7.1 and remains the same for the axisymmetric source. The solutions for the equations are as follows:

$$B = \frac{4}{5}\alpha\zeta \tag{46}$$

$$W = \sqrt{\frac{4}{3}\Psi}\zeta^{1/2} \tag{47}$$

$$\Phi = 2\Psi \tag{48}$$

For the same reasons presented in section 3.5, empirical correlations for temperature and velocity are given at this time.

The temperature equation, (48), in empirical format:

$$\Phi = C_{T_f}\Psi$$

McCaffrey [33] burned methane on 0.3 m square porous burners and found that temperature in the flame zone was a steady 800 °C. Using this value for temperature and solving for Ψ, C_{Tf} can be found easily.

$$\Phi = \frac{\Delta T}{T_o} = \frac{800K}{293K} = 2.73$$

$$\Psi = \frac{(1-\chi_r)\Delta H_a}{c_p T_o} = \frac{(1-.20)2{,}910}{1.01(293)} = 7.87$$

Note that a value of 20 % was used for the radiation fraction. McCaffrey [18] also performed extensive radiation experiments on these burners and found that χ_r varies from 10 % to 24%. These experiments are discussed in greater detail in sec. 4.6.

$$C_{T_f} = \frac{2.73}{7.87} = 0.347$$
$$\Phi = 0.347\Psi$$
$$-or-$$
$$\Phi = 0.434(1-\chi_r)\Psi$$

The empirical correlation for velocity is also solved from the same data set. The velocity equation in empirical format:

$$W = C_{v_f}\zeta^{1/2}$$

Choosing one representative point and changing the data presented by McCaffrey [18] into our format yields:

$$v = 1.70 \, {}^{m}\!/_{s}$$
$$z = 0.0726m$$
$$Z^* = 0.175m$$
$$\zeta = \frac{z}{Z^*} = 0.414$$

Next solve for W and Ψ:

$$W = \frac{v}{\sqrt{gZ^*}} = \frac{1.70}{\sqrt{9.81 \cdot 0.175}} = 1.30$$
$$\Psi = 7.87 \text{ (from before)}$$

Thus:

$$C_{v_f} = \frac{W}{\sqrt{\Psi\zeta}} = \frac{1.30}{\sqrt{7.87\cdot 0.414}} = 0.720$$

$$W = 0.720\zeta^{1/2}$$

$$-\mathit{or}-$$

$$W = 0.805(1-\chi_r)^{1/2}\zeta^{1/2}$$

3.8 Summary of Near Field Results

Table 3: Near Field Summary

Dimensionless Variable	Axisymmetric	Infinite Line
B	$\frac{4}{5}\alpha\zeta$	$\left(\frac{4\alpha}{3\sqrt{\pi}}\right)\zeta$
W	$\sqrt{\frac{4}{3}\Psi}\zeta^{1/2}$	$\sqrt{\Psi}\zeta^{1/2}$
Φ	2Ψ	$\sqrt{2}\Psi$

3.9 Entrainment in the Combustion Zone, $0 \le z \le Z_{fl}$

The same basic equations for entrainment in the far field, found from the continuity equations, can be used in our analysis of entrainment in the near field or combustion zone. The main difference between these two analyses is the inclusion of geometry effects in the combustion zone. Recall from section 2.3, (Methodology), that both near field entrainment and flame height are developed through an iterative process where "point source" solutions are modified to incorporate geometry effects.

In the far field, the role of geometry is secondary to the energy release rate which dominates all processes. However, close to the fire source and in the flame both the source geometry and energy release rate play an important role and need to be considered.

The inclusion or exclusion of geometry effects is achieved through the plume width term, b, found in the generic entrainment equation. In the far field, the solution of plume width in the form, $C_l\zeta^n$, is substituted into the mass entrainment equation. This solution only takes into account the change in plume width with height. There are no diameter or width effects inherent to this solution. Thus none are included in the far field entrainment correlation. However, source effects are inserted into plume width, b, in the near field through a term which includes the change in plume width with height, used in the far field solution, and the sources initial width or diameter; $b = b_o + C_l\zeta^n$. Where b_o is either D/2 (axisymmetric radius) or D/2 (line half width).

3.9.1 Line Source

Basic entrainment equation:

$$\dot{m}'_e = \sqrt{\pi}\,\rho_o w_m b \tag{15}$$

Terms to be substituted into equation 15:

$$w_m = \sqrt{gZ^{**}}\sqrt{\Psi}\,\zeta^{1/2}$$

$$b = b_o + C_l z = \frac{D}{2} + Z^{**}\frac{4\alpha}{3\sqrt{\pi}}\zeta$$

$$\text{Where } \frac{D}{2} = \text{half width}$$

Remember, w_m and C_l are both taken from the combusting plume region, section 3.7.1. Substitution of the above terms into the entrainment equation yields:

$$\dot{m}'_e = \sqrt{\pi}\,\rho_o\sqrt{gZ^{**}}\sqrt{\Psi}\,\zeta^{1/2}\left(\frac{D}{2} + Z^{**}\frac{4\alpha}{3\sqrt{\pi}}\zeta\right)$$

$$-\mathit{or}-$$

$$\frac{\dot{m}'_e}{\rho_o\sqrt{gD}D} = \sqrt{\pi}\sqrt{\Psi}\left(\frac{z}{D}\right)^{1/2}\left(\frac{1}{2} + \frac{4\alpha}{3\sqrt{\pi}}\left(\frac{z}{D}\right)\right) \tag{49}$$

$$\text{Where } \Psi = \frac{(1-\chi_r)\Delta H_c}{c_p T_o ns}$$

In order to develop useful analytical correlations, the above equation must be put into an empirical format where the theoretical constants can be replaced by numerical constants fitted from available data.

Empirical form:

$$\frac{\dot{m}_e'}{\rho_o\sqrt{gDD}} = \sqrt{\pi}\sqrt{\Psi}\left(\frac{z}{D}\right)^{1/2}\left(\frac{1}{2}+\frac{4\alpha}{3\sqrt{\pi}}\left(\frac{z}{D}\right)\right)\cdot\frac{2}{2}$$

$$= \frac{1}{2}\sqrt{\pi}\sqrt{\Psi}\left(\frac{z}{D}\right)^{1/2}\left(1+\frac{8\alpha}{3\sqrt{\pi}}\left(\frac{z}{D}\right)\right)$$

$$-or-$$

$$\frac{\dot{m}_e'}{\rho_o\sqrt{gDD}} = C_1\sqrt{\Psi}\left(\frac{z}{D}\right)^{1/2}\left(1+C_2\left(\frac{z}{D}\right)\right) \qquad (50)$$

$$\text{Where } C_1 = \frac{\sqrt{\pi}}{2}; C_2 = \frac{8\alpha}{3\sqrt{\pi}}$$

Note- C_1 and C_2 will be determined in section 4.11.

3.9.2 Axisymmetric Source

Basic entrainment equation, 3-(30):

$$\dot{m}_e = \pi\rho_o w_m b^2$$

Terms to be substituted:

$$w_m = \sqrt{\frac{4}{3}\Psi}\sqrt{gZ^*}$$

$$b = b_o + C_1 z = \frac{D}{2} + Z^*\frac{4}{5}\alpha\zeta$$

$$\text{Where } \frac{D}{2} = \text{radius}$$

Substitution of the above terms into the entrainment equation yields:

$$\dot{m}_e = \pi\rho_o\sqrt{gZ^*}\sqrt{\frac{4}{3}\Psi}\zeta^{1/2}\left(\frac{D}{2}+Z^*\frac{4}{5}\alpha\zeta\right)^2$$

$$-\ or\ -$$

$$\frac{\dot{m}_e}{\rho_o\sqrt{gD}D^2} = \pi\sqrt{\frac{4}{3}\Psi}\left(\frac{z}{D}\right)^{1/2}\left(\frac{1}{2}+\frac{4}{5}\alpha\left(\frac{z}{D}\right)\right)^2 \qquad (51)$$

Empirical form:

$$\frac{\dot{m}_e}{\rho_o\sqrt{gD}D^2} = \pi\sqrt{\frac{4}{3}\Psi}\left(\frac{z}{D}\right)^{1/2}\left(\frac{1}{2}+\frac{4}{5}\alpha\left(\frac{z}{D}\right)\right)^2\cdot\frac{4}{4}$$

$$= \frac{\pi}{2\sqrt{3}}\sqrt{\Psi}\left(\frac{z}{D}\right)^{1/2}\left(1+\frac{8}{5}\alpha\left(\frac{z}{D}\right)\right)^2$$

$$-\ or\ -$$

$$\frac{\dot{m}_e}{\rho_o\sqrt{gD}D^2} = C_1\sqrt{\Psi}\left(\frac{z}{D}\right)^{1/2}\left(1+C_2\left(\frac{z}{D}\right)\right)^2 \qquad (52)$$

Where $C_1 = \frac{\pi}{2\sqrt{3}};\ C_2 = \frac{8}{5}\alpha$

Note- C_1 and C_2 will be determined in section 4.9.

3.10 Flame Height

Multiplying the equation for entrainment in the flame zone by a parameter containing the heat of combustion of air, ΔH_a, results in a simple transition from entrainment to flame height.

3.10.1 Line Source

A useful relationship follows that energy release rate be related to the amount of air entrained into the flame zone times the heat of combustion of a certain amount of that entrained air.

$$\dot{Q}' = \dot{m}_e'(Z_f)\cdot\frac{\Delta H_c}{ns} \qquad (53)$$

Using the above relation an equation for flame height can easily be deduced from the entrainment equations:

$$\frac{\dot{Q}'}{\rho_o\sqrt{gD}Dc_pT_o} = \frac{\sqrt{\pi}}{2}\sqrt{\Psi}\left(\frac{Z_f}{D}\right)^{1/2}\left(1+\frac{8\alpha}{3\sqrt{\pi}}\left(\frac{Z_f}{D}\right)\right)\frac{\Delta H_c}{c_pT_o ns}$$

$$-\,or\,-$$

$$Q_D^{**} = \left(\frac{Z^{**}}{D}\right)^{3/2} = \frac{\sqrt{\pi}\Psi^{3/2}}{2(1-\chi_r)}\left(\frac{Z_f}{D}\right)^{1/2}\left(1+\frac{8\alpha}{3\sqrt{\pi}}\left(\frac{Z_f}{D}\right)\right) \tag{54}$$

As before with the entrainment equations, the flame height equation is put into an empirical form.

Empirical form:

$$Q_D^{**} = C\left(\frac{Z_f}{D}\right)^{1/2}\left(1+C_2\left(\frac{Z_f}{D}\right)\right) \tag{55}$$

Where $C = C_1\frac{\Psi^{3/2}}{(1-\chi_r)}$

Note- C and C_2 will be determined in section 4.10.

3.10.2 Axisymmetric Source

Equality of the heat of combustion of air times entrainment and energy release rate:

$$\dot{Q} = \dot{m}_e(Z_f)\cdot\frac{\Delta H_c}{ns} \tag{56}$$

Using the above relation an equation for flame height can easily be deduced from the entrainment equations:

$$\frac{\dot{Q}}{\rho_o c_p T_o \sqrt{gD}\, D^2} = \frac{\pi}{2\sqrt{3}}\sqrt{\Psi}\left(\frac{Z_f}{D}\right)^{1/2}\left(1+\frac{8}{5}\alpha\left(\frac{Z_f}{D}\right)\right)^2 \cdot \frac{\Delta H_c}{c_p T_o n s}$$

$$-\,or\,-$$

$$Q_D^* = \left(\frac{Z^*}{D}\right)^{5/2} = \frac{\pi}{2\sqrt{3}}\frac{\Psi^{3/2}}{(1-\chi_r)}\left(\frac{Z_f}{D}\right)^{1/2}\left(1+\frac{8}{5}\alpha\left(\frac{Z_f}{D}\right)\right)^2 \qquad (57)$$

Empirical form:

$$Q_D^* = C\left(\frac{Z_f}{D}\right)^{1/2}\left(1+C_2\left(\frac{Z_f}{D}\right)\right)^2 \qquad (58)$$

$$\text{Where } C = C_1\frac{\Psi^{3/2}}{(1-\chi_r)}$$

Note- C and C_2 will be determined in section 4.8.

Chapter 4 EMPIRICAL CONSTANTS

4.1 Introduction

In this chapter, empirical constants are fitted to the theory developed in Chapter 3. Generally, a discussion of the data and the graphs that these empirical constants are taken from will proceed the explanation of how the constants were mathematically obtained.

It is important to note that the data presented on all of our graphs and used to develop our correlations has not been weighted or selected under any mathematical pretenses whatsoever. Selection of data points was made in an effort to capture the range of data and was otherwise taken on a purely random basis. In many cases only limited data points were selected from a source graph so as not to overshadow data from other authors.

4.2 Infinite Line Temperature Data

Empirical correlations for temperature both in the smoke plume and the combustion zone are taken from Figure 1. The solid lines represent our correlations of the data with the flat line corresponding to the near field or combustion zone and the following line, having a slope of $^{-}1$, representing the far field or smoke plume. The dashed lines depict Cox's [9] definition of the transition and intermittent zones. Remember that our theory models a simplified plume containing only two regimes. However, an actual plume can be more accurately broken into four parts, as were described earlier, with the addition of the transition and intermittent zones.

To get a sense of the range of data plotted on the temperature graph lets take a look at the two extremes; the bottom of the flame zone and top of the smoke plume.

Figure 1: Dimensionless Temperature vs. Height for the Infinite Line
$X_r = 30$ %

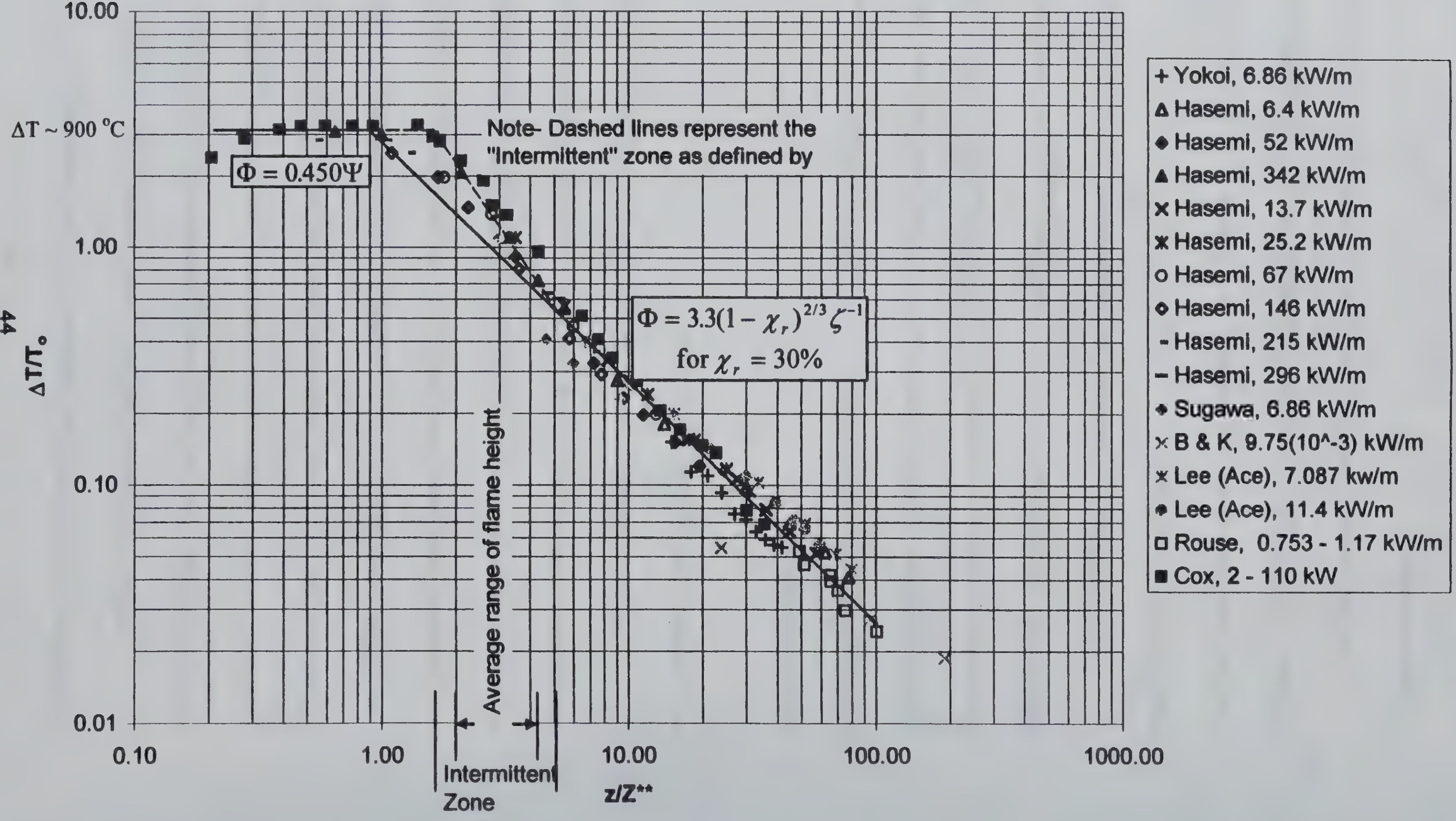

At the bottom of the flame zone $z/Z^{**} = 0.20$. In this area measurements were taken so close to the burner that they actually dip into the fuel rich zone slightly above the burner's surface where combustion is just beginning to occur. Thus, these temperature readings are slightly lower than the other readings taken throughout the combustion zone.

For large values, $z/Z^{**} = 100$, energy release rates are extremely small compared to the heights where they are measured. Two sets of data in this area give a physical illustration of the large ratios between height, [m], and energy release rate, [m], corresponding to the very top of the smoke plume. Brodowicz and Kierkus [12] measured temperatures above a heated wire with a very small energy release rate, 9.75×10^{-3} kW. Thus, even measurements close to this source will yield a large ratio between height and energy. In the other data set, Rouse, Yih, and Humphreys were attempting to model atmospheric disturbances. They took measurements a couple of meters above recessed gas burners emitting weak blue flames.

Note that when developing the far field temperature correlation data points corresponding to large values of z/Z^{**} were given more weight than those low in the smoke plume to avoid complications inherent to the intermittent zone. The same methodology was used when choosing the location of the far field velocity line. Thus, both of these far field correlations may provide erroneous answers low in the smoke plume. However, this area is generally not as important to the fire engineer as temperatures high in the developed smoke plume where interactions with detectors and sprinklers occur. Using these far field correlations for modelling purposes or prediction of device activation is merited because they will yield conservative values of both temperature and the convective heat transfer coefficient, h.

4.3 Infinite Line Velocity Data

Empirical correlations for velocity both in the smoke plume and the combustion zone are taken from Figure 2. Once again, the solid lines represent our correlations of the data. The flat line corresponds to velocity in the far field or smoke plume. The preceding line, having a slope of ½, represents velocity in the near field or combustion zone. As in Figure 1, the dashed lines represent Cox's depiction of the intermittent and transition regions.

Although the velocity data falls together in the same general area it does not plot as tightly together as its corresponding temperature data. This could be expected since it is a lot harder to take accurate velocity measurements than temperature measurements, therby resulting in a lack of precision among different data sets.

4.4 Infinite Line Far Field Correlations

C_T and C_V are determined from Figures 1 and 2 respectively by simply applying a best fit line through the data while maintaining the predetermined powers of dimensionless height from Chapter 3. These constants are then used to determine α, β, and C_l. Hence, $C_T = 2.6$ and $C_V = 2.0$ from the far field "fits" on Figures 1 and 2.

Looking at either of the graphs, the constants depicted as C_T and C_V may not be apparent as they are expressed in a generic form to incorporate radiation loss. To get the values of C_T and C_V listed above a radiation fraction of 30 % has been

Figure 2: Axisymmetric Dimensionless Velocity vs. Height
Xr = 15 % Near Field & 30 % Far Field

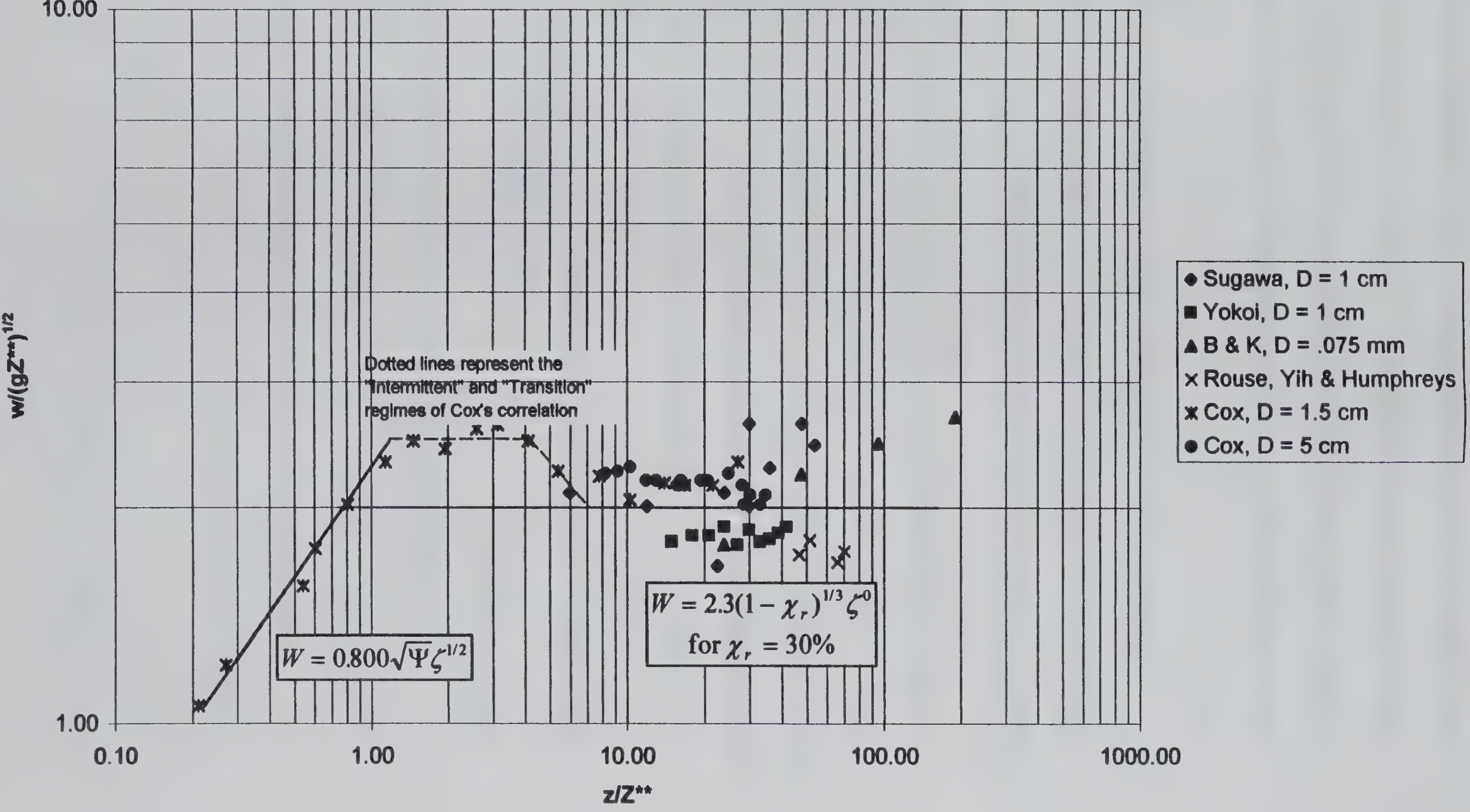

incorporated. For C_T, the radiation fraction was set at 30 % to maintain consistency with the propane fuel used by Hasemi [1]. For C_V, 30 % was chosen for the radiation fraction because it did the best job of fitting available data. A detailed explanation of the reasons for setting $\chi_r = 30$ % is presented later in the thesis in sections 4.6.1 and 4.6.2.

The above values for temperature and velocity agree well with the new data published by Cox [9] and that of more historic works including Yokoi [3], Rouse et al [4], Lee and Emmons [2], and Hasemi and Nashimeti[1].

β is first solved from the relation $\frac{W^2}{\Phi\zeta} = \frac{C_v^2}{C_T} = \sqrt{\frac{2}{\beta}}$ and found to equal 0.845. With knowledge of β, α is easily solved through the definition of C_v.

$\alpha = 0.091$

C_l is found easily as it is proportional to α.

$C_l = 0.103$

4.5 Infinite Line Near Field Correlations

4.5.1 Temperature

First put the theoretical equation, (40), into an empirical form.

$$\Phi = C_{T_f}\Psi$$

Next choose a value for Φ in the combustion zone that represents the majority of data points and solve for Ψ.

$\Phi = 3.1$

$$\Psi = \frac{(1-\chi_r)\Delta H_a}{c_p T_o} = \frac{(1-.30)2{,}910}{1.01 \cdot 293} = 6.89$$

Here χ_r was also assumed equal to 30% to match Hasemi's propane data [1].

Solve for C_{Tf}

$$C_{T_f} = \frac{\Phi}{\Psi} = \frac{3.1}{6.89} = .450$$

Therefore:

$$\Phi = 0.450\Psi$$

4.5.2 Velocity

As was the case in the previous section, put the theoretical equation, (39), into an empirical form.

$$W = C_{v_f}\sqrt{\Psi}\zeta^{1/2}$$

In order to solve for the empirical constant an "average" data point is selected and Ψ is solved for with a different radiation fraction, χ_r, of 15%. Here the radiation fraction was set at 15 % to match Cox's methane data [9].

$W=2.00; \zeta=0.748$

$$\Psi = \frac{(1-\chi_r)\Delta H_a}{c_p T_o} = \frac{(1-.15)2{,}910}{1.01\cdot 293} = 2.89$$

Solve for C_{vf}:

$$C_{v_f} = \frac{\sqrt{\Psi}\zeta^{1/2}}{W} = \frac{\sqrt{2.89(0.748)}}{2.00} = 0.800$$

Therefore:

$$W = 0.800\sqrt{\Psi}\zeta^{1/2}$$

4.6 Radiation Effects

The effects of radiation are considerable on our empirical correlations as was illustrated above. Therefore, choosing the correct χ_r is of the utmost importance. Unfortunately, χ_r was either not reported or not measured by any of the authors. An example depicting the severity of this oversight can be found on Figure 1. One would expect Yokoi's alcohol data to have higher temperatures than Hasemi's propane data. However, this is not the case. Had the authors reported radiation losses these values could have been used to correct the data.

In most cases, the types of fuel burned were given. Although this information is useful it does not convey the whole picture. Radiation loss, χ_r, varies with both source size and configuration, fuel flow rate, combustion inefficiencies, and most importantly how the fuel is burned, or how the fuel and oxidant are mixed and ignited [18].

Because χ_r's were not given we were forced to pick values based upon sound reasoning. Sections 4.6.1 and 4.6.2 discuss both the reasoning behind our choices and the effect of radiation on our temperature and velocity data respectively.

4.6.1 Temperature

Recall that a value of 30 % was selected for the radiation fraction, χ_r, in both the far and near fields, and was used primarily for determining α and C_v in the far field and C_{Tf} in the near field. The radiation fraction was set at 30 % to maintain consistency with the propane fuel used by Hasemi [1]. The value was determined from Tewarson's chapter in the SFPE Handbook[32] as follows:

$$E_{ch} = E_{con} + E_{rad}$$

$$\chi_{r_{propane}} = \frac{E_{rad}}{E_{ch}} x100 = \frac{12.5}{43.7} x100 = 28.6\% \cong 30\%$$

In addition, a value of 30 % gave the most reasonable radiation curves found on Figure 3.

Figure 3 illustrates the effects of radiation ranging from no radiation loss to a hefty 60 % radiation loss. Increments of 15 % are spaced out evenly between these two extremes, where 30 % was taken as our baseline radiation value. As can be seen on Figure 3, no radiation loss will result in higher temperatures than an entity which radiates a fraction of its energy away. In the far field, zero percent energy loss results in temperatures that are at least twice as high as their counterparts loosing 60 % of their energy to radaiation loss and as much as 2.6 times greater in the flame zone.

The strong effect of radiation on temperature or vice-versa was alluded to above. The hotter the temperature the stronger the effect of radiation. Thus, radiation loss in the flame zone is far more significant than losses in the smoke plume. The larger gap between the radiation curves in the flame zone than those in the smoke plume are a testament to this phenomenon.

All of the data points within the flame zone and the smoke plume, with the exception of those points falling in the designated intermittent zone, are captured by our theory incorporating a range of radiation losses.

4.6.2 Velocity

Both the far and near field correlations were originally intended to be fitted to the natural gas data of Cox [9] and to other points belonging to low radiation loss

Figure 3: Temperature Radiation Curves for the Infinite Line
$X_r = 30\ \%$

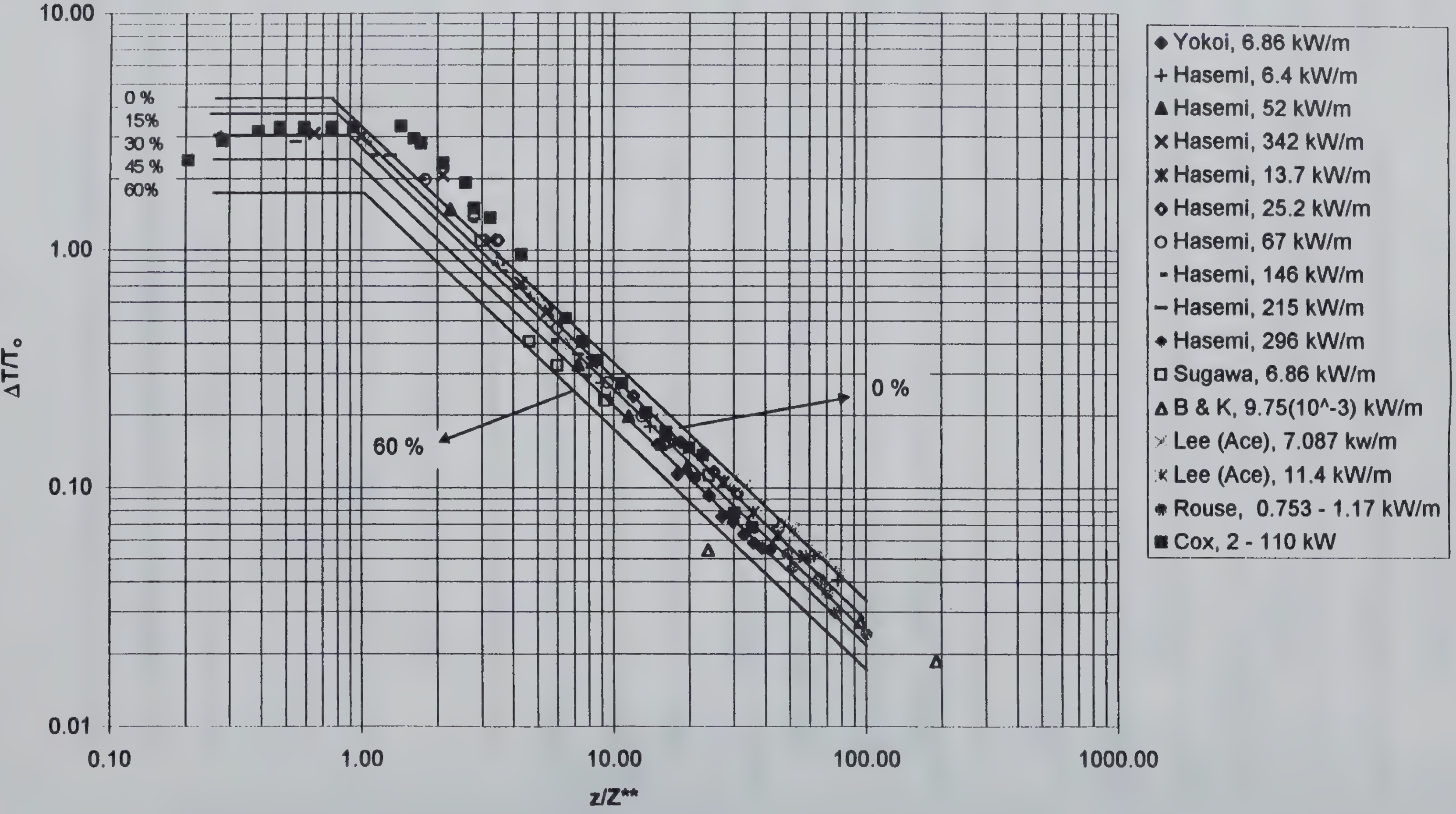

fuels. Because this LNG was composed of 94 % methane a χ_r suitable for methane was chosen.

McCaffrey [18] burned methane on 0.3 m square porous burners and found that radiation loss varies from 10 % for low energy fires to an asymptotic value of 24 % for high energy fires. From Figure 1 of his report we chose a value closer to 10 %. First of all, McCaffrey's burners were much larger than any of those used in this paper. Because radiation loss increases with increasing source size[ ], we were inclined to pick a small χ_r to match our small burners. In order to get a more refined value we once again turned to Tewarson's chapter in the SFPE Handbook [32].

$$\chi_{r_{methane}} = \frac{E_{rad}}{E_{ch}} x100 = \frac{7.0}{49.6} x100 = 14.1\% \cong 15\%$$

Figures 4 and 5 illustrate the effects of radiation loss on vertical velocity. As was the case with the temperature plot, Figure 2, a range of radiation losses from zero to 60 percent was plotted with 15 percent increments between these two extremes on both graphs.

Figure 5 was plotted in conjunction with Figure 4 to show the dramatic effects associated with choosing the baseline radiation fraction used in developing our correlations. Assuming an initial radiation fraction of 30 %, for both the far and near fields, instead of 15 % shifts all of the radiation curves upwards and captures many of the data points missed in the far field when assuming an initial radiation fraction of 15 %. As a result, an initial radiation fraction of 30 % rather than 15 % was used to fit far field data. McCaffrey [18] offers an explanation for this unexpected behavior: "Short bluish flames at low flow rates will obviously radiate proportionally less than the larger, yellower sooty flames of higher flow rates." Since Cox's [9] flow rates

Figure 4: Velocity Radiation Curves for the Infinite Line
Initial X_r = 15 %

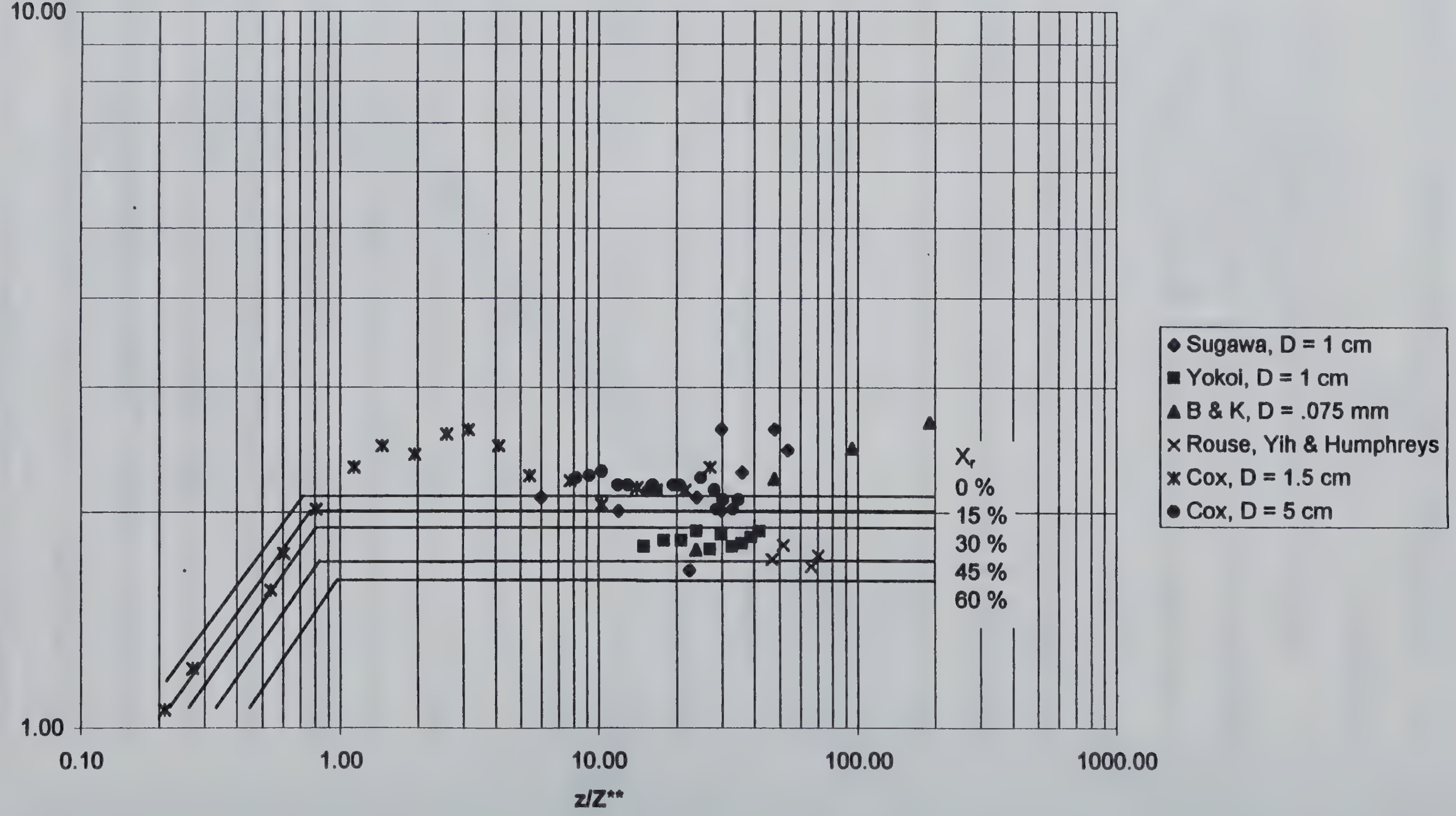

Figure 5: Velocity Radiation Curves for the Infinite Line
Initial X_r = 30 %

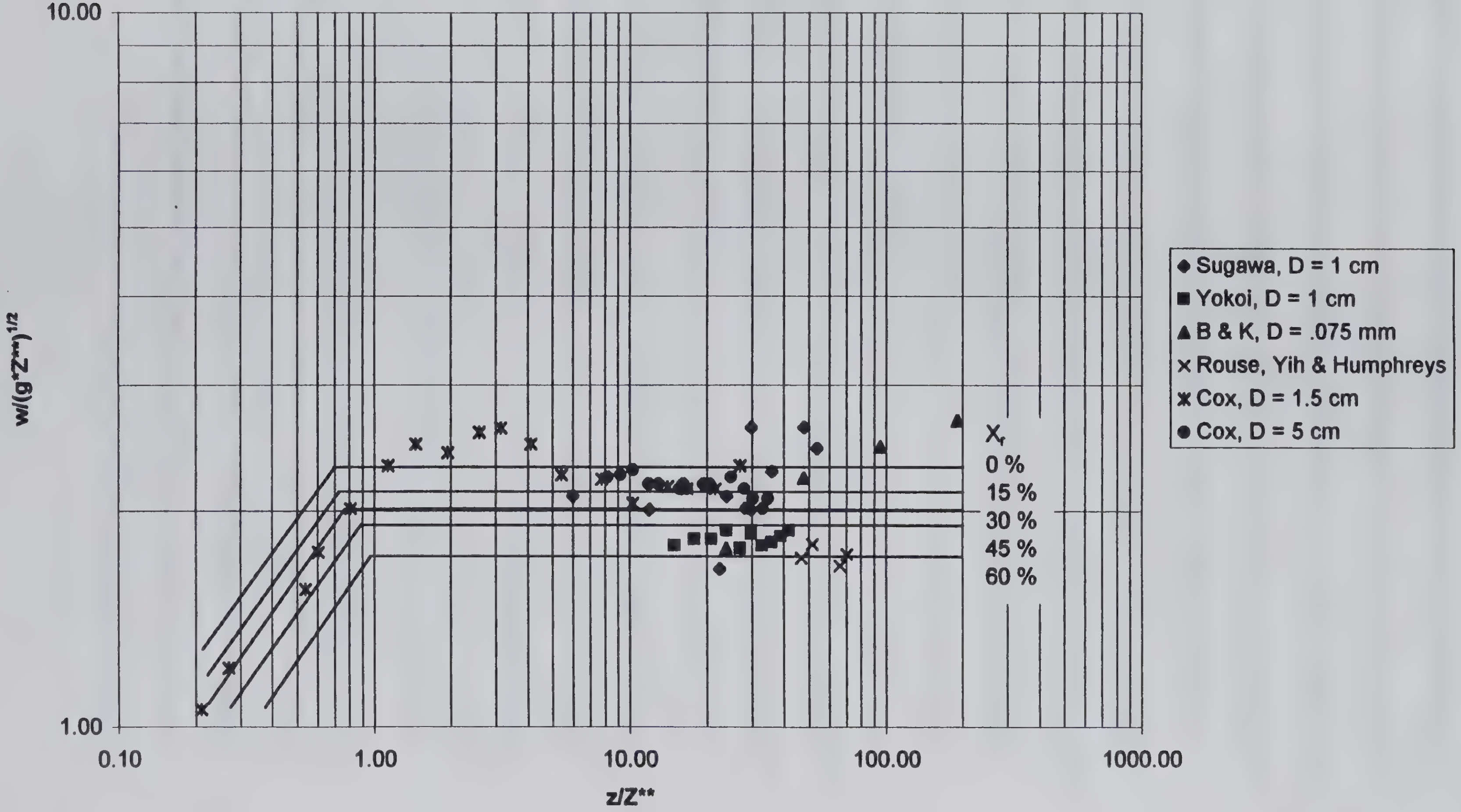

ranged from 2 – 110 kW and Sugawa [13] used propane it is possible that some of the data actually do approach higher radiation losses. Therefore, χ_r = 15 % was used in the flame zone and χ_r = 30 % was used in the far field. A short explanation of how radiation loss affects velocity through temperature is presented below.

Theoretically, lower radiation loses yield higher velocities through a direct relation between temperature and velocity. Less radiation loss results in higher temperatures, Figure 2. Higher temperatures cause a greater expansion of the plume gases through the Ideal Gas Law corresponding to lighter, less dense gases resulting in a stronger buoyancy force. The stronger the force of buoyancy the faster plume gases will be driven up and away from colder ambient gases. In short, the lower the radiation loss the faster the plume gases will rise. Hence, the zero percent radiation loss curve is found above all curves depicting a radiation loss, Figures 4 and 5.

A mistaking assertion of the radiation curves shows several of these curves spaced unequally amongst themselves. This is a manifestation of rounding errors and not a part of the theory or other underlying assumptions. These curves should be spaced equidistantly.

4.7 Introduction to Near Field Entrainment and Flame Height

In Chapter 3, the equations for entrainment were modified to develop equations for flame height. However, the process is reversed when fitting empirical constants to those equations. Entrainment correlations are developed using previously determined flame height constants because flame height is easier to measure and more accurately quantified than entrainment.

In addition, empirical constants for the infinite line are determined with knowledge of their axisymmetric counterparts because axisymmetric data is far more prevalent and accepted/established than that of infinite line data. More exactly, both the profile and entrainment constants from the axisymmetric flame height correlation are used to determine the correlation for infinite line flame height and entrainment. From the theory developed in chapter three, the profile constants for axisymmetric entrainment and flame height should equal infinite line constants for entrainment and flame height. A flow chart depicting this methodology can be found on page 58.

4.8 Axisymmetric Flame Height Correlations

The empirical constants for axisymmetric flame height were developed from the data on Figure 6. The region enclosed by the solid black line in the center of the graph represents a range of data compiled by Zukoski [10]. Where large fuel source diameters have accumulated at the top of the region and small diameters have accumulated at the bottom of the enclosed region. Obviously, there is a diameter effect exhibited by the data. Although we have included diameter as a term in our dimensionless parameters, we are still unaware exactly how and to the extent with which it affects our correlations

Recall the axisymmetric, empirical, flame height correlation from Chapter 3.

$$Q_D^* = C\left(\frac{Z_f}{D}\right)^{1/2}\left(1+C_2\left(\frac{Z_f}{D}\right)\right)^2 \qquad 3\text{-}58$$

$$\text{where } C = C_1\frac{\Psi^{3/2}}{(1-\chi_r)}$$

Flow Chart Depicting Methodology Behind Near Field Entrainment and Flame Height

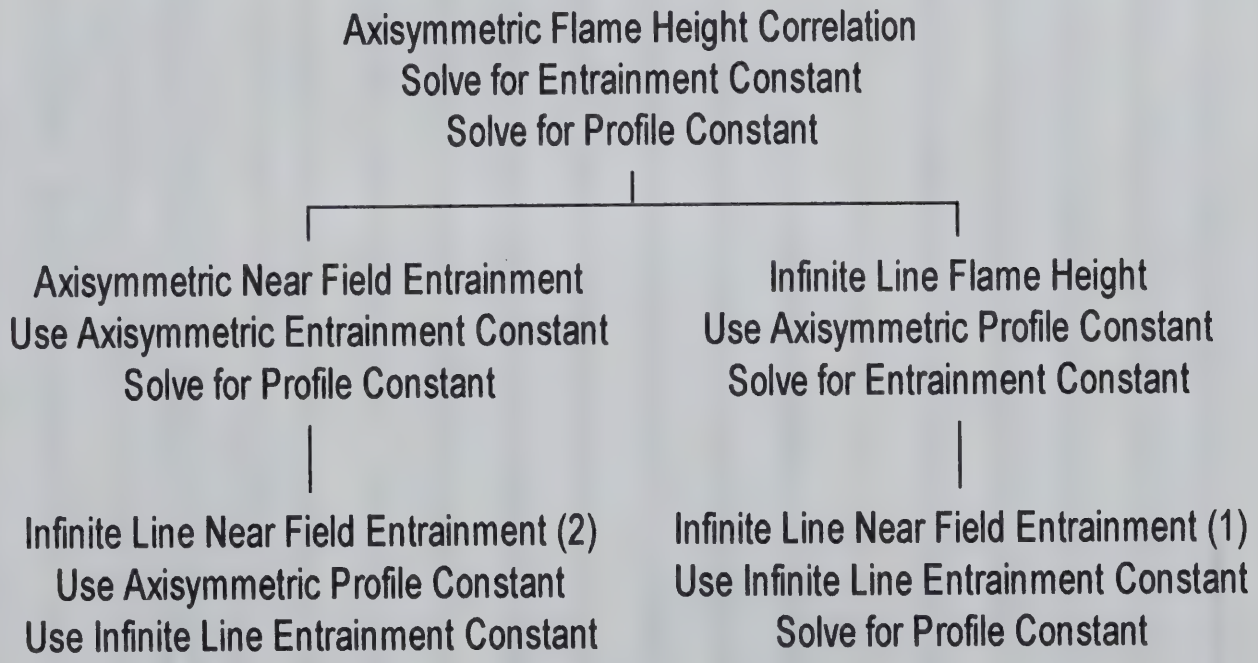
Axisymmetric Flame Height Correlation
Solve for Entrainment Constant
Solve for Profile Constant
Axisymmetric Near Field Entrainment
Use Axisymmetric Entrainment Constant
Solve for Profile Constant
Infinite Line Flame Height
Use Axisymmetric Profile Constant
Solve for Entrainment Constant
Infinite Line Near Field Entrainment (2)
Use Axisymmetric Profile Constant
Use Infinite Line Entrainment Constant
Infinite Line Near Field Entrainment (1)
Use Infinite Line Entrainment Constant
Solve for Profile Constant

Figure 6: Axisymmetric Smooth Fit of Dimensionless Flame Height, Z_f/D, vs. Energy Release Rate, Q_D^*

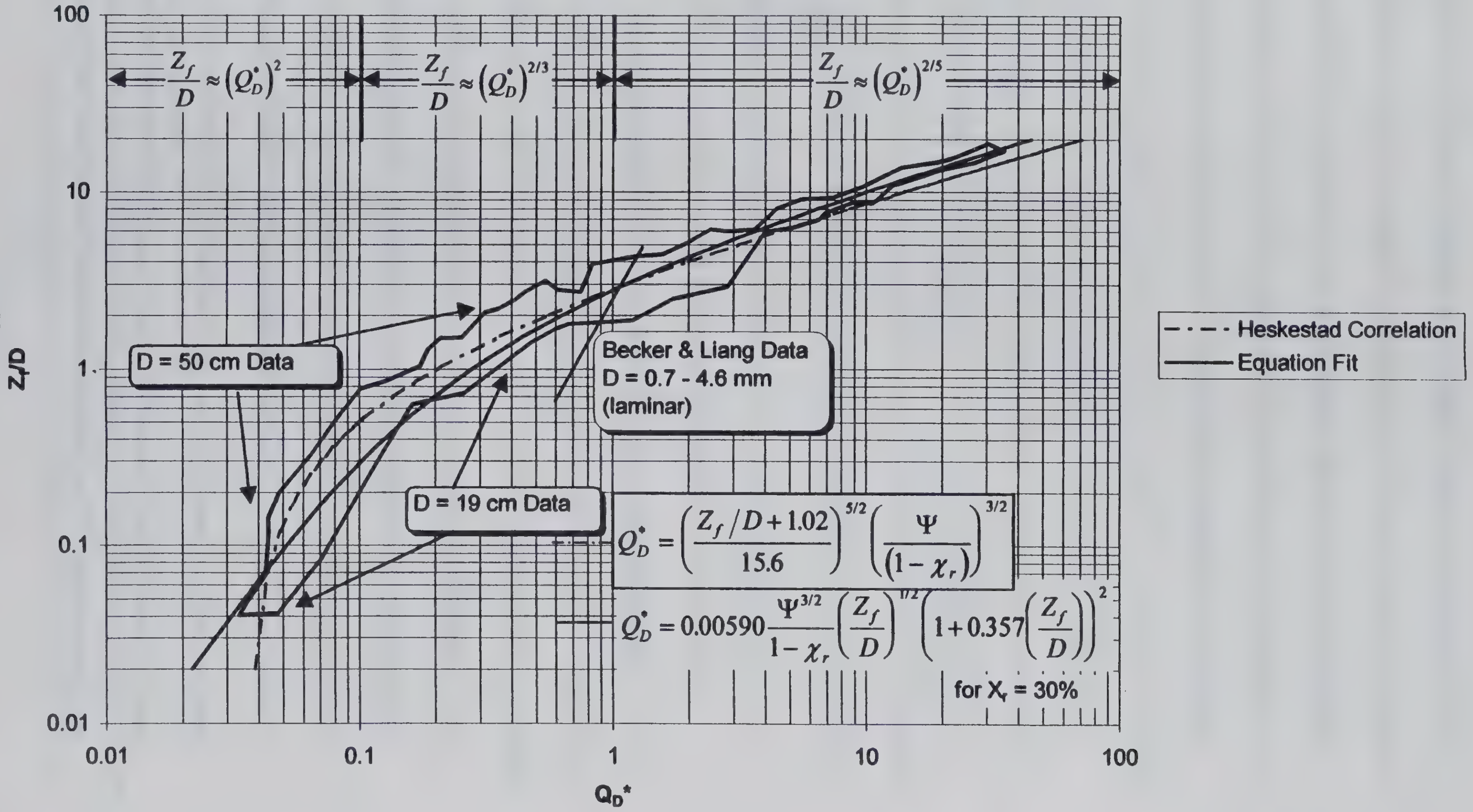

In order to solve for C and C_2 two points, not shown on the graph, are taken from the enclosed region. The first point is taken from the top of the data range corresponding to tall flames. The second point is taken from the bottom of the data corresponding to small flames. In an attempt to get the best correlation numerous data points were fitted to equation (58). The points below represent the best fit.

Table 4: Axisymmetric Flame Height Data Fit Points

	Q^*_D	$\frac{Z_f}{D}$
Top data point	30.0	16.7
Bottom data point	0.0415	0.068

Solving the empirical equation, (58), for C and C_2 yields:

$C = 0.152$
$C_2 = 0.357$
$C_1 = 0.00590$ (from the relation above)

Substituting these constants into equation 3-(58) yields:

$$Q_D^* = 0.00590\frac{\Psi^{3/2}}{(1-\chi_r)}\left(\frac{Z_f}{D}\right)^{1/2}\left(1+0.357\left(\frac{Z_f}{D}\right)\right)^2$$

The solid black line on Figure 6 represents this correlation. It can be shown that the correlation fits the powers mapped out by Zukoski [20] shown at the top of the graph. For a small flame height to diameter ratio corresponding to a weak energy release rate Zukoski finds that flame height over diameter varies with dimensionless energy release rate to the second power. Our correlation exhibits the same behavior. If the ratio of flame height to diameter is small 1 becomes the dominant term in the second set of parentheses. Thus the entire term turns into one and energy release rate varies with flame height to the ½ or flame height varies with energy release rate to the 2nd power as was depicted by Zukoski [20]. On the other extreme, for a large flame height over diameter ratio corresponding to a large energy release rate Zukoski finds that flame height varies with energy release rate to the 2/5 power. In our correlation, a large Z_f/D will overwhelm the value of 1 found in the second set of parentheses. Thus, the simplified equation will yield $Z_f/D^{5/2} = Q^*$ or $Q^{*2/5} = Z_f/D$ as was depicted by Zukoski. Between the two extremes, Zukoski finds $Z_f/D = Q^{*2/3}$, but says realistically the exponent could vary anywhere between 2 and 2/5. A value of 2/3 should be used with caution.

Also placed on the graph is a correlation by Becker and Liang [14] whose data follow the slope of a line exhibiting laminar behavior equal to $Q_D^{*\,2}$. The dashed line found in the enclosed region is a well known purely empirical correlation by Heskestad [34]. It was placed on the graph as a comparison to our equation. Heskestad did not design his correlation to fit the entire range of data that we have plotted, but rather used a subset of this range. Heskestad reports that for low Z_f/D ratios smaller than about 0.5 there is a transition from coherent flaming to distributed flamelets, and that data in this area and lower is very scattered. Therefore, correlations in this area are subject to a large degree of freedom resulting in a substantial difference in the rate of decay between the two equations. It is not obvious which correlation is better in this regime.

4.8.1 Radiation Effects

Figure 7 shows how our correlation for flame height, presented in figure 6, is affected by radiation. Similar to the other graphs portraying radiation we have incorporated a

Figure 7: Axisymmetric Smooth Fit Radiation Curves of Z_f/D vs. Q_D^*

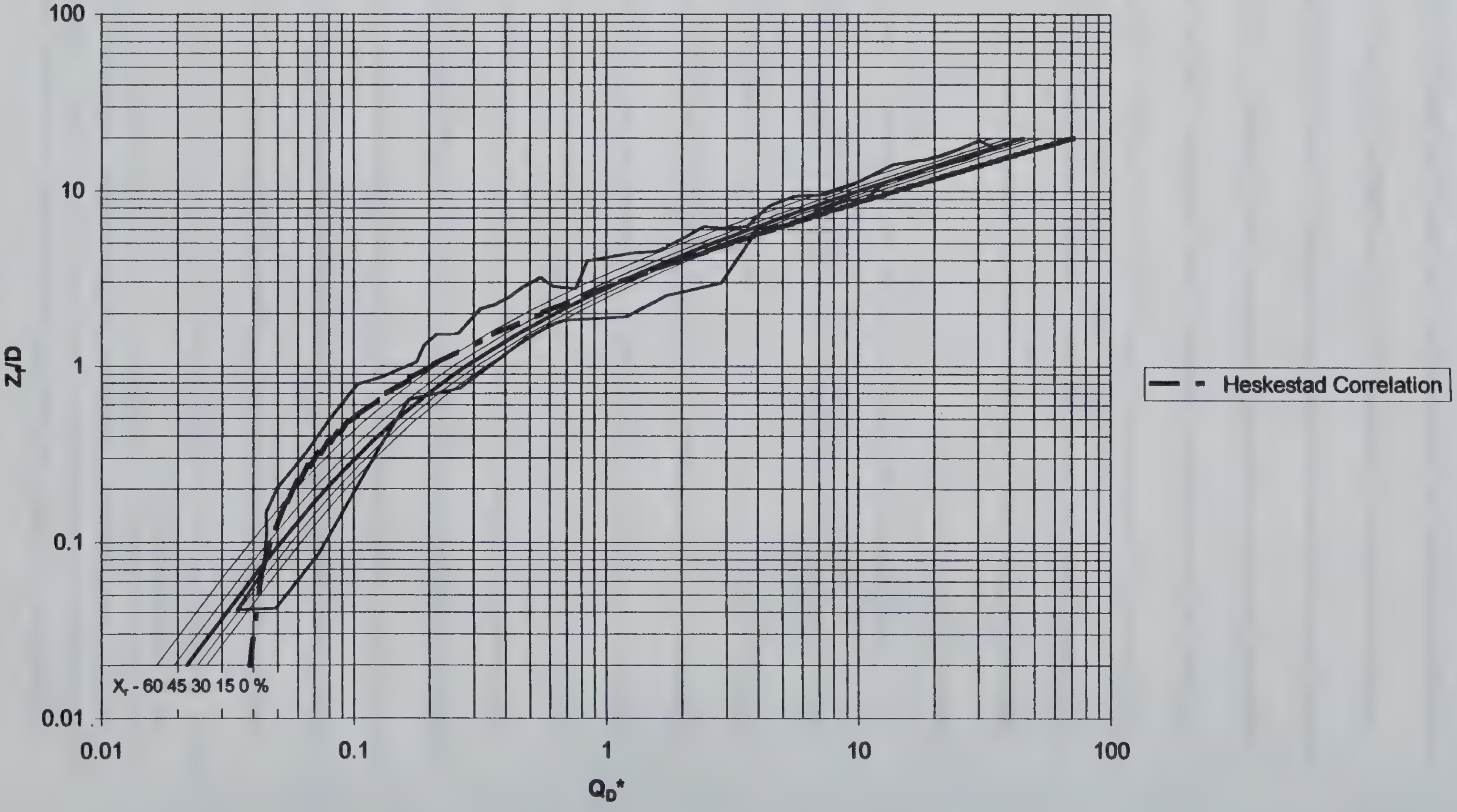

range of radiation curves from no radiation loss to 60 % radiation loss with 15 % intervals between these two extremes. As can be seen from Figure 7, the larger the radiation loss the taller the flames. This phenomenon can be explained through an extension of the theory presented for the effect of radiation on velocity, Figures 4 and 5. Recall that less radiation loss results in higher plume temperatures which corresponds directly to larger velocities. Flame height is determined indirectly by the magnitude of this vertical velocity, w. Remember also from earlier theory that entrainment is a function of centerline velocity times a constant. Hence, the larger the vertical velocity the faster new air needs to be entrained into the plume to make up for this lost velocity, (see the continuity equation). As was shown earlier, flame height is proportional to entrainment times the heat of combustion of air, ΔH_a. From here out, we will examine the effects of radiation on flame height by looking at the two extreme cases; no radiation loss and 60 % radiation loss.

No radiation loss results in a high temperature plume with a large centerline velocity that is capable of entraining large amounts or air in a short distance. Because the plume has entrained a large amount of air combustible fuel vapors need not travel vary far to find the oxidizer necessary for combustion. Thus, little or no radiation loss results in short flames. On the other hand, a plume which has lost a lot of its energy to radiation will have low temperatures that produce a weak force of buoyancy incapable of driving hot combustible gases upwards at a large velocity. Thus, the plume has a weak entrainment rate and combustible gases are required to travel a greater distance in search of the oxidizer necessary for their combustion. In conclusion, large radiation losses result in tall flames and small radiation losses result in short flames.

4.9 Axisymmetric Entrainment

Recall from section 4.7, (Introduction), that although flame height equations were developed from entrainment equations the process is reversed when fitting empirical constants to entrainment equations. C_2 which physically represents the expansion of the plume through the entrainment constant, α, should remain the same for both of these equations. However, the profile constants C or C_1 will not be the same due to a partial addition of the Ψ term in flame height. Thus, both correlations will grow the same way with height but will acquire different profile constants as the result of different powers of Ψ.

Figure 8 shows our correlation for entrainment in the flame zone against data compiled by Zukoski [20]. Recall the axisymmetric, empirical, entrainment equation from section 3.9.2:

$$\frac{\dot{m}_e}{\rho_o\sqrt{gD}D^2} = C_1\sqrt{\Psi}\left(\frac{z}{D}\right)^{1/2}\left(1+C_2\left(\frac{z}{D}\right)\right)^2$$

$$\text{where } C_1 = \frac{\pi}{2\sqrt{3}};\, C_2 = \frac{8}{5}\alpha$$

The correlation was determined by keeping the same entrainment constant, C_2, developed from flame height data and solving for $C_1\sqrt{\Psi}$. Solving for $C_1\sqrt{\Psi}$ is easily done by picking a specific entrainment point from Figure 8; inserting its values into the entrainment equation; and then solving for the constant.

Figure 8: Near Field Axisymmetric Dimensionless Entrainment vs. Height

$X_r = 30\ \%$

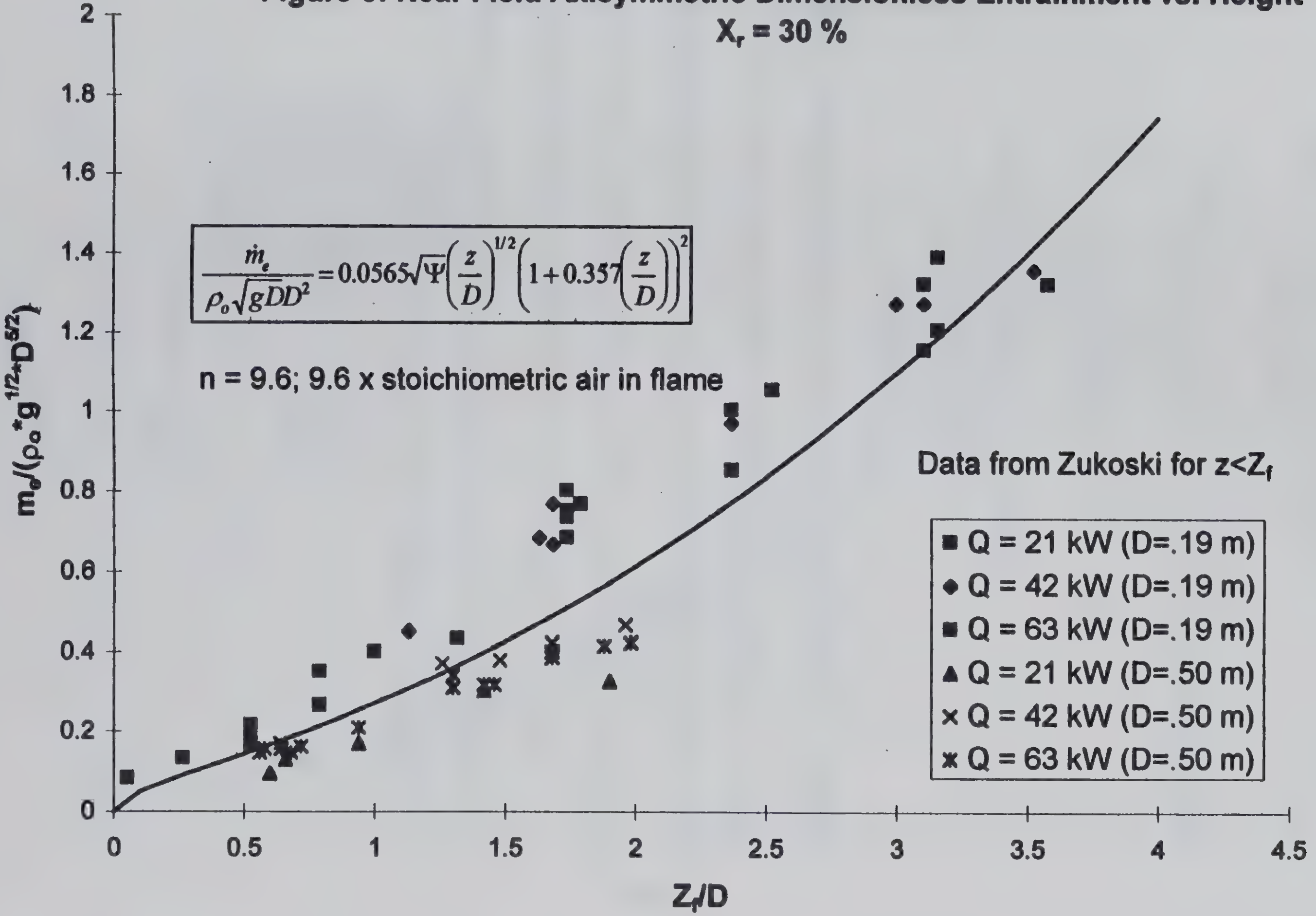

From Figure 8 the point selected is:

$$\frac{\dot{m}_e}{\rho_o\sqrt{g}D^{5/2}} = 0.536; \quad \frac{Z_f}{D} = 1.8$$

Recall $C_2 = 0.357$ from the flame height equation.

Inserting these values into the entrainment equation yields:

$$0.536 = C_1\sqrt{\Psi}(1.8)^{1/2}[1 + 0.357(1.8)]^2$$
$$C_1\sqrt{\Psi} = 0.148$$

Through the definition of $C_1\sqrt{\Psi}$,n was found to equal 9.6.

$$C = C_1\sqrt{\Psi}\left(\frac{\Delta H_c}{c_p T_o s n}\right)$$
$$C_1\sqrt{\Psi} = \frac{C}{\dfrac{\Delta H_c}{c_p T_o s n}} = \frac{0.152n}{\dfrac{2{,}910}{1.01(293)}} = 0.148$$
$$n = 9.57 = 9.6$$

Tamanini [21] applied an improved version of the k-ε-g model of turbulence to buoyancy controlled turbulent diffusion flames issuing from a variety of fuel arrays and found that at the flame tip a plume entrains 9 times the oxygen stoichiometric requirement. Commonly accepted values of n range from 5 – 15, Delichatsios [16].

Figure 9 shows entrainment in both the far and near fields on the same graph by putting far field entrainment correlations in near field terms. Recall from section 3.5.1, (Far Field Entrainment for the Axisymmetric Source):

$$\frac{\dot{m}_e}{\rho_o\sqrt{gz}z^2} = \pi C_v C_l^2 Q_z^{*1/3}$$

$$-or-$$

$$\frac{\dot{m}_e}{\rho_o\sqrt{gz}z^2} = \pi C_v C_l^2 \left(\frac{Z^*}{z}\right)^{5/6}$$

Figure 9: Near and Far Field Axisymmetric Entrainment

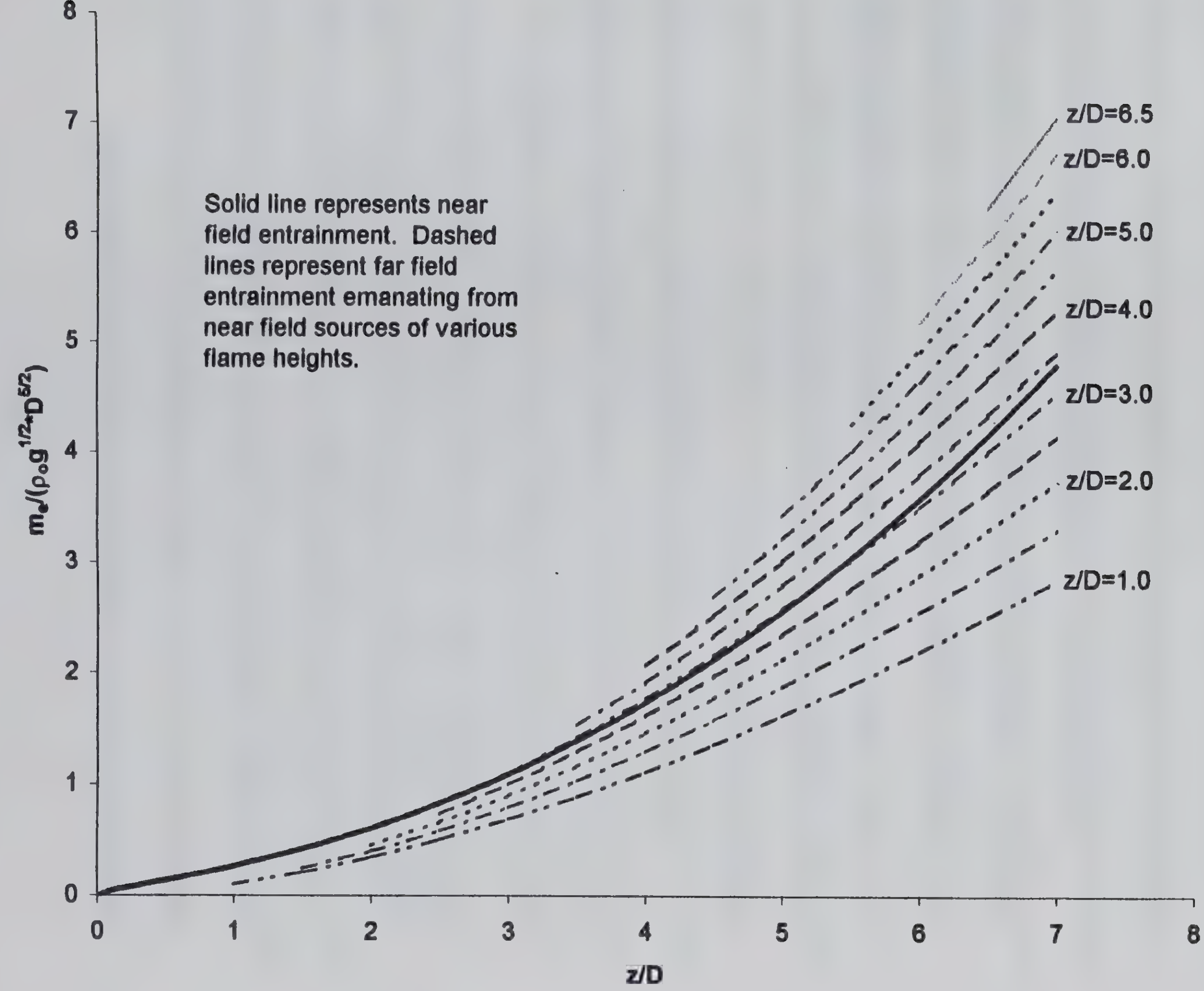
Solid line represents near field entrainment. Dashed lines represent far field entrainment emanating from near field sources of various flame heights.

To convert far field entrainment into near field terms multiply both sides of the equation by $Z^{5/2}$ and divide both sides of the equation by $D^{5/2}$.

$$\frac{\dot{m}_e}{\rho_o\sqrt{gD}D^2} = \pi C_v C_l^2 \left(\frac{Z^*}{D}\right)^{5/6} \left(\frac{z}{D}\right)^{5/3}$$

$$-or-$$

$$\frac{\dot{m}_e}{\rho_o\sqrt{gD}D^2} = \pi C_v C_l^2 Q_D^{*1/3} \left(\frac{z}{D}\right)^{5/3}$$

Note- From section 3.5, (Far Field Theory for the Axisymmetric Source), C_v = 3.87 and C_l = 0.118 for χ_r = 20 %. Therefore $\pi C_v C_l^2 = 0.169$.

Thus, it is possible to represent entrainment in both the far and near fields on one graph. As before, the solid black line represents entrainment in the combustion zone, whereas the dashed spurs coming off this line model far field entrainment for fire plumes of different flame heights. The graph is read by starting on the solid line representing entrainment in the flame zone and branching off onto one of the far field spurs at a desired flame height.

At z/D between 3 and 3.5 both regimes of the fire plume entrain about the same amount of air. However, for weak fire plumes exhibiting small flame heights, the far field entrains considerably less air than the near field. The opposite phenomenon is observed for high energy fires yielding flames larger than z/D = 3.5. These large flames result in a smoke plume that is capable of entraining larger amounts of fluid than its issuing near field. The gaps between various far field correlations and the solid near field line can not be attributed to the length of the intermittent zone. They are merely a manifestation of the near field correlation being incapable of describing entrainment in the far field and vice-versa.

4.10 Infinite Line Flame Height

Figure 10 shows flame height data for the line. The two long lines extending from the upper right of the graph to the lower left are linear fits of the data. Notice that there is a large gap between these two linear fits ranging from 4.3Z** to 2Z**. This discrepancy could be due to individual researcher's varying definitions of flame height itself. More specifically, how they dealt with the intermittent zone defined as the fraction of time during which at least part of the flame lies above a horizontal plane located at elevation z above the burner [20]. For example, did they define the end of the flame zone to be where flame exists 10 % of the time, 50 % of the time, or 90 % of the time? Definition of this zone is extremely important since it can occupy anywhere from 40-60% of the total flame height. In most cases, authors did not report how they defined flame height.

Even if two authors used the same definition of flame height it is still quite possible to get offset values based on their measurement techniques. Several examples of popular measurement techniques include (1) infrared-imaged pictures, (2) judgments by eyes, (3) usual photographs, (4) video tape recordings [13]. All of these techniques could yield different values of flame height assuming the same source and flame height definition. For example, eye-averaged results are consistently 10 –15 % higher than flame heights determined from video pictures assuming 50 % intermittency [20]. A detailed explanation of measurement techniques and definition of flame height made available by individual authors, where possible, can be found in the Appendix A.

Figure 10: Dimensionless Flame Height for the Infinite Line

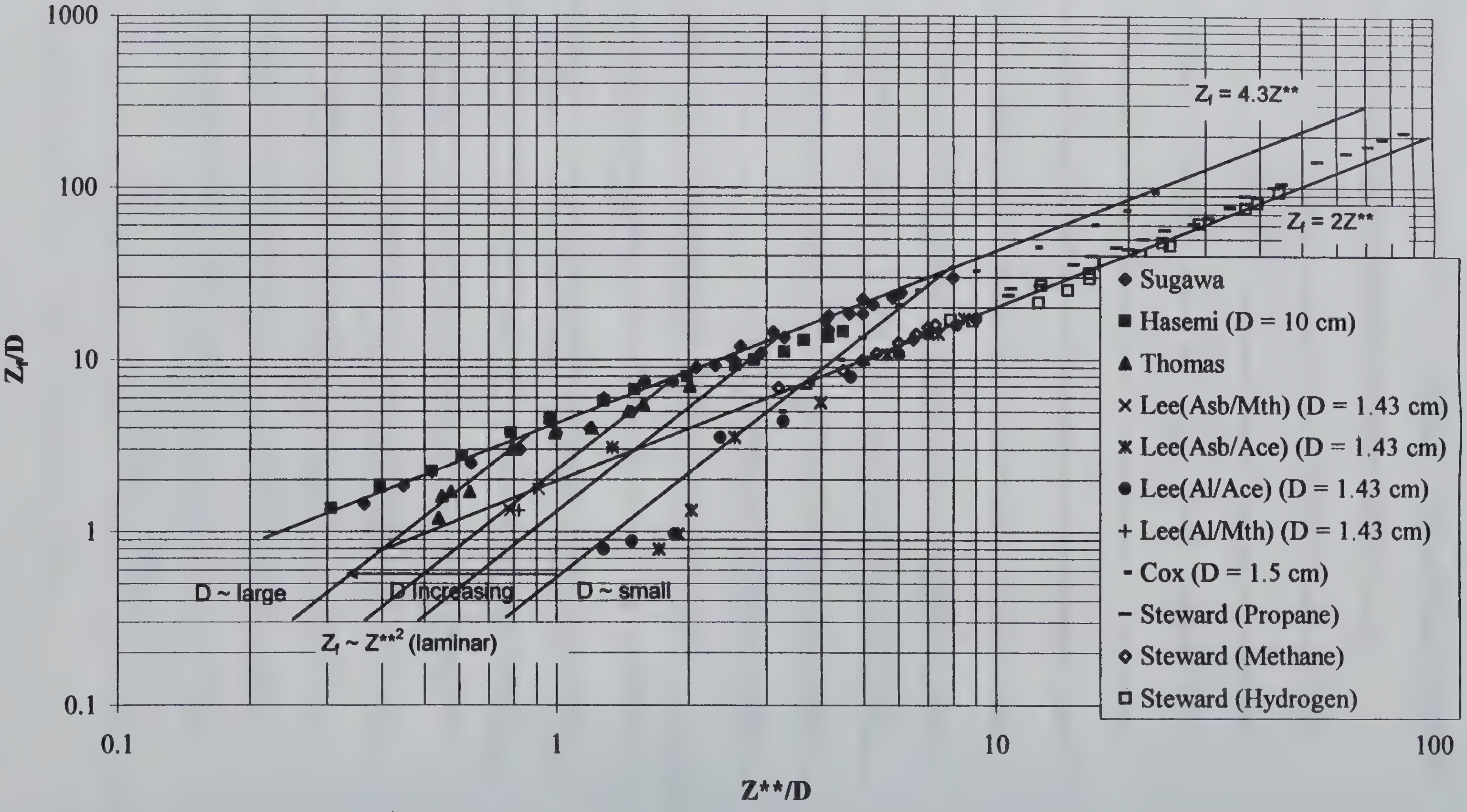

As was the case with the data presented by Zukoski in Figure 6 for axisymmetric flame height, sources having large widths or diameters tend to conglomerate at the top of the data range while those with small diameters or widths are found near the bottom of the range. In other words, for a given Z_f/D "large" sources require less energy release rate per diameter or width, Z**/D, than "small" sources. Thus, diameters or widths will increase when travelling along a constant Z_f/D from right to left. This effect is not that important for large Z_f/D ratios found on the upper right section of the graph where Z** is the dominant term and D has a minimal effect. However, for short flames found on the lower left section of the graph the width, D, is the dominant parameter and this effect is extremely important when determining whether or not data is laminar or turbulent.

One of the problems encountered when developing our empirical correlations was the possibility of encountering laminar flame height data. Our theoretical correlations were developed for purely turbulent data in order to take advantage of all the assumptions listed at the beginning of the theory section. If laminar data were to contaminate the data pool it could throw off our empirical constants because assumptions (1) – (3) would no longer be valid.

If laminar data is present it will more than likely be found on the right side of the data range where the widths are predominantly small. Fluid flow is a function of the Reynolds Number, $\mathrm{Re} = \frac{Dv^2}{\nu}$. For a given fluid flow and viscosity the smaller the width the better the chance of encountering laminar data. Roper [7] [8] details how to predict laminar flames based on nozzle or fuel source size and developed a correlation for laminar data which has Z**/D raised to the 2/3 power. Cox [9] used this correlation to fit some of his own data which he specifies to be laminar. Cox's laminar fit, on Figure 10, is the first line all the way to the right of the others that comes off of the two linear fits discussed earlier. The other lines are drawn with different coefficients but the same slope to pick up other possible laminar data. Thus laminar data, if present at all, would be found on the right side of the data range. For this reason our correlation, found on Figure 11, was placed on the upper left of the data range.

Figure 11 shows our correlation of flame height for a line source. The correlation is developed by using the same profile constant, C, from axisymmetric flame height and solving for the entrainment constant by choosing a "middle of the road" data point from Figure 11. Rectangular theory, which will be presented in more detail later, says that the profile constant should be the same for both of these extreme cases.

General rectangular flame height equation:

$$\frac{\dot{Q}}{\rho\sqrt{g}c_pT_oA^{3/2}B} = Q^*_{\mathrm{mod}} = C_3\frac{\Psi^{3/2}}{(1-\chi_r)}\left(\frac{Z_f}{A}\right)^{1/2}\left(1+C_{2a}\frac{Z_f}{A}\right)\left(1+C_{2b}\left(\frac{A}{B}\right)\frac{Z_f}{A}\right)$$

The two subscripts, a and b, for the C_2 constant are required because the rate of entrainment on two different size lengths is not necessarily the same. Where a represents the rate of entrainment on the short side and b the long side. In addition, A represents the short side and B represents the long side.

For the axisymmetric case A=B:

Figure 11: Dimensionless Flame Height Equation for the Infinite Line

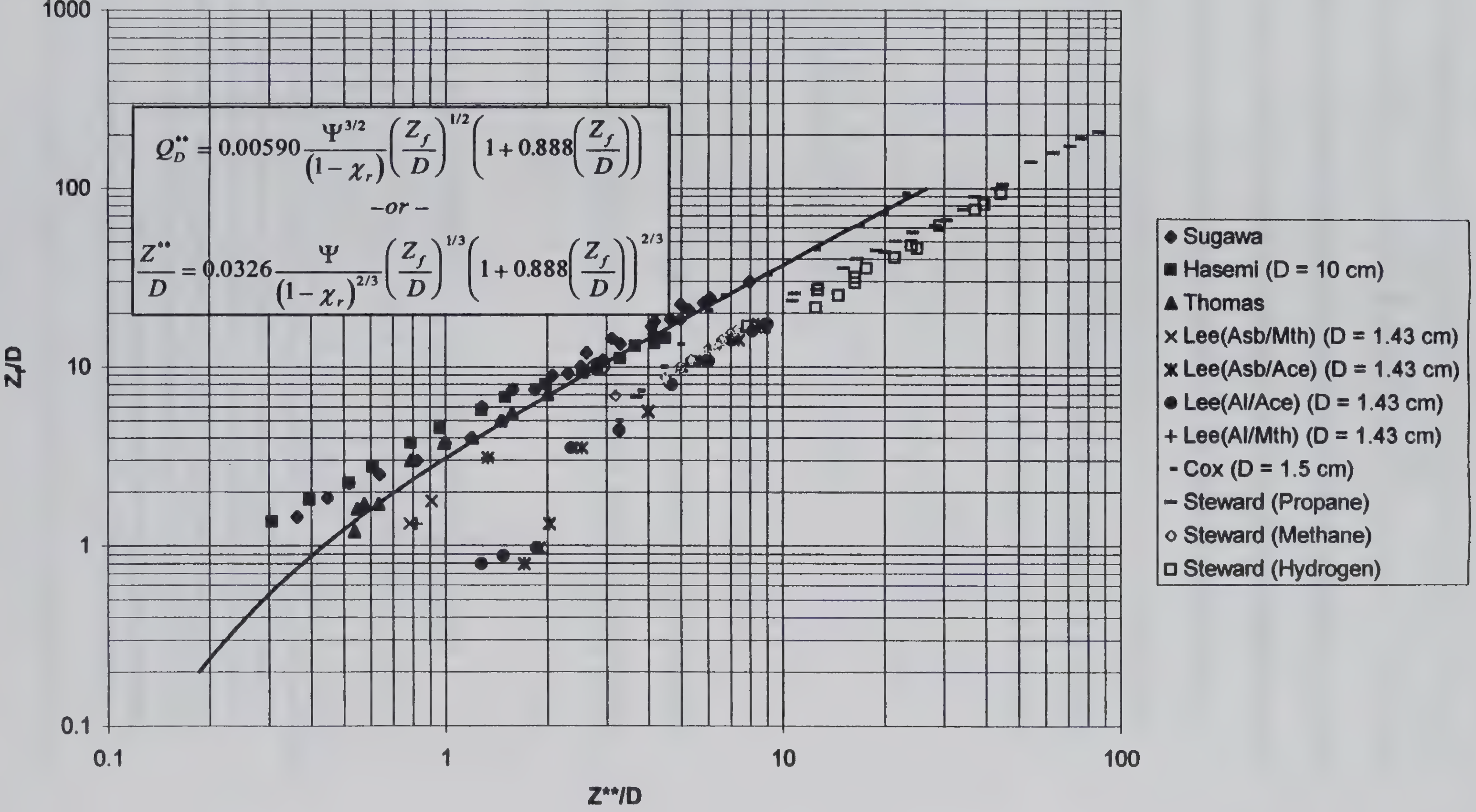

$$Q_D^* = C_3 \frac{\Psi^{3/2}}{(1-\chi_r)} \left(\frac{Z_f}{D}\right)^{1/2} \left(1 + C_2 \frac{Z_f}{D}\right)^2$$

As expected, this is the same equation developed for axisymmetric flame height. Both C_3 and C_2 should match axisymmetric "fitted" values. Note that if the two sides of the rectangle are equivalent, as in the axisymmetric case, C_{2a} will be the same constant as C_{2b}. As a result, the multiplication of these two terms will simply be denoted C_2. In addition, because there is no longer a difference in length between A and B the two terms have both been denoted D.

For the infinite line source A<<B:

$$Q_D^{**} = C_3 \frac{\Psi^{3/2}}{(1-\chi_r)} \left(\frac{Z_f}{D}\right)^{1/2} \left(1 + C_{2a} \frac{Z_f}{D}\right)$$

The third set of parentheses on the RHS of the equation reduces to one. In addition, the $A^{3/2}$ term found on the LHS of the rectangular flame height equation becomes minimal when compared to B and thus drops out. Therefore, Q_{mod}^* turns into Q_D^*.

Comparing the two equations, (A=B and A<<B), it is obvious that the profile constant, C_3, should be the same for both the axisymmetric and infinite line flame height correlations. Recall that we have used the axisymmetric constant to develop our linear flame height correlation rather than vice-versa because we felt more comfortable with the data available for this source. Note that the entrainment constants for the two equations are not the same.

To solve for the entrainment constant C_2 we set C_3 equal to 0.152 from the axisymmetric flame height correlation and pick a point from Figure 11. The chosen point is located in the center of the top cluster of data. Reasons for picking the point here were covered earlier. Recall that the chances of correlating only turbulent data are the best at the top of the data range.

Table 5: Infinite Line Flame Height Data Fit Point

Q_D^{**}	$\frac{Z_f}{D}$
4.75	10.0

Solving for C_2 knowing $C_3 = 0.152$:

$$\begin{aligned}4.75 &= 0.152(10)^{1/2}(1+C_2(10))\\ 9.88 &= 1+10C_2\\ C_2 &= 0.888\end{aligned}$$

Plugging C_2 and the axisymmetric, flame height, profile constant into the infinite line, flame height equation yields:

$$Q_D^{**} = 0.00590\frac{\Psi^{3/2}}{(1-\chi_r)}\left(\frac{Z_f}{D}\right)^{1/2}\left(1+0.888\left(\frac{Z_f}{D}\right)\right)$$

4.11 Infinite Line Entrainment

Figure 12 shows two possible near field entrainment equations for the infinite line. The bottom correlation was developed by using the same profile constant developed for the axisymmetric entrainment equation and the same entrainment constant from the linear flame height equation, Figure 11. The axisymmetric, entrainment, profile constant was put into this equation for the same reasons outlined

Figure 12: Near Field Entrainment Equations for the Infinite Line
$X_r = 30\ \%$

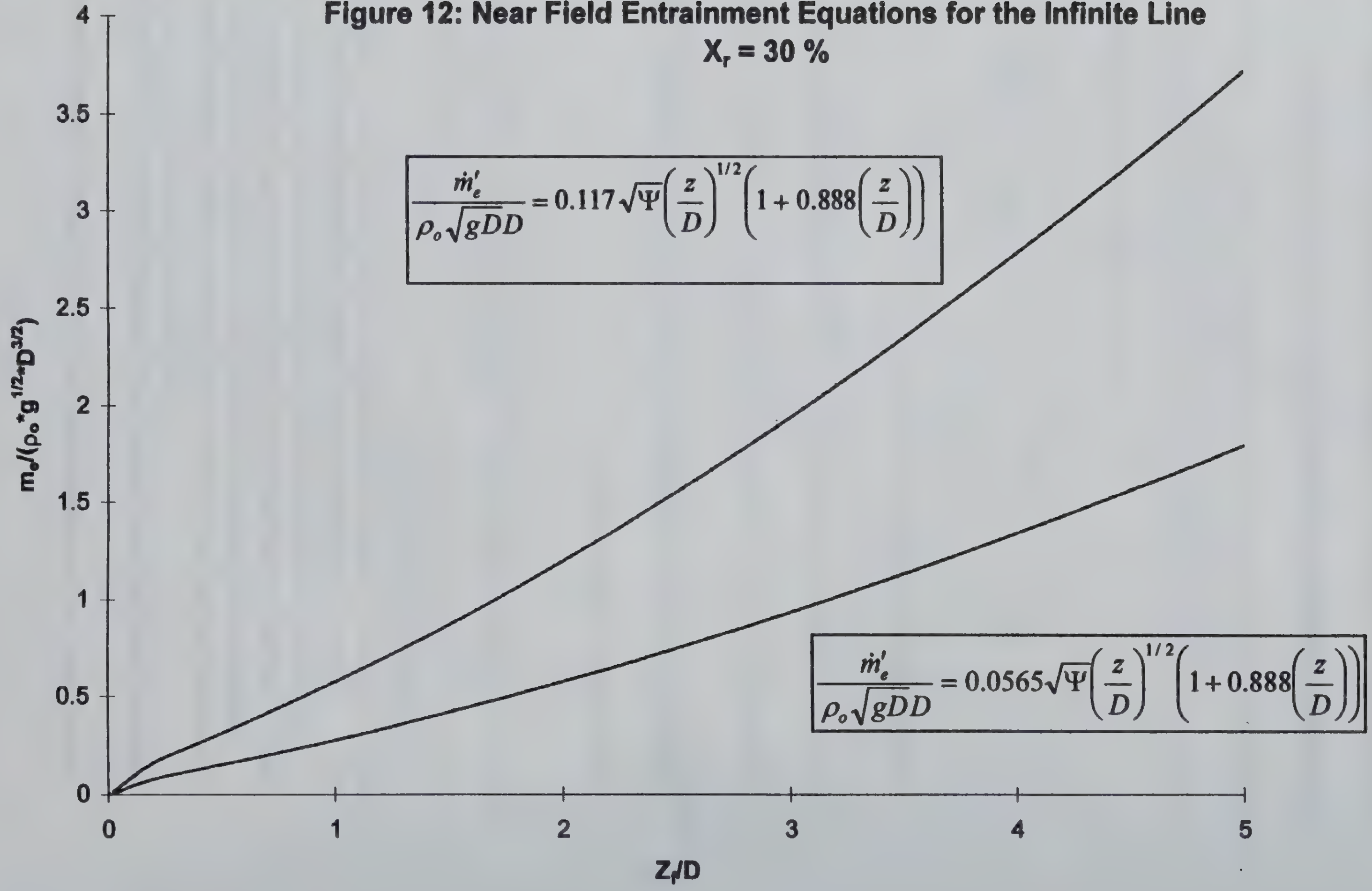

above for substituting the axisymmetric, flame height, profile constant into the linear flame height correlation.

The top correlation was developed by keeping the same entrainment coefficient but determining a new profile constant based on one data point extracted from Cox [9]. Unfortunately, we were forced to more or less fabricate this data point because to the best of our knowledge no other reliable data was available. The first step in creating our mock entrainment point was to take the lowest point on a graph of mass flux in a thermal plume by Cox [9]. Our hopes are that this point is at the flame's tip or just slightly above the flame.

$$\frac{m_l}{Q_l} = 0.0055$$

$$\frac{z}{Q_l^{2/3}} = 0.03$$

To get a ballpark value for Q_l, because none were explicitly reported, 100 kW was chosen which corresponds to the average visible flame height for turbulent flames on Figure 2 of Cox's paper.

Thus:

$$m_l = 0.0055(100) = 0.55 \,{}^{kg}\!\big/_{s \cdot m}$$

$$z = 0.03(100)^{2/3} = 0.647m$$

Making the terms dimensionless yields:

$$\frac{\dot{m}'_e}{\rho_o\sqrt{gD}D} = \frac{0.55}{1.21\sqrt{9.81}(0.015)^{3/2}} = 78.9$$

$$\frac{Z_f}{D} = \frac{0.647}{0.015} = 43.1$$

Inserting the data point into the linear entrainment equation along with the value of C_2 developed from our flame height correlation and solving for C_1:

$$\frac{\dot{m}'_e}{\rho_o\sqrt{gDD}} = C_1\sqrt{\Psi}\left(\frac{z}{D}\right)^{1/2}\left(1+C_2\left(\frac{z}{D}\right)\right)$$
$$78.9 = \mathrm{C}_1(2.615)\sqrt{43.1}(1+0.888(43.1))$$
$$\mathrm{C}_1 = 0.117$$

Hopefully, these two correlations found on two totally different premises represent the upper and lower bounds of the uncertainty for our entrainment correlation. No data exist in the flame zone to verify either of the correlations.

The process of converting far field infinite line entrainment into near field terms is detailed below. Recall the equation for far field entrainment, (16), from section 3.4.1:

$$\frac{\dot{m}'_e}{\rho_o\sqrt{gz}z} = .\sqrt{\pi}C_vC_l(Q_Z^{**})^{1/3}; Q_Z^{**} = \left(\frac{Z^{**}}{z}\right)^{3/2}$$
$$-or-$$
$$\frac{\dot{m}'_e}{\rho_o\sqrt{gz}z} = \sqrt{\pi}C_vC_l\left(\frac{Z^{**}}{z}\right)^{1/2}$$

Convert far field entrainment into near field terms by multiplying both sides of the equation by $Z^{3/2}$ and dividing both sides of the equation by $D^{3/2}$.

$$\frac{\dot{m}'_e}{\rho_o\sqrt{gD}\,D} = .\sqrt{\pi}C_vC_l\left(\frac{Z^{**}}{D}\right)^{1/2}\left(\frac{z}{D}\right)$$
$$-\ or\ -$$
$$\frac{\dot{m}'_e}{\rho_o\sqrt{gD}\,D} = \sqrt{\pi}C_vC_l(Q_D^{**})^{1/3}\left(\frac{z}{D}\right); Q_D^{**} = \left(\frac{Z^{**}}{D}\right)^{3/2}$$

Applying these correlations to the near field, as was done in the axisymmetric case, makes little sense because we are not sure whether the near field correlations are reasonable.

The five tables below are a compilation of all of the theoretical and empirical constants developed thus far. Several key points will be noted.

Table 6: Far Field Correlations

Dimensionless Variable	Axisymmetric	Infinite Line
B	$\left(\frac{6}{5}\alpha\right)\zeta$ 0.118ζ	$\left(\frac{2}{\sqrt{\pi}}\alpha\right)\zeta$ 0.103ζ
W	$\left[\left(\frac{25}{24\pi}\right)\left(\frac{\beta+1}{\beta}\right)\alpha^{-2}(1-\chi_r)\right]^{1/3}\zeta^{-1/3}$ $4.17(1-\chi_r)^{1/3}\zeta^{-1/3}$	$\left[\left(\frac{\beta+1}{2\beta}\right)^{1/6}\alpha^{-1/3}(1-\chi_r)^{1/3}\right]$ $2.3(1-\chi_r)^{1/3}\zeta^{0}$
Φ	$\left[\frac{2}{3}\left(\frac{25}{24\pi}\right)^{2/3}\frac{(\beta+1)^{2/3}}{\beta^{-1/3}\alpha^{4/3}}(1-\chi_r)^{2/3}\right]\zeta^{-5/3}$ $10.58(1-\chi_r)^{2/3}\zeta^{-5/3}$	$\left[\frac{(\beta+1)^{1/3}}{2^{5/6}\beta^{-1/6}}\alpha^{-2/3}(1-\chi_r)^{2/3}\right]\zeta^{-1}$ $3.3(1-\chi_r)^{2/3}\zeta^{-1}$
α	0.098	0.091
β	0.913	0.845

Theoretically, if the entrainment coefficient, α, is the same for both the combusting zone and the smoke plume, Tables 6 and 5 respectively, the plume will expand at a faster rate in the far field for both sources. Yokoi [3] documents this behavior in Figure 13. (The empirical solutions do not support the constancy of α as it is much higher in the combusting region.) The assumption of a constant α and similarity profiles close to the fuel source can not be correct.

Table 7: Near Field Correlations

Dimensionless Variable	Axisymmetric	Infinite Line
B	$\left(\frac{4}{5}\alpha\right)\zeta$ 0.176ζ	$\left(\frac{4\alpha}{3\sqrt{\pi}}\right)\zeta$ 0.272ζ
W	$\sqrt{\frac{4}{3}\Psi}\zeta^{1/2}$ $0.720\sqrt{\Psi}\zeta^{1/2}$	$\sqrt{\Psi}\zeta^{1/2}$ $0.800\sqrt{\Psi}\zeta^{1/2}$
Φ	2Ψ 0.347Ψ	$\sqrt{2}\Psi$ 0.450Ψ
α	0.22	0.590
β	1	1

Figure 13: Qualitative Depiction of Plume Width in both the Far and Near Fields, Yokoi [3]

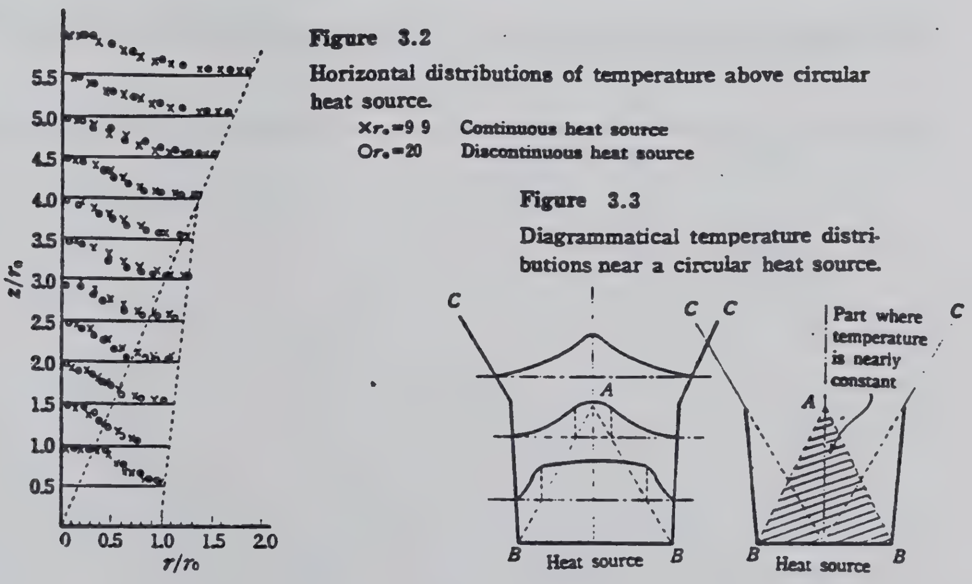

Figure 3.2

Horizontal distributions of temperature above circular heat source.

$\times r_0 = 9.9$ Continuous heat source

$\circ r_0 = 20$ Discontinuous heat source

Figure 3.3

Diagrammatical temperature distributions near a circular heat source.

Table 8: Far Field Entrainment Correlations

Axisymmetric	Infinite Line
$\frac{\dot{m}_e}{\rho_o\sqrt{gz}z^2} = \pi C_v C_l^2 \zeta^{-5/6}$	$\frac{\dot{m}_e'}{\rho_o\sqrt{gz}z} = \sqrt{\pi} C_v C_l \zeta^{-1/2}$
$\frac{\dot{m}_e}{\rho_o\sqrt{gz}z^2} = 0.169\zeta^{-5/6}$	$\frac{\dot{m}_e'}{\rho_o\sqrt{gz}z} = 0.647\zeta^{-1/2}$

Table 9: Flame Height Correlations

Axisymmetric	Infinite Line
$Q_D^* = \left(\frac{Z^*}{D}\right)^{5/2} = \frac{\pi}{2\sqrt{3}} \frac{\Psi^{3/2}}{(1-\chi_r)} \left(\frac{Z_f}{D}\right)^{1/2} \left(1+\frac{8}{5}\alpha\left(\frac{Z_f}{D}\right)\right)^2$	$Q_D^{**} = \left(\frac{Z^{**}}{D}\right)^{3/2} = \frac{\sqrt{\pi}\Psi^{3/2}}{2(1-\chi_r)} \left(\frac{Z_f}{D}\right)^{1/2} \left(1+\frac{8\alpha}{3\sqrt{\pi}}\left(\frac{Z_f}{D}\right)\right)$
$Q_D^* = 0.00590\frac{\Psi^{3/2}}{(1-\chi_r)} \left(\frac{Z_f}{D}\right)^{1/2} \left(1+0.357\left(\frac{Z_f}{D}\right)\right)^2$	$Q_D^{**} = 0.00590\frac{\Psi^{3/2}}{(1-\chi_r)} \left(\frac{Z_f}{D}\right)^{1/2} \left(1+0.888\left(\frac{Z_f}{D}\right)\right)$

Further justification for using the same empirical profile constant developed from axisymmetric data for the infinite line stems from the fact that the theoretical constants, $\frac{\pi}{2\sqrt{3}}$ and $\frac{\sqrt{\pi}}{2}$, are almost equal in the above equations for Q_D^* and Q_D^{**}.

Table 10: Near Field Entrainment Correlations

Axisymmetric	Infinite Line
$\frac{\dot{m}_e}{\rho_o\sqrt{gD}D^2}=\frac{\pi}{2\sqrt{3}}\sqrt{\Psi}\left(\frac{z}{D}\right)^{1/2}\left(1+\frac{8}{5}\alpha\left(\frac{z}{D}\right)\right)^2$	$\frac{\dot{m}'_e}{\rho_o\sqrt{gD}D}=\frac{1}{2}\sqrt{\pi}\sqrt{\Psi}\left(\frac{z}{D}\right)^{1/2}\left(1+\frac{8\alpha}{3\sqrt{\pi}}\left(\frac{z}{D}\right)\right)$
$\frac{\dot{m}_e}{\rho_o\sqrt{gD}D^2}=0.0565\sqrt{\Psi}\left(\frac{z}{D}\right)^{1/2}\left(1+0.357\left(\frac{z}{D}\right)\right)^2$	$\frac{\dot{m}'_e}{\rho_o\sqrt{gD}D}=0.117\sqrt{\Psi}\left(\frac{z}{D}\right)^{1/2}\left(1+0.888\left(\frac{z}{D}\right)\right)$ $\frac{\dot{m}'_e}{\rho_o\sqrt{gD}D}=0.0565\sqrt{\Psi}\left(\frac{z}{D}\right)^{1/2}\left(1+0.888\left(\frac{z}{D}\right)\right)$

Note – The two empirical correlations in the infinite line column represent the upper and lower limits of near field entrainment.

Chapter 6 Rectangular Theory

6.1 Introduction

Having developed empirical correlations for the infinite line and axisymmetric source it should be possible to determine correlations for source geometries between these two extremes. More specifically, this section utilizes the knowledge gained in previous chapters to develop correlations for temperature, entrainment and flame height for rectangular sources. The following studies were not exhaustive nor meant to be thorough. Their purpose for being was to illustrate the possibility of subtending simplified 2-D theory to a 3-D problem. Hopefully, the following discussion will spark interest in this possibility.

6.2 Assumptions

All of the assumptions listed in section 3.2 are carried over into this chapter. In addition, we have added two more.

(1) Plume cross section maintains rectangular shape.

(2) $$\frac{W^2}{\Phi\zeta} = \frac{w_m^2}{g\left(\frac{T_m - T_o}{T_o}\right)z} = \text{constant} \qquad (1)$$

The implication of the first assumption is that the plume will keep its original geometry by maintaining crisp corners as it ascends. In reality, the plume will become more and more rounded as it rises away from its source. The hazards appreciated by incorporating assumption (1) are minor. The second assumption was actually proven for both the axisymmetric and infinite line source, and therefore assumed to be true here.

In addition, we will utilize the following Gaussian profiles and set β=1:

$$\frac{\Phi}{\Phi_m}=\frac{w}{w_m}=\exp\left[-\left(\frac{y}{a}\right)^2\right]\exp\left[-\left(\frac{x}{b}\right)^2\right] \qquad (2)$$

6.3 Far Field Non-Combusting Plume Temperature

Assume an appropriate point source energy equation:

$$\dot{Q}(1-\chi_r)=4\iint_{\infty}\rho_o c_p w(T-T_o)dydx \qquad (3)$$

Integrating this energy equation over ¼ of the source area and multiplying by 4 yields the amount of energy liberated over the entire plume cross section.

Substituting the above Gaussian profiles for vertical velocity and temperature into equation (3) yields:

$$\dot{Q}(1-\chi_r)=4\rho_o c_p\left(\frac{ab}{2}\right)w_m\Phi_m T_o\iint_{\infty}e^{-y'^2}e^{-x'^2}dy'dx'$$

$$\text{where } y'=\sqrt{2}\frac{y}{a} \text{ and } x'=\sqrt{2}\frac{x}{b}$$

Using the following relationship, $\int_0^{\infty}e^{-x^2}dx=\frac{\sqrt{\pi}}{2}$, the integrals can be solved:

$$\dot{Q}(1-\chi_r)=\frac{\pi}{2}\rho_o c_p w_m\Phi_m T_o ab$$

$$-or-$$

$$\frac{\dot{Q}(1-\chi_r)}{\rho_o c_p T_o\sqrt{g}}=\frac{\pi}{2}\frac{w_m}{\sqrt{g}}\Phi_m ab \qquad (4)$$

Recall equation (1) from section 6.2:

$$\frac{w_m^2}{g\left(\frac{T_m - T_o}{T_o}\right)z} = C_1^2$$

Substituting equation (1) into equation (4) yields:

$$\frac{\dot{Q}(1-\chi_r)}{\rho_o c_p T_o \sqrt{g}} = \frac{\pi}{2} C_1 \Phi_m^{\ 3/2} z^{1/2} ab$$

Now let:

$$a = \frac{A}{2} + C_2 z$$
$$b = \frac{B}{2} + C_2 z \qquad (5)$$

Substituting for a and b:

$$\frac{\dot{Q}(1-\chi_r)}{\rho_o c_p T_o \sqrt{g} A^{3/2} B} = \frac{\pi}{2} C_1 \Phi_m^{\ 3/2} \left(\frac{z}{A}\right)^{1/2} \left(\frac{1}{2} + C_2 \frac{z}{A}\right)\left(\frac{1}{2} + C_2 \frac{z}{B}\right)$$

$$-or-$$

$$Q^*_{\text{mod}}(1-\chi_r) = \frac{\pi}{8} C_1 \Phi_m^{\ 3/2} \left(\frac{z}{A}\right)^{1/2} \left(1 + 2C_2 \frac{z}{A}\right)\left(1 + 2C_2 \frac{z}{B}\right)$$

$$Where\ Q^*_{\text{mod}} = \frac{\dot{Q}}{\rho_o c_p T_o \sqrt{g} A^{3/2} B} \qquad (6)$$

Note, Q^*_{mod} becomes Q^*_D or Q^{**}_D in either the axisymmetric or infinite line limit respectively.

Solve for Φ_m:

$$\Phi_m = \left(\frac{8(1-\chi_r)}{\pi C_1}\right)^{2/3} \left\{ Q^{*2/3}_{\text{mod}} \Big/ \left[\left(\frac{z}{A}\right)^{1/2} \left(1 + 2C_2 \frac{z}{A}\right)\left(1 + 2C_2 \frac{z}{B}\right)\right]^{2/3} \right\} \qquad (7)$$

The above equation is graphed on Figure 14 as $y = Cx^{-1}$.

Where:

$$
\begin{aligned}
y &= \Phi_m \\
C &= \left(\frac{8(1-\chi_r)}{\pi C_1} \right)^{2/3} \\
x^{-1} &= \left\{ Q_{\mathrm{mod}}^{*2/3} \Big/ \left[\left(\frac{z}{A} \right)^{1/2} \left(1 + 2C_2 \frac{z}{A} \right) \left(1 + 2C_2 \frac{z}{B} \right) \right]^{2/3} \right\}
\end{aligned}
\qquad (8)
$$

Data points of various aspect ratios ranging from 0.2 to 1.0 were taken from Hasemi [1]. In order to convert Hasemi's data points into our format a value for the entrainment constant, C_2, had to be assumed. Far away from the source, $\left[\frac{z}{A} \cong 6\sqrt{\frac{B}{A}} \right]^{[3]}$, the rectangular plume will resort to point source axisymmetric behavior. Therefore, C_2 was assumed to equal $\frac{6}{5}\alpha$ which was taken from axisymmetric plume theory developed earlier in section 3.5. The entrainment coefficient, α, was taken as 0.11 from Zukoski [20]. However, our value of 0.098 could just have easily been used. Recall that the difference between these two values results from the inclusion of a 20 % radiation loss when determining our value.

In the combustion region, temperature remains constant. The value on Figure 13 falls below temperatures for the infinite line and above temperatures for the axisymmetric source.

In the far field, a best fit of the representative data yields a coefficient of 2.3 which is slightly higher than the coefficient calculated by manipulation of equation

Figure 14: Dimensionless Temperature vs. Height for a Rectangular Source

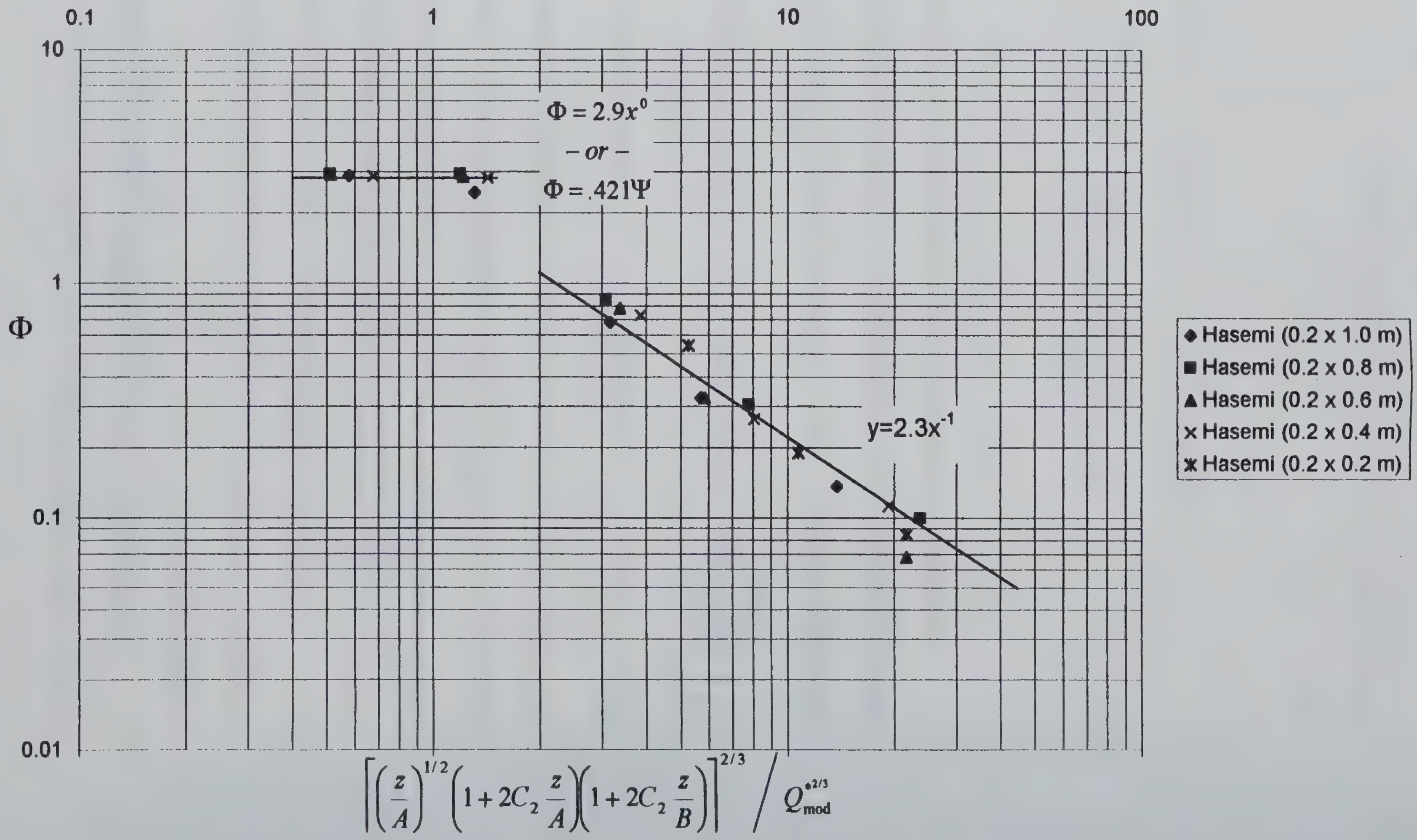

(7). As B approaches A in the far field equation (7) reduces to an axisymmetric expression for far field temperature. This is rather fortuitous because we can then use the far field axisymmetric constant for temperature, C_T, to determine C_1 found in the profile constant of equation (7). The process is illustrated below.

Setting A = B into equation (7) yields:

$$\Phi_m \to \frac{(1-\chi_r)^{2/3}(8Q^*_{\mathrm{mod}})^{2/3}}{(\pi C_1)^{2/3}\left(z/B\right)^{5/3}(2C_2)^{4/3}} \tag{9}$$

Setting A = B into equation (6) gives:

$$Q^*_{\mathrm{mod}} = \left(\frac{Z^*}{B}\right)^{5/2} \tag{10}$$

Substituting equation (10) into equation (9) gives:

$$\Phi_m \to \frac{4(1-\chi_r)^{2/3}\left(Z^*/z\right)^{5/3}}{(\pi C_1)^{2/3}(2)^{4/3}C_2^{\;4/3}} = C_T\left(\frac{Z^*}{z}\right)^{5/3}$$

C_1 can now be solved by setting C_T equal to 9.115 from Yokoi [3]; C_2 equal to $6/5\alpha$ from axisymmetric far field theory; α equal to 0.11 from Zukoski [20]; and χ_r equal to 30 %. The constant, C, in equation (8) can now be solved by substituting the value for C_1. C is found to equal 1.54; a value slightly lower than the fitted value of 2.31. The discrepancy between the calculated constant and the fitted constant could be attributed to the fact that β was assumed equal to one here in the far field. Because $\alpha = 0.11$ was determined from $\beta \neq 1$provisions should have been made to include β in our calculations, or a new α should have been calculated for β = 1. If either of these methods were carried out our calculated C should fall a little closer to the fitted value.

6.4 Far Field Entrainment

An expression for rectangular entrainment can be assumed:

$$\dot{m}_e = 4\iint \rho_o w\,dy\,dx \tag{11}$$

Substituting Gaussian profiles into the above equation yields:

$$\dot{m}_e = 4\rho_o w_m ab \iint e^{-\frac{y^2}{a^2}} e^{-\frac{x^2}{b^2}} \frac{dy}{a}\frac{dx}{b}$$

Solving the integrals gives:

$$\dot{m}_e = 4\rho_o w_m ab \frac{\sqrt{\pi}}{2}\frac{\sqrt{\pi}}{2}$$

$$-\mathit{or}-$$

$$\dot{m}_e = \pi \rho_o w_m ab \tag{12}$$

6.5 Flame Height

As before, an equation for flame height can be developed by multiplying a near field entrainment equation, which includes provisions for source geometry, by a parameter containing ΔH_a.

First, the general entrainment equation, (12), is modified through equation (1):

$$\dot{m}_e = \pi \rho_o C_1 \sqrt{g \frac{T_m - T_o}{T_o} z}\, ab \tag{13}$$

From equation (5) for a and b and the solution for dimensionless temperature in the combustion zone developed below, an expression for near field entrainment can be ascertained.

Assume an appropriate energy equation in the combustion zone:

$$\rho_o c_p \frac{d}{dz}\iint w(T-T_o)dxdy = (1-\chi_r)\iint \dot{Q}'''dxdy = \left(\frac{1}{4}\right)\frac{d\dot{m}_e}{dz}\cdot\frac{\Delta H_c}{ns}(1-\chi_r) \qquad (14)$$

Note that the relation between energy release rate and air entrainment was shown earlier in section 3.7.1 equation (33) and section 3.7.2 equation (42).

In order to solve for Φ integrate the LHS with the appropriate Gaussian profiles and ignore effects at the source, z = 0. Integrating the entrainment derivative on the RHS and substituting from equation (12) yields:

$$\rho_o c_p w_m \Phi_m T_o \frac{ab}{2}\frac{\pi}{4} = \frac{1}{4}\rho_o \pi w_m ab\left(\frac{\Delta H_c}{ns}\right)(1-\chi_r)$$

$$-or-$$

$$\Phi = 2\left(\frac{\Delta H_c}{nsc_pT_o}\right)(1-\chi_r) = 2\Psi \qquad (15)$$

Substituting the values for a and b from equation (5) and Φ from equation (15) into equation (13) yields:

$$\dot{m}_e = \pi\rho_o C_1\sqrt{gz}\sqrt{2\Psi}\left(\frac{A}{2}+C_2 z\right)\left(\frac{B}{2}+C_2 z\right)$$

Simplifying yields an equation for near field entrainment:

$$\frac{\dot{m}_e}{\rho_o\sqrt{g}A^{3/2}B}=\left[\frac{\pi C_1\sqrt{2\Psi}}{4}\right]\left(\frac{z}{A}\right)^{1/2}\left(1+2C_2\frac{z}{A}\right)\left(1+2C_2\frac{z}{B}\right)$$

$$-\,or\,-$$

$$\frac{\dot{m}_e}{\rho_o\sqrt{g}A^{3/2}B}=C_3\left(\frac{z}{A}\right)^{1/2}\left(1+2C_2\frac{z}{A}\right)\left(1+2C_2\frac{z}{B}\right) \qquad (16)$$

$$Where\ C_3=\left[\frac{\pi C_1\sqrt{2\Psi}}{4}\right]$$

Since $\dot{m}_e\left(Z_f\right)=ns\dot{m}_f=ns\cdot\dfrac{\dot{Q}}{\Delta H_c}$, the near field entrainment equation is easily converted into flame height.

$$\frac{\dot{Q}}{\rho_o c_p T_o\sqrt{g}A^{3/2}B}=C_3\sqrt{\pi}\left(\frac{Z_f}{A}\right)^{1/2}\left(1+2C_2\frac{Z_f}{A}\right)\left(1+2C_2\frac{Z_f}{B}\right)\cdot\frac{\Delta H_c}{nsc_pT_o}$$

$$-\,or\,-$$

$$Q^{*}_{\mathrm{mod}}=C_3\frac{\Psi^{3/2}}{\left(1-\chi_r\right)}\left(\frac{Z_f}{A}\right)^{1/2}\left(1+2C_2\frac{Z_f}{A}\right)\left(1+2C_2\left(\frac{A}{B}\right)\frac{Z_f}{A}\right) \qquad (17)$$

Because the profile constant, C_3, was set at 0.00590 for both the infinite line and axisymmetric sources we will use the same value for our rectangular solutions. The entrainment constant, C_2, was found by fitting the equation to a point in the center of the data range.

Table 11: Rectangular Flame Height Data Fit Point

Geometry	Q^{*}_{mod}	Z_f/A
(0.2 x 1.0 m)	1.3	4.7

Note that this point's geometry should have no "lasting" effect on the flame height correlation thereby favoring sources of (0.2 x 1.0 m).

The data used to fit this correlation was taken from Hasemi [1] and includes aspect ratios ranging from 0.1 to 1. The data was plotted directly onto Figure 15, thus avoiding any assumptions or manipulation.

Figure 15: Dimensionless Flame Height for Rectangular Sources

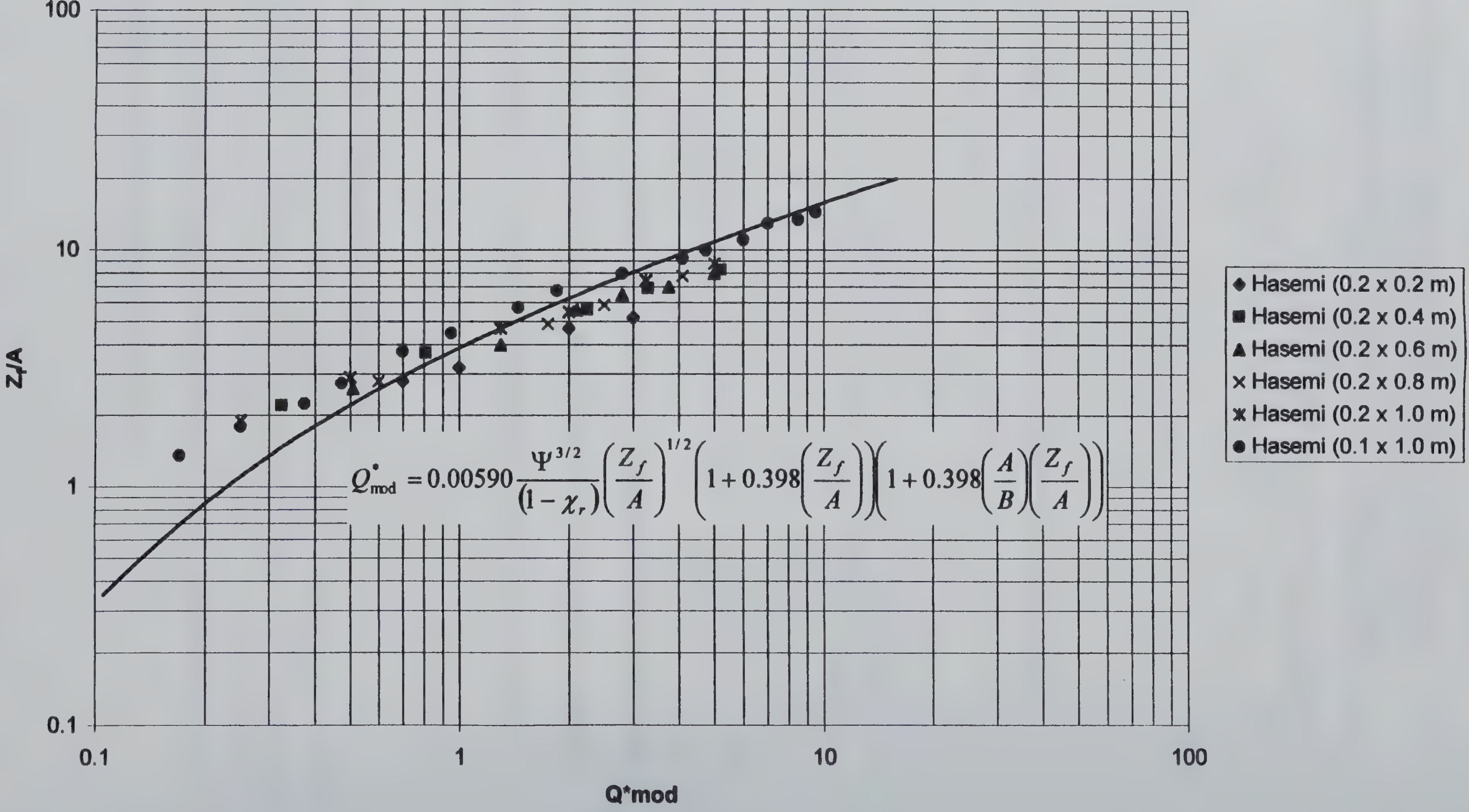

Chapter 7 Conclusion

Empirical correlations were developed for the infinite line for temperature, velocity, and plume width in both the far and near fields through dimensionless plots. Correlations were also developed for the axisymmetric source for all of the above characteristics. However, due to the acceptance of previous correlations and data comparisons of these correlations were not made on dimensionless plots.

Point and line source theory was modified with a diameter correction to determine flame height and near field entrainment correlations for the axisymmetric and infinite line source respectively. For the axisymmetric source, results were consistent with data and n was found to equal 9.6. For the line source an empirical correlation for flame height was developed. However, no entrainment data was available for this source making it impossible to develop an exact entrainment correlation. As a result, two entrainment correlations were created that hopefully embody the upper and lower bounds of a “true” entrainment equation.

The theory and empirical correlations developed for axisymmetric and infinite line solutions were applied to rectangular sources in a fairly rough manner. Future research should center around refining this theory and developing more data for rectangular sources. In addition, entrainment data for the infinite line source would prove extremely valuable.

References

1. Hasemi, Y. & Nishita, M., Fuel shape effect on the deterministic properties of turbulent diffusion flames. *In Proc. 2nd Int. Symp. on Fire Safety Science*. Hemisphere, New York, 1988, pp. 275-284

2. Lee, S. L. & Emmons, H. W., A study of natural convection above a line fire. *J. of Fluid Mech.*, 11 (1961) pp. 353-368

3. Yokoi, S., Study on the prevention of fire spread caused by hot upward current. Building Research Report 34, Japanese Ministry of Construction, 1960

4. Rouse, H., Yih, C. S. & Humphries, H. W., Gravitational convection from a boundary source. *Tellus*, 4 (1952) pp. 202 –210

5. Thomas P. H., The size of flames from natural fires. *In 9th Int. Symp. on Combustion*. Academic Press, New York, 1963, pp. 844-859

6. Steward, F. R., Linear flame heights for various fuels. *Combust. Flame*, 8 (1964) pp. 171 –178

7. Roper, F. G., The prediction of laminar jet diffusion flame sizes: part I. Theoretical Model. *Combust. Flame*, 91 (1992) pp. 226 –238

8. Roper, F. G., The prediction of laminar jet diffusion flame sizes: part II.

9. Yuan, L. & Cox, G., An experimental study of some line fires. *Fire Safety J.* 27 (1996) pp. 123- 139

10. Zukoski, E. E., Fluid dynamic aspects of room fires. *In Proc. 1st Int. Symp. on Fire Safety Science*. 1985, pp. 1-11

11. Sugawa, O., Yasushi, O. & Hirofumi, H., Fire induced flow in a clean room with downward vertical laminar flow.

12. Brodowicz, K. & Kierkus, K. T., Experimental investigation of laminar free-convection flow in air above horizontal wire with constant heat flux. *Int. J. Heat Mass Transfer*, 9 (1966) pp. 81 –94

13. Sugawa, O., Yasushi, O. & Satoh, H., Flame height from rectangular fire sources considering mixing factor. *In. Proc. 3rd Int. Symp. on Fire Safety Science*. pp. 435-444

14. McCaffrey, B., Flame heights. *SFPE Handbook of Fire Protection Engineering*, Sec. Ed., P. J. DiNenno, National Fire Protection Assoc., Quincy, MA, 1995

15. Heskestad, G., Fire plumes. ibid.

16. Delichatsios, M. A., Air entrainment into buoyant jet flames and pool fires. ibid.

16 a. Delichatsios, M. A., Air entrainment into buoyant jet flames and pool fires. *Comb. and Flame* 70 (1987) pp. 33-46

17. Drysdale, D., *An introduction to fire dynamics*. John Wiley and Sons Inc., 1992

18. McCaffrey, B. J., Some measurements of the radiative power output of diffusion flames. NBS Paper No WSS/CI 81-15, *Comb. Inst. Meeting*, Pullman, WA, 1981

19. McCaffrey, B. J., Momentum implications for buoyant diffusion flames. *Comb. and Flame* 52 (1983) pp. 149-167

20. Zukoski, E. E., Properties of fire plumes. *Combustion Fundamentals of Fire*, Ed. G. Cox, Academic Press, London, 1995

21. Taminini F., Reaction rates, air entrainment and radiation in turbulent fire plumes. *Comb. and Flame* 30 (1977) pp. 85-101

22. Morton, B. R., Sir Geoffrey Taylor, Turner, F.R.S. and J. S., Turbulent gravitational convection from maintained and instantaneous sources. *Proc. of the Royal Soc. Of London* 234. A. (1956)

23 Gupta, A. K., Kumar, S., Singh, B., One-dimensional mathematical modeling of enclosure fire dynamics. *Fire and Materials*, Vol. 12, No. 2 (1988)

24. Gupta, A. K., Kumar, S., Singh, B., Plume analysis above finite size fire sources. *Fire Safety Science- Proc. of the Third Int. Symp.*, pp. 445-454

25. Gupta, A. K., Fire plume-theories and their analysis. *J. of Applied Science*, Vol. 2(4) (1992-93) pp. 269-298

26. Gupta, A. K., Mathematical modeling of two-dimensional plume flows. *J. of Applied Science*, Vol. 3(1) (1994-94) pp. 19-33

27. Gupta, A. K., Transient analysis of fire plumes. *J. of Applied Fire Science*, Vol. 3(4) (1994-94) pp. 373-390

28. Gebhart, B., Pera, L., Schorr, A. W., Steady laminar natural convection plumes above a horizontal heat source. *Int. J. of Heat Mass Transfer* 13 (1970) pp. 161-171

29. Spalding, D.B., Cruddace, R. G., Theory of the steady laminar buoyant flow above a line heat source… *Int. J. Heat Mass Transfer* 3 (1961) pp. 55-59

30. Incropera, F. P., DeWitt, D. P., *Fundamentals of heat and mass transfer*. 3rd ed. John Wiley and Sons Inc., 1990 p. 6

31. McCaffrey, B. J., Purely buoyant diffusion flames: some experimental results. National Bureau of Standards, NSBIR 79-1910, (1979)

32. Tewarson, A., B., Generation of heat and chemical compounds in fires. *SFPE Handbook of Fire Protection Engineering*, Sec. Ed., P. J. DiNenno, National Fire Protection Assoc., Quincy, MA, 1995 pp. 3-76 to 3-78

33. McCaffrey, B. J., Purely buoyant diffusion flames: Some experimental results. NSBIR 79-1910, National Bureau of Standards, Washington, D. C., October 1979

34 Heskestad, G., A reduced-scale mass fire experiment. *Combustion and Flame* 83 (1991) pp. 293 – 301

35 Thomas, P. H., Webster, C. T., Raftery, M. M., Some experiments on buoyant diffusion flames. *Combustion and Flame* 5 (1961) pp. 359 – 367

Appendix A

Description of Experimental Apparatus and Procedures

Natural Convection Above a Line Fire
(Shao-Lin Lee)

- Temperature
- Flame Height

Experimental Apparatus

The burner is 78" long by .564" wide and .282" deep. A 1/4" diameter copper circular tube is soldered onto both sides of the length of the burner. The tube is filled with water and serves as a water cooling jacket. Fuel is fed into the bottom of the burner through six equally separated ports along the length of the burner. Such a configuration in conjunction with the "Steady Fuel Supply System" allows for equal filling and combustion of fuel in the channel burner. Both methyl alcohol and acetone are used as fuels, where the first fuel is used to produce a flame with little heat loss due to radiation and the latter produces the opposite effect.

The burner is housed in a "combustion cage" made out of wire mesh with dimensions of 4 feet wide, 8 feet long, 8 feet high and 3 feet above the laboratory floor. The base of the combustion cage is made out of 1/4" thick asbestos board and rests on a table. On either side of the channel burner, which runs down the length of the combustion cage, lie a 1/4" thick 18" wide piece of asbestos board. The asbestos board lies flat on the base of the combustion cage and is the exact length of the channel burner. Against each end of the side plates stands a vertical asbestos end plate 4 feet wide and 8 feet tall which serves to cut off the entrainment of air from the ends. At times the end plates are wrapped with aluminum foil to alter the effects of radiation.

Temperature measurements are made with a 40 inch piece of pure nickel resistance wire 0.002 inches in diameter. The resistance wire is suspended parallel to the channel burner between two metal poles and is stretched slightly to account for thermal elongation during the experiment.

Experimental Procedures

The combustion cage was centered in the middle of a large room measuring approximately 40 feet long, 25 feet wide, and 30 feet high. To insure a minimal amount of disturbance in the ambient air all detectable leaks around doors and windows for example were sealed with adhesive tape. In addition, local heating of certain areas by radiation from the sun was reduced by employing window curtains. Before each experiment at least one half hour was allowed for the air in the room to equilibrate.

Flame Height from Rectangular Fire Sources
(Sugawa, Satoh, & Oka)

- Flame Height

Experimental Apparatus

The gas diffusion burner contained fine sand as a diffuser in a rectangular stainless steel vessel. Propane with a monitored flow rate was used in the vessel. The authors report aspect ratios of 1:6, 1:8.8, 1:12, 1:17.8, 1:40, 1:60 however, no exact burner dimensions were given. In later tests, burner dimensions included 1 cm X 40 cm, 1 cm X 60 cm, 2 cm X 60 cm and 2 cm X 120 cm. Most likely the burners used in the first set of tests were of the same order of magnitude as those used in the second and third set of tests. The authors concluded that flame height is a function of HRR and practically independent of fuel and aspect ratio.

Experimental Procedures

Three minutes were allowed for flame heights to reach a quasi-steady state at which the flame height was recorded by four different methods.

- Infrared-imaged pictures
- judgments by eyes
- photographs
- video tape recordings

However, the data from the video tapes was primarily used to report flame heights in order to eliminate bias inherent in the other three methods.

Measurements of flame height issued form a single line burner were taken with and without both walls and floors. The data reported on my flame length graph is only from a burner on the floor and out in the open.

- Temperature
- Velocity

Experimental Apparatus

All of the experiments were performed in a "clean room" with dimensions of 9m long, 6.4m wide, and 3.2m high. A 22 cm/sec downward vertical flow was achieved as a direct result of the ventilation system which changed the air in the room 200 times/hr. The line burner was positioned just off-center at a height 78 cm above the free access floor.

The burner itself was 1cm wide by 85 cm long. Methanol was supplied to the burner at a constant rate of .37-.4 ml/sec. The delivery procedure was not documented nor is it deemed to be important.

Experimental Procedures

Combustion of the fuel was kept constant for about one hour before any data was recorded. Thirty three 0.32 mm diameter alumel-chromel thermocouples were spaced equally at 10 cm across a movable wire approximately three meters in length. The wire was moved horizontally and vertically so as to measures temperatures at different points of interest. Thermocouples were maintained at each position for approximately two to three minutes. Velocities were measured by a bi-directional tube measuring dynamic pressure which was also moved both horizontally and vertically. A smoke wire system was used to visualize where velocities were almost zero and indicate a balance between upward and downward flows. The wire was also used to indicate the size and position of eddies and flow patterns.

“Heat flux was calculated based on the consumption rate of the fuel and its heat of combustion at 25 ^{0}C to gaseous CO_2 and H_2O. The estimated heat flux was about 6 kW/m^2. This is the only HRR given by Sugawa, therefore I followed the author’s advice using an average value of the flow rates given and a HRR from Tewarson’s chapter in the SFPE Handbook.

Velocity measurements are taken from approximately 0.2 -1.8 m above the free access floor. When extracting these velocity values careful attention must be used because the graph starts its datum at the free access floor not at the fire source level.

Fuel Shape Effect on the Deterministic Properties of Turbulent Diffusion Flames
(Hasemi, Nishihata)

- Temperature
- Flame Height

Experimental Apparatus

The experiments were conducted using a 0.1 by 1.0 m and a 0.2 by 1.0 m rectangular porous burner with propane as the fuel. The 0.2 by 1.0 m burner could be sealed off into five equally sized square burners thereby making aspect ratios of 1,2,3,4,5, and 10 available. The burners were filled with ceramic beads of approximately 5 mm in diameter. The heat input ranged from 20 kW to 300 kW corresponding to a Q^*_{mod} between 0.3 and 5.

The burner was placed 0.50 m above the ground in a large room measuring 27m by 20 m in plan and 27m high.

Experimental Procedures

Flame height was monitored by a video camera during each experiment. The reported values of flame height are the average of the height of flame tips observed for more than three minutes at the intervals of one sec. The flame heights measured during the 0.1 by 1 m burner experiments range from 0.1 to 1.5 m.

Temperature measurements were made using 0.20 mm diameter chromel-alumel thermocouples. (The time constant of the temperature measurement system is approximately ten sec..) The authors report an under estimation of gas temperatures ranging from 2-20 % over 300-1,000 °C. These errors are a direct result of radiation and conduction losses at thermocouple junctions and soot buildup on the thermocouples themselves. To eliminate the effect of accidental sway of the flame on temperature measurements, temperatures were measured not only above the burner center but at two different points 5 cm apart from the center in the direction of the burner's shorter side. Reported temperature values are the average of the maximum temperature at each height at the interval of 10 s over three minutes during which the temperature above the burner center was higher than the other two. The temperatures measured during the 0.1 by 1 m burner experiments range from 10 to 1000 °C.

Report of the Building Research Institute
Study on Prevention of Fire Spread Caused by Hot Upward Current
(Yokoi)

- Temperature
- Velocity

Experimental Apparatus

The burner was made out of tin and measured 100 cm long by 1 cm wide. Alcohol was supplied to the burner via one communicating tube. Yokoi never mentions exactly what type of alcohol was used for his experiments however Sugawa reports that Yokoi used methyl alcohol on pg. 365 of "Fire Induced Flow in a Vertical Clean Room..."

Experimental Procedures

Yokoi found that slight draughts markedly disturb upward currents. Therefore, he conducted his experiments in a dark room used for photo processing. The room measured approximately 4.5m x 4.5m x 4.5m. In addition, experiments were only conducted on calm days where there was not much wind and only lasted for a maximum of two hours, so as to avoid draughts due to the difference in temperature between inside and outside the room.

A temperature compensating type hot wire anemometer measured upward velocity. The meter is not suitable for measuring the velocity of gas at temperatures above 100 ^{0}C.

Gas temperatures were measured using a copper-constantan thermocouple having a 0.2 mm diameter. The thermocouples were connected to a simple slow rotating oscillograph where the average values were recorded by eye for a time period of ten minutes. The automatic recording instrument could record no more than six points at a time, therefore one of the points was selected as the standard point and the other five points, distributed at various points on the same vertical line, were moved in relation to the fire source. As temperatures and velocities gradually changed with time adjustments were made in analyzing the results of experiments according to the value of the temperature at the base point.

Both temperatures and velocities were measured between the range of 50-140 cm. A HRR of approximately 6 kW was given off by the burner.

- Temperature
- Velocity

Experimental Apparatus

A wire 0.075 mm O.D. and 250 mm long was stretched horizontally and heated by a direct electric current passing through it. Heat supply to the wire was measured at 9.75 kW by means of a wattmeter.

Experimental Procedures

The velocity distribution was determined by introducing small dust particles into the air around the wire. These particles were then illuminated by a thin light beam and their trajectories were recorded on photograph. Velocity components could then be determined from the distance between two positions of a dust particle on a photograph.

The temperature distribution was determined by means of the Mach-Zehnder interferometer.

Measurements of velocity and temperature were taken at points 1, 2, 4, and 8 cm above the wire.

Gravitational Convection from a Boundary Source
Hunter Rouse, C. S. Yih, and H. W. Humphreys

- Temperature
- Velocity

Experimental Apparatus

The room was approximately circular with a diameter of 25 feet and a height of 11 feet. The burner was housed between two parallel walls measuring 4 feet high by 8 feet long and 4 feet apart. The burner was placed in the middle of a low platform extending the length of the walls. The authors never reported a detailed description of the burner including dimensions, fuel used, and other relevant intricacies. The only available description describes a "...recessed gas burner yielding low, blue flames..."

Experimental Procedures

Temperature measurements were made by a copper constantan thermocouple in combination with a potentiometer reading to 0.002 millivolt. Velocity measurements were obtained from a vane anemometer 1 1/4 inch in diameter. Velocities as low as 0.2 feet per second were measured. Both instruments were mounted alternatively on remotely controlled traversing mechanisms.

An Experimental Study of Some Line Fires
Li-Ming Yuan and G. Cox

- Temperature
- Velocity
- Flame Height

Experimental Apparatus

Natural gas, 94% Methane, was burned in three different burners including two porous refractory burners measuring 15mm x 0.20 m, 15 mm x 0.50 m, and a sandbox burner 50mm x 0.5m. The fuel supply could be adjusted to achieve theoretical heat release rates ranging from 2 to 110 kW. Similar to the setup by Lee and Emmons, experiments were conducted in a large laboratory with a fine mesh screen surrounding the burner to minimize the effects of ambient air movements. The burner surface was elevated 0.7 m above the floor.

Experimental Procedures

Flame height measurements were obtained from 3 min samples of video records. Temperature measurements were made using 150 micrometer chromel alumel thermocouples, and velocity measurements were recorded through 10 mm diametre bi-directional pressure probes. Both sets of measurements were taken up to 1.2 m above the burner and midway across its width. Similar to flame height measurements, both centerline time-mean temperatures and gas velocities where determined over three min samples. More specifically, temperature measurements were determined by averaging the maximum temperature exhibited by three thermocouples at the same elevation.

One thermocouple was placed at the center of the burner with two the other two offset 50 mm across the burner's width.

Mass flux was also determined for the 0.5 m long burners through a hood and duct technique.

Linear Flame Heights for Various Fuels
F. R. Steward

- Flame Height

Steward did not describe any of the experimental procedures or the apparatus used to develop the data he used in his paper.

The Size of Flames from Natural Fires
P. H. Thomas

- Flame Height

Thomas also has limited information regarding experimental procedures and apparatus.

Appendix B Data in Chart Format

Experimental Investigation of Laminar Free-Convection Flow...
(Brodowicz, Kierkus)

Velocity			
Z (m)	Z/Z*	u (m/s)	$u/(gZ^*)^{1/2}$
0.01	23.81	0.11	1.78
0.02	47.62	0.14	2.23
0.04	95.24	0.16	2.46
0.08	190.48	0.17	2.68

Temperature (9.75 W/m)			
dT	dT/T_o	Z	Z/Z*
16.00	0.05	0.01	23.75
8.00	0.03	0.04	95.01
5.50	0.02	0.08	190.02

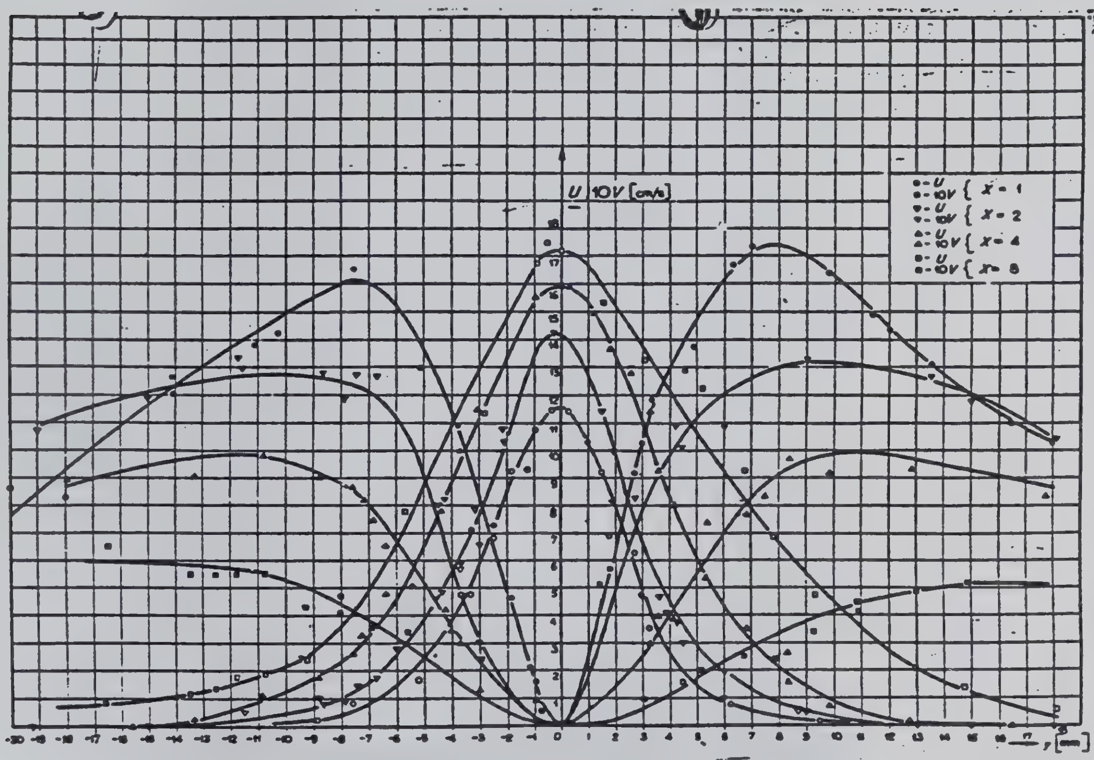

FIG. 3. Velocity distribution in the wake.

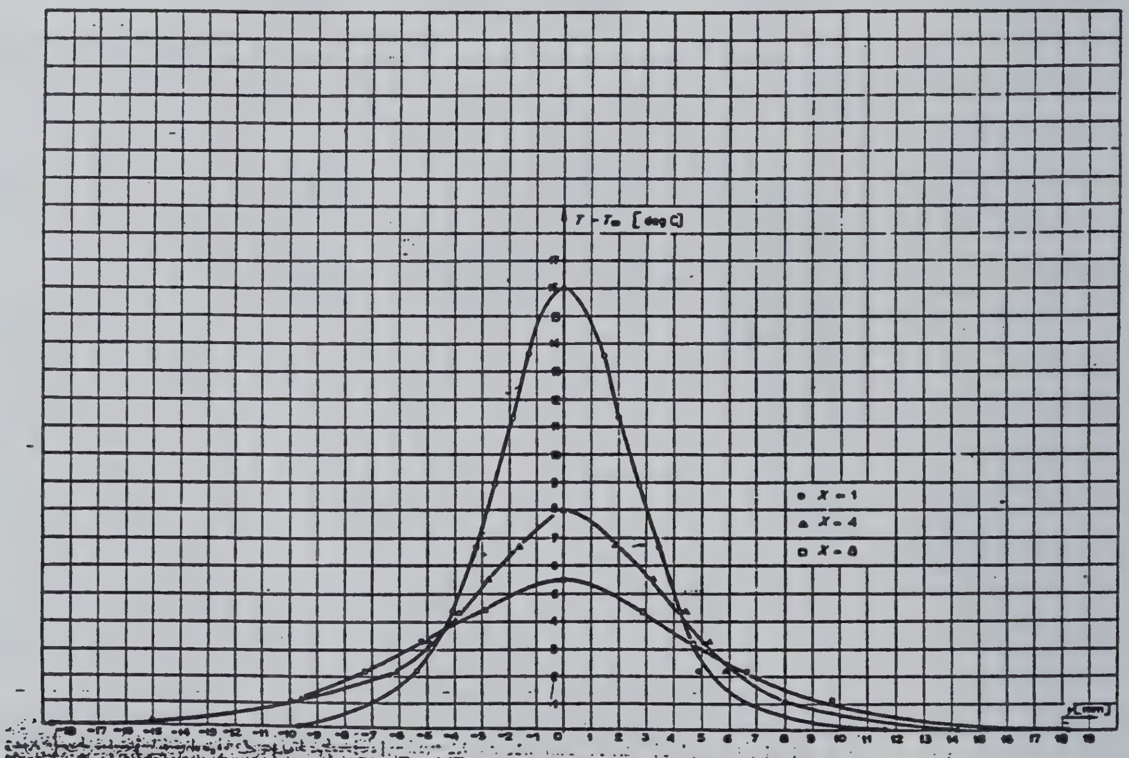

FIG. 4. Temperature distribution in the wake.

Velocity			
$u/Q_l^{1/3}$	$u/(gZ^*)^{1/2}$	$Z/Q_l^{1/3}$	Z/Z^*
0.32	1.05888	0.00195	0.21099
0.365	1.207785	0.0025	0.2705
0.47	1.55523	0.005	0.541
0.53	1.75377	0.0056	0.60592
0.61	2.01849	0.0075	0.8115
0.7	2.3163	0.0105	1.1361
0.75	2.48175	0.0135	1.4607
0.73	2.41557	0.018	1.9476
0.78	2.58102	0.024	2.5968
0.79	2.61411	0.029	3.1378
0.75	2.48175	0.038	4.1116
0.68	2.25012	0.05	5.41
0.67	2.21703	0.072	7.7904
0.62	2.05158	0.095	10.279
0.655	2.167395	0.13	14.066
0.65	2.15085	0.155	16.771
0.65	2.15085	0.2	21.64
0.7	2.3163	0.25	27.05

Flame Height			
L_f	L_f/D	Q_l	Z^*/D
0.052	3.466667	7.4	2.341311
0.075	5	12	3.232179
0.11	7.333333	15	3.75089
0.15	10	19	4.391472
0.2	13.33333	22.5	4.915721
0.31	20.66667	30	5.955543
0.375	25	35	6.60047
0.49	32.66667	55	8.922846
0.675	45	90	12.39257
0.91	60.66667	140	16.63983
1.1	73.33333	180	19.67652
1.4	93.33333	225	22.83427

Temperature			
dT	dT/T_o	$Z/Q_l^{2/3}$	Z/Z^*
700.00	2.389078	0.0019	0.20558
840.00	2.866894	0.0026	0.28132
925.00	3.156997	0.0036	0.38952
960.00	3.276451	0.0044	0.47608
960.00	3.276451	0.0055	0.5951
960.00	3.276451	0.0071	0.76822
960.00	3.276451	0.01	0.93052
970.00	3.31058	0.01	1.4066
860.00	2.935154	0.02	1.623
820.00	2.798635	0.02	1.7312
680.00	2.320819	0.02	2.1099
560.00	1.911263	0.02	2.5968
440.00	1.501706	0.03	2.8132
400.00	1.365188	0.03	3.246
280.00	0.955631	0.04	4.328
150.00	0.511945	0.06	6.492
120.00	0.409556	0.07	7.574
100.00	0.341297	0.08	8.656
80.00	0.273038	0.10	10.82
60.00	0.204778	0.13	13.525
50.00	0.170648	0.15	16.23
43.00	0.146758	0.19	20.017
40.00	0.136519	0.21	22.722
23.00	0.078498	0.28	30.296
20.00	0.068259	0.33	35.706

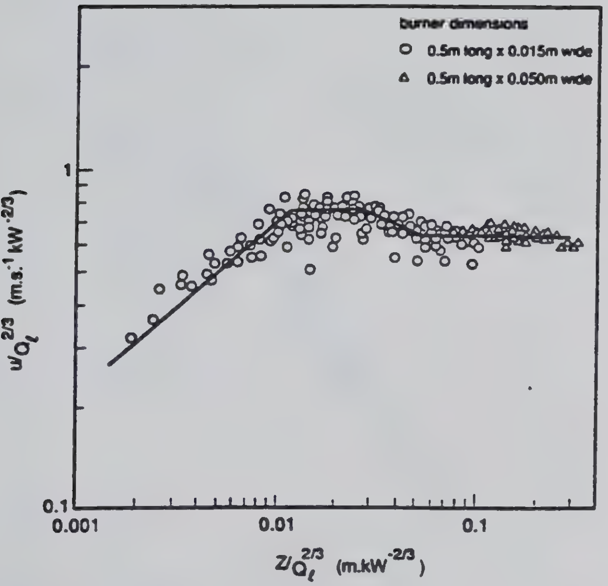

Fig. 3. Reduced centreline velocity with height.

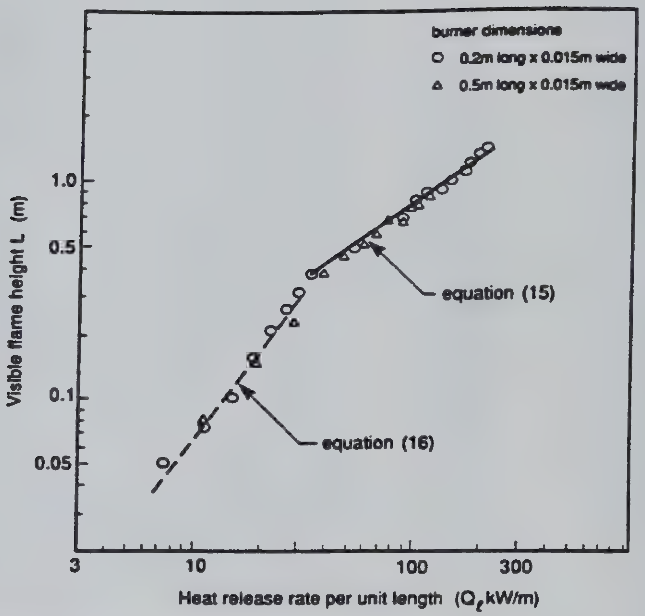

Fig. 2. Visible flame height as a function of Q_l.

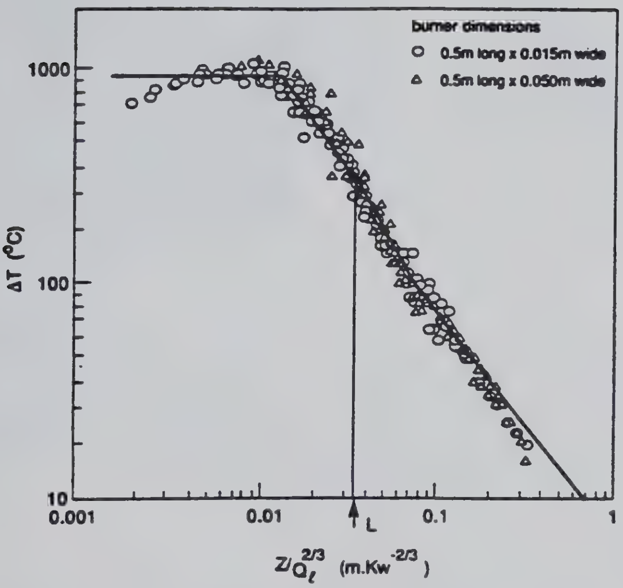

Fig. 4. Centreline temperature rise with reduced height.

Fuel Shape Effect on the Deterministic Properties of Turbulent Diffusion Flames
(Hasemi, Nishihata)

Flame Height		
L_f/D	Q^*_{mod}	Z^*/D
1.36	0.17	0.306697
1.8	0.25	0.396667
2.25	0.375	0.519851
2.75	0.475	0.608632
3.75	0.7	0.78828
4.5	0.95	0.966366
5.75	1.45	1.281246
6.75	1.85	1.507313
8	2.8	1.987259
9.25	4.1	2.562872
10	4.75	2.827188
11.1	6	3.3039
13	7	3.66168
13.5	8.5	4.167949
14.5	9.5	4.488918

Temperature (w = .20 m)						
Hasemi (49.6 kW)				**Hasemi (132.3 kW)**		
dT	dT/T_o	Z/Z*		dT	dT/T_o	Z/Z*
460	1.59	2.4		780	2.69	1.25
310	1.07	3.95		625	2.16	2.1
120	0.41	8		310	1.07	4.2
69	0.24	12.2		150	0.52	6.25
50	0.17	17		97	0.33	8.5
39.5	0.14	20		70	0.24	11
Hasemi (200 kW)				**Hasemi (331 kW)**		
dT	dT/T_o	Z/Z*		dT	dT/T_o	Z/Z*
700	2.41	1.7		845	2.91	0.645
450	1.55	3.2		800	2.76	1.15
245	0.84	4.8		635	2.19	2.21
160	0.55	6.4		370	1.28	3.42
120	0.41	7.9		242	0.83	4.45
				175	0.60	5.5
Hasemi (409 kW)						
dT	dT/T_o	Z/Z*				
845	2.91	0.575				
780	2.69	0.92				
720	2.48	1.9				
440	1.52	2.8				
290	1.00	3.8				
205	0.71	4.65				

			Temperature (w = .10 m)					
Hasemi (6.4 kW)			**Hasemi (34.2 kW)***			**Hasemi (170 kW)***		
dT	dT/T_o	Z/Z*	dT	dT/T_o	Z/Z*	dT	dT/T_o	Z/Z*
12.00	0.04	77.50	30	0.10	25	100	0.34	10
15.00	0.05	62.50	36	0.12	20	120	0.41	8.25
20.00	0.07	45.00	47.5	0.16	15	170	0.59	6
28.50	0.10	30.00	75	0.26	9.5	325	1.12	3.8
52.50	0.18	14.00	109	0.38	4.5	750	2.59	1.85
80.00	0.28	9.00	136	0.47	2.8	860	2.97	1.15
Hasemi (9.6 kW)*			**Hasemi (52 kW)**			**Hasemi (215 kW)**		
dT	dT/T_o	Z/Z*	dT	dT/T_o	Z/Z*	dT	dT/T_o	Z/Z*
15	0.05	57.5	35.00	0.12	19.50	105.00	0.36	7.25
18	0.06	47	44.00	0.15	15.50	200.00	0.69	4.30
24	0.08	35	57.50	0.20	11.50	390.00	1.34	2.80
77.5	0.27	10.5	95.00	0.33	7.25	725.00	2.50	1.30
140	0.48	6.75	265.00	0.91	3.50	825.00	2.84	0.55
			430.00	1.48	2.25			
Hasemi (13.7 kW)			**Hasemi (67 kW)**			**Hasemi (252 kW)***		
dT	dT/T_o	Z/Z*	dT	dT/T_o	Z/Z*	dT	dT/T_o	Z/Z*
15.00	0.05	57.50	45.00	0.16	16.00	125	0.43	6.75
18.50	0.06	45.00	57.50	0.20	13.00	260	0.90	3.8
23.00	0.08	36.00	80.00	0.28	9.50	480	1.66	2.5
31.00	0.11	27.50	135.00	0.47	6.00	825	2.84	1.2
45.00	0.16	17.50	400.00	1.38	2.80	875	3.02	0.76
97.50	0.34	8.25	575.00	1.98	1.80			
Hasemi (17.3 kW)*			**Hasemi (100 kW)***			**Hasemi (296 kW)**		
dT	dT/T_o	Z/Z*	dT	dT/T_o	Z/Z*	dT	dT/T_o	Z/Z*
22.5	0.08	38	69	0.24	12	175.00	0.60	5.25
25	0.09	32	120	0.41	7.25	185.00	0.64	4.75
34.5	0.12	24	220	0.76	4.75	260.00	0.90	3.50
55	0.19	15	560	1.93	2.25	825.00	2.84	1.05
120	0.41	7	725	2.50	1.4	875.00	3.02	0.28
Hasemi (25.2 kW)			**Hasemi (146 kW)**			**Hasemi (342 kW)**		
dT	dT/T_o	Z/Z*	dT	dT/T_o	Z/Z*	dT	dT/T_o	Z/Z*
27.50	0.09	31.00	67.50	0.23	9.50	160.00	0.55	5.50
34.00	0.12	25.00	85.00	0.29	7.75	210.00	0.72	4.30
45.00	0.16	18.50	120.00	0.41	5.75	320.00	1.10	3.25
70.00	0.24	12.00	235.00	0.81	3.60	600.00	2.07	2.10
165.00	0.57	5.50	575.00	1.98	1.70	875.00	3.02	1.00
320.00	1.10	3.50	725.00	2.50	1.10	900.00	3.10	0.65

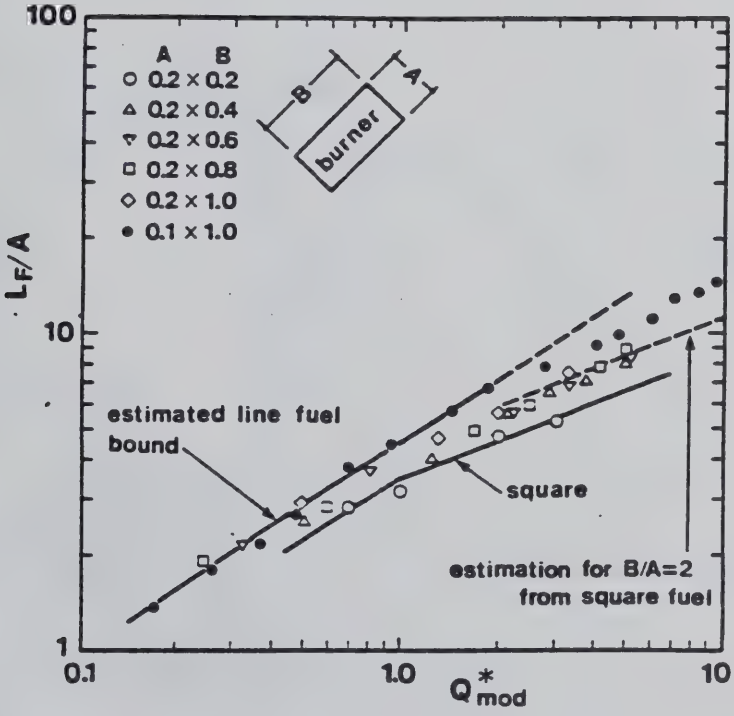

Figure 3 L_F/A vs. Q_{mod}^*

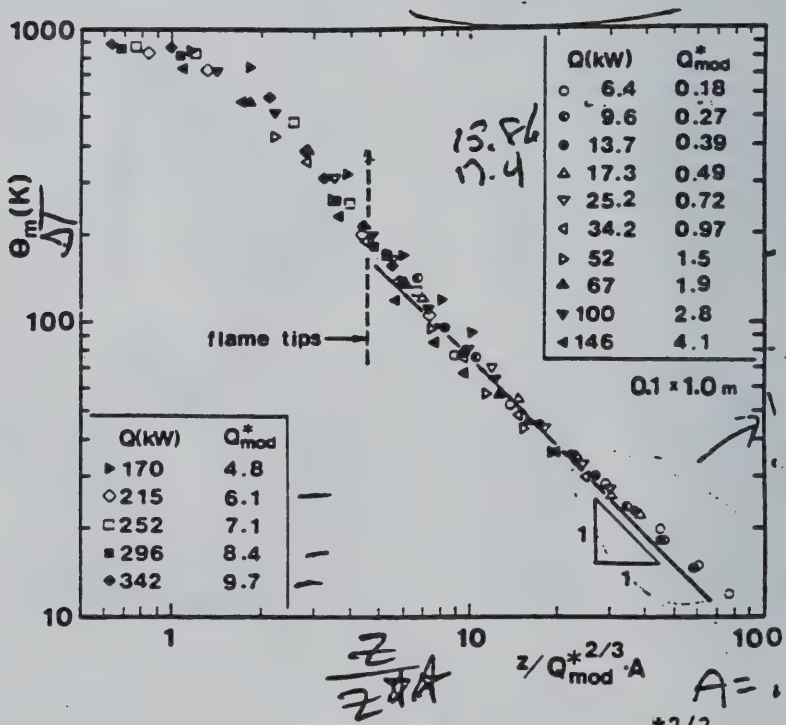

13.86
17.4

$\frac{Z}{Z^* A}$

A = .

Figure 4 Maximum excess temperature vs. normalized height($z/Q_{mod}^{*2/3}A$), 0.10m x 1.0m burner.

Figure 6
Maximum excess temperature vs.
normalized height$(z/Q_{mod}^{*2/3}A)$
0.20m x 1.0m burner

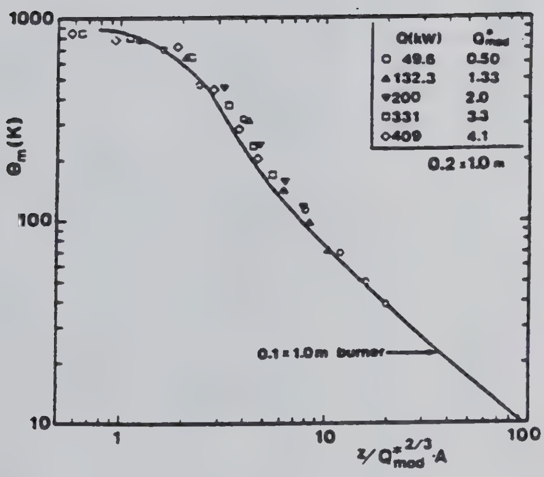

Natural Convection Above a Line Fire
(Shao-Lin Lee)

Flame Height (Asbestos/Methanol)

L_f	L_f/D	g/s*cm	kj/s*m	$Q_l^{2/3}$	Z*	Z*/D
0.75	1.329787	0.0007	1.337	1.213634	0.011214	0.784194
1	1.77305	0.000875	1.67125	1.408297	0.013013	0.909977
1.75	3.102837	0.00156	2.9796	2.070643	0.019133	1.337954

Flame Height (Asbestos/Acetone)

L_f	L_f/D	g/s*cm	kj/s*m	$Q_l^{2/3}$	Z*	Z*/D
0.45	0.797872	0.00155	4.3245	2.654344	0.024526	1.715115
0.55	0.975177	0.0018	5.022	2.932589	0.027097	1.894903
0.75	1.329787	0.002	5.58	3.145981	0.029069	2.032788
2	3.546099	0.0028	7.812	3.937085	0.036379	2.543963
3.2	5.673759	0.0055	15.345	6.175109	0.057058	3.99007
6.1	10.8156	0.0093	25.947	8.764452	0.080984	5.663184
8	14.1844	0.0139	38.781	11.45722	0.105865	7.403128
9.8	17.37589	0.017	47.43	13.10294	0.121071	8.466515

Flame Height (Aluminum/Acetone)

L_f	L_f/D	g/s*cm	kj/s*m	$Q_l^{2/3}$	Z*	Z*/D
0.45	0.797872	0.001	2.79	1.981844	0.018312	1.280576
0.5	0.886525	0.00125	3.4875	2.299726	0.021249	1.485977
0.55	0.975177	0.00175	4.8825	2.878027	0.026593	1.859648
2	3.546099	0.0025	6.975	3.650588	0.033731	2.358841
2.5	4.432624	0.0041	11.439	5.076823	0.04691	3.280409
4.5	7.978723	0.007	19.53	7.252173	0.06701	4.68602
6.1	10.8156	0.01025	28.5975	9.351588	0.086409	6.042565
8	14.1844	0.0128	35.712	10.8445	0.100203	7.007214
9	15.95745	0.016	44.64	12.58393	0.116275	8.131152
9.8	17.37589	0.0187	52.173	13.96252	0.129014	9.021937

Flame Height (Aluminum/Methanol)

L_f	L_f/D	g/s*cm	kj/s*m	$Q_l^{2/3}$	Z*	Z*/D
0.75	1.329787	0.00075	1.4325	1.270759	0.011742	0.821106
1.75	3.102837	0.00156	2.9796	2.070643	0.019133	1.337954

Temperature

Lee (Acetone/m=.0010) Al/q=2.79

T_o/dT	dT/T_o	Z(in)	Z(m)	Z/Z**
2.10	0.48	2.50	0.06	3.47
3.60	0.28	5.00	0.13	6.94
7.90	0.13	13.00	0.33	18.04
13.20	0.08	24.50	0.62	34.01
18.90	0.05	34.50	0.88	47.89

Lee (Acetone/m=.0070) Al/q=19.53

T_o/dT	dT/T_o	Z(in)	Z(m)	Z/Z**
2.30	0.43	9.00	0.23	3.41
5.80	0.17	25.00	0.64	9.46
8.90	0.11	40.00	1.02	15.14
11.80	0.08	56.00	1.42	21.20
14.40	0.07	70.00	1.78	26.50

Lee (Acetone/m=.00134) Al/q=3.74

T_o/dT	dT/T_o	Z(in)	Z(m)	Z/Z**
3.30	0.30	5.00	0.13	5.70
7.10	0.14	13.00	0.33	14.81
11.60	0.09	23.00	0.58	26.20
16.20	0.06	34.50	0.88	39.30
21.00	0.05	44.50	1.13	50.69

Lee (Acetone/m=.0103) Al/q=28.74

T_o/dT	dT/T_o	Z(in)	Z(m)	Z/Z**
2.50	0.40	10.00	0.25	2.93
4.20	0.24	20.00	0.51	5.85
5.80	0.17	30.00	0.76	8.78
7.00	0.14	40.00	1.02	11.71
8.90	0.11	50.00	1.27	14.63
10.00	0.10	60.00	1.52	17.56
11.90	0.08	70.00	1.78	20.48

Lee (Acetone/m=.00157) Al/q=4.38

T_o/dT	dT/T_o	Z(in)	Z(m)	Z/Z**
2.70	0.37	4.00	0.10	4.11
3.70	0.27	5.00	0.13	5.14
4.70	0.21	6.00	0.15	6.17
5.70	0.18	7.00	0.18	7.20
6.70	0.15	8.00	0.20	8.23
7.70	0.13	9.00	0.23	9.26

Lee (Acetone/m=.0127) Al/q=35.43

T_o/dT	dT/T_o	Z(in)	Z(m)	Z/Z**
2.20	0.45	12.50	0.32	3.18
4.00	0.25	22.00	0.56	5.60
6.00	0.17	35.00	0.89	8.91
7.10	0.14	46.50	1.18	11.83
8.90	0.11	58.00	1.47	14.76
10.30	0.10	70.00	1.78	17.82

Lee (Acetone/m=.00254) Al/q=7.087

T_o/dT	dT/T_o	Z(in)	Z(m)	Z/Z**
2.50	0.40	6.00	0.15	4.47
5.00	0.20	13.00	0.33	9.68
9.75	0.10	28.50	0.72	21.23
14.50	0.07	44.00	1.12	32.77
19.50	0.05	58.50	1.49	43.57
22.50	0.04	68.00	1.73	50.65

Lee (Acetone/m=.0165) Al/q=46.04

T_o/dT	dT/T_o	Z(in)	Z(m)	Z/Z**
2.40	0.42	16.00	0.41	3.42
4.00	0.25	24.50	0.62	5.24
5.70	0.18	36.50	0.93	7.80
7.00	0.14	47.00	1.19	10.05
8.20	0.12	58.00	1.47	12.40
9.50	0.11	70.00	1.78	14.97

Lee (Acetone/m=.0041) Al/q=11.439

T_o/dT	dT/T_o	Z(in)	Z(m)	Z/Z**
2.50	0.40	8.00	0.20	4.33
3.80	0.26	12.00	0.30	6.50
7.00	0.14	25.00	0.64	13.54
9.20	0.11	35.00	0.89	18.96
11.75	0.09	46.50	1.18	25.18
14.00	0.07	55.00	1.40	29.79
15.20	0.07	61.00	1.55	33.04
17.80	0.06	70.00	1.78	37.91

Lee (Acetone/m=.0187) Al/q=52.17

T_o/dT	dT/T_o	Z(in)	Z(m)	Z/Z**
2.1	0.48	15	0.38	2.95
3.8	0.26	25	0.64	4.91
5.4	0.19	35	0.89	6.88
6.6	0.15	45	1.14	8.85
7.7	0.13	55	1.40	10.81
8.7	0.11	64.5	1.64	12.68
9.15	0.11	70	1.78	13.76

Lee (Methanol/m=.00074) Al/q=1.413

T_o/dT	dT/T_o	Z(in)	Z(m)	Z/Z**
8	0.13	10	0.25	21.90
16	0.06	20	0.51	43.79
23	0.04	30	0.76	65.69
31	0.03	38.5	0.98	84.30
38.00	0.03	49.50	1.26	108.39
46.00	0.02	59.00	1.50	129.19

Lee (Methanol/m=.00158) Al/q=3.018

T_o/dT	dT/T_o	Z(in)	Z(m)	Z/Z**
3	0.33	7	0.18	9.21
7	0.14	16.5	0.42	21.72
12	0.08	25	0.64	32.90
15	0.07	33	0.84	43.43
21	0.05	42	1.07	55.27
23.5	0.04	51.5	1.31	67.78
28	0.04	60	1.52	78.96
32	0.03	70	1.78	92.12

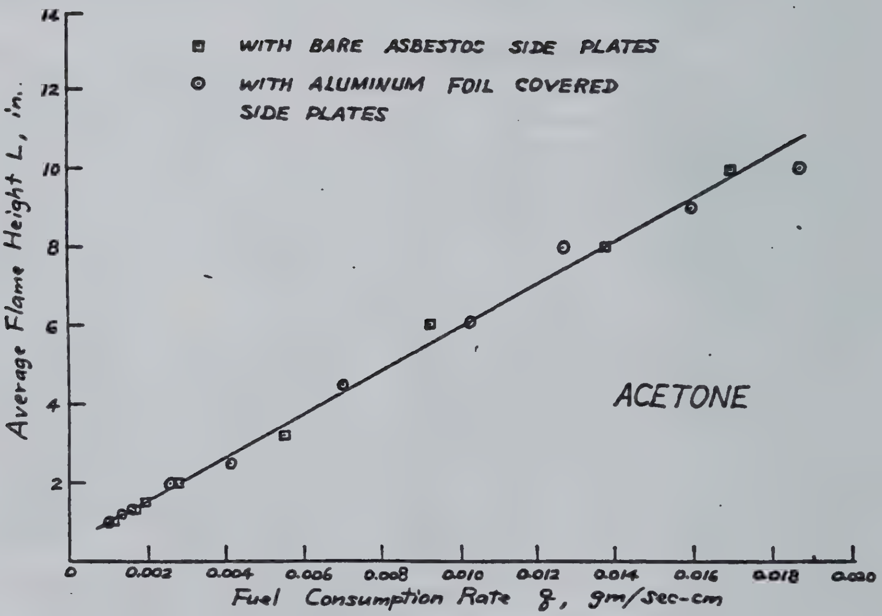

Figure 5-11 Measurements of Average Height of Acetone Flame

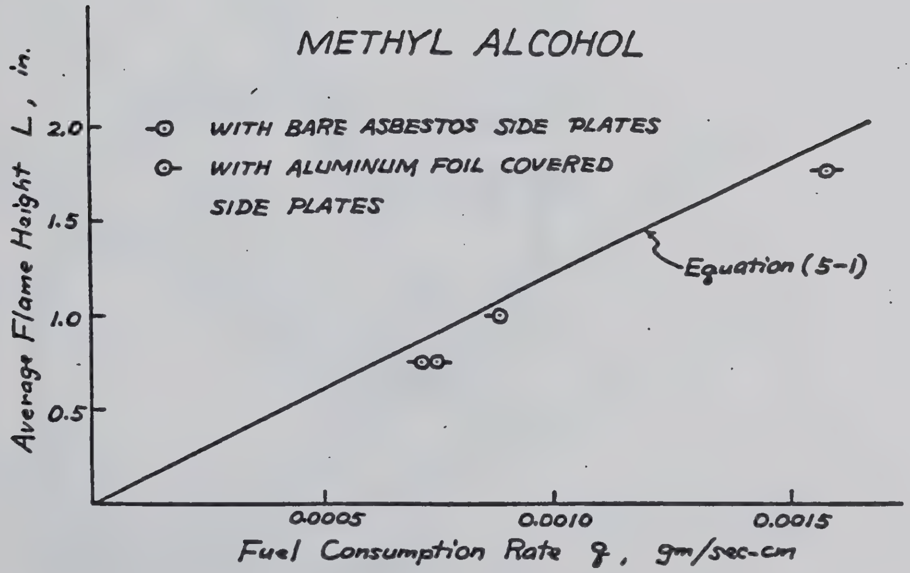

Figure 5-10 Measurements of Average Height of Methyl Alcohol Flame

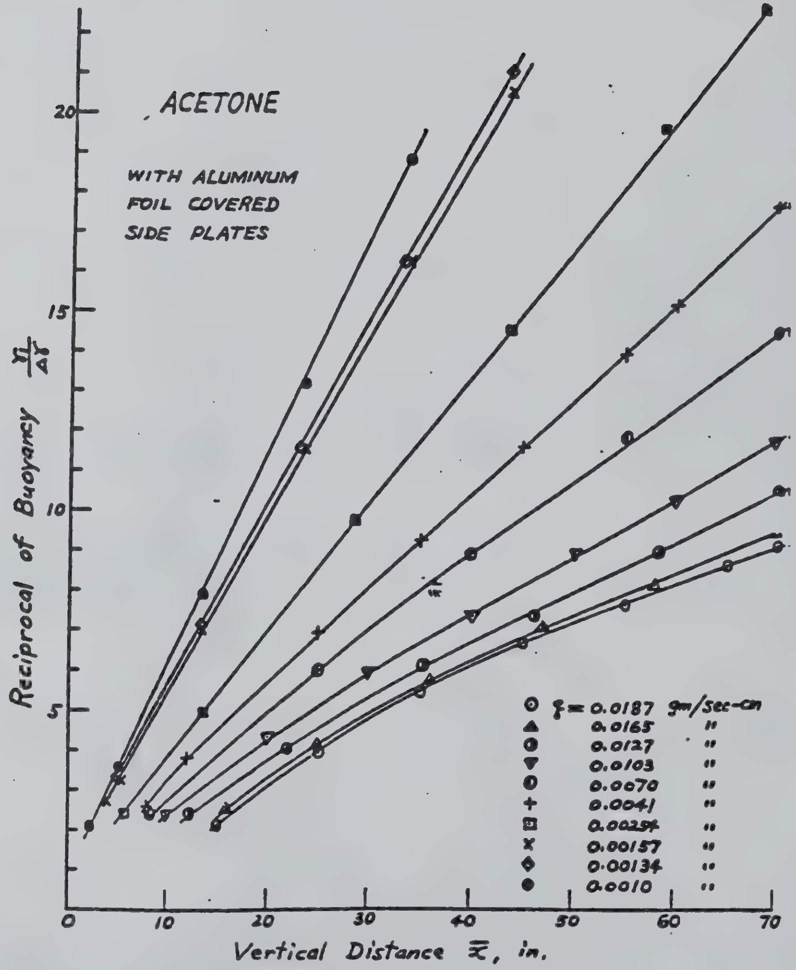

Figure 5-7 Buoyancy Measurements for the Plume above a Flame of Acetone with Aluminum Foil Covered Side Plates

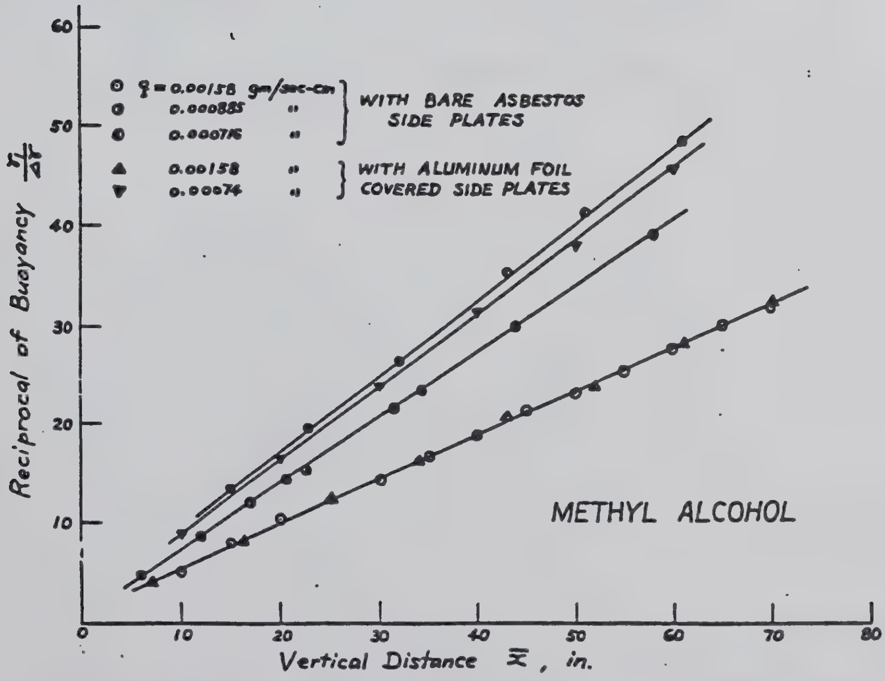

Figure 5-3 Buoyancy Measurements for the Plume above a Flame of Methyl Alcohol

Gravitational Convection from a Boundary Source
Hunter Rouse, C. S. Yih, and H. W. Humphreys

Velocity						
$u/(gZ^*)^{1/2}$	$-W/L$	Z(ft)	Z(m)	Q/l	Z*	Z/Z*
1.80	.001710	1.30	0.39624	0.752981	0.007667	51.67813
1.68	.005220	3.50	1.0668	2.298575	0.016135	66.11732
1.74	.003040	2.60	0.79248	1.338634	0.011252	70.42905
1.72	.006590	2.90	0.88392	2.901841	0.018847	46.89954

Temperature (Scientific Units)								
Y-axis	$-W/L$	Z(ft)	Z(m)	Q_l	Z*	Z/Z*	Z*/Z	dT/T_o
2.40	0.0017	1.30	0.39624	0.752981	0.01	51.80	0.019303	0.05
2.60	0.0023	1.50	0.4572	1.003975	0.01	49.34	0.020269	0.05
2.25	0.0017	1.90	0.57912	0.752981	0.01	75.71	0.013208	0.03
2.75	0.0023	2.00	0.6096	1.003975	0.01	65.78	0.015201	0.04
2.55	0.0024	2.20	0.67056	1.039202	0.01	70.72	0.014141	0.04
2.45	0.0027	3.40	1.03632	1.166901	0.01	101.16	0.009885	0.02
2.60	0.0052	3.50	1.0668	2.298575	0.02	66.25	0.015093	0.04

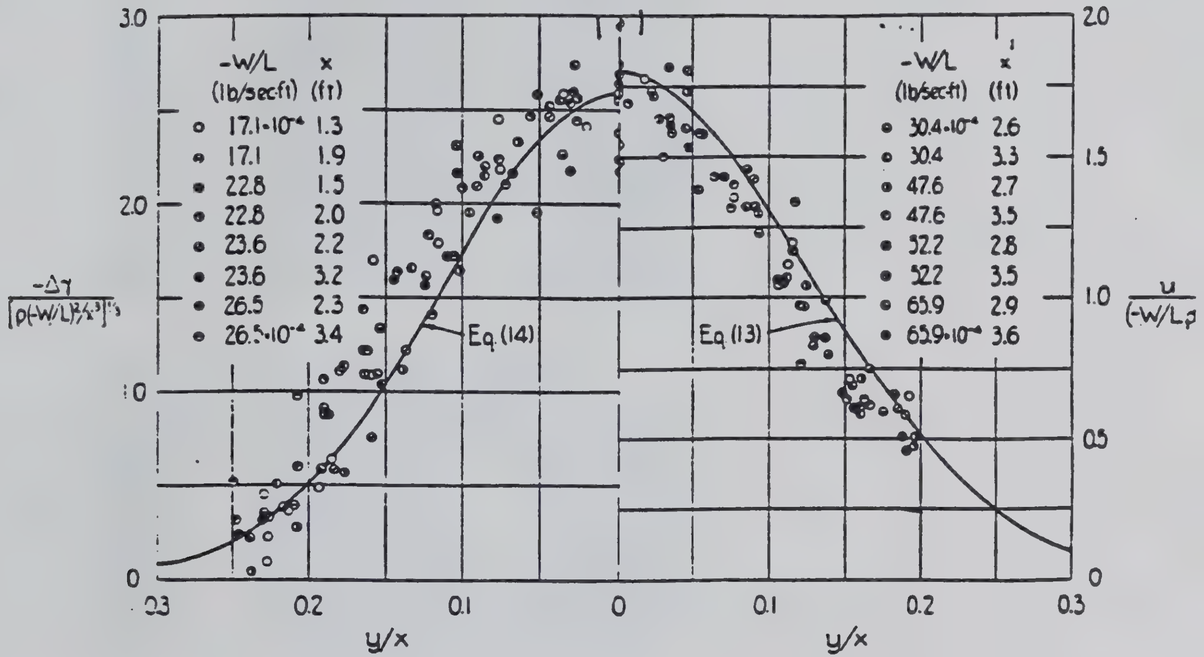

Fig. 2. Distribution functions for two-dimensional convection.

Fire Induced Flow in a Clean Room with Downward Vertical Laminar Flow

(Sugawa, Oka, Hotta)

Velocity			
Z (m)	Z/Z*	u (m/s)	$u/(gZ^*)^{1/2}$
0.20	5.99	1.20	2.10
0.40	11.98	1.15	2.01
0.75	22.46	0.95	1.66
0.80	23.95	1.20	2.10
1.00	29.94	1.50	2.62
1.00	29.94	1.15	2.01
1.20	35.93	1.30	2.27
1.60	47.90	1.50	2.62
1.80	53.89	1.40	2.45

Temperature (5.83 kW)			
dT	dT/T_o	Z	Z/Z*
33.00	0.11	0.80	23.95
67.50	0.23	0.31	9.28
95.00	0.32	0.20	5.99
120.00	0.41	0.16	4.64
320.00	1.09	0.10	2.99

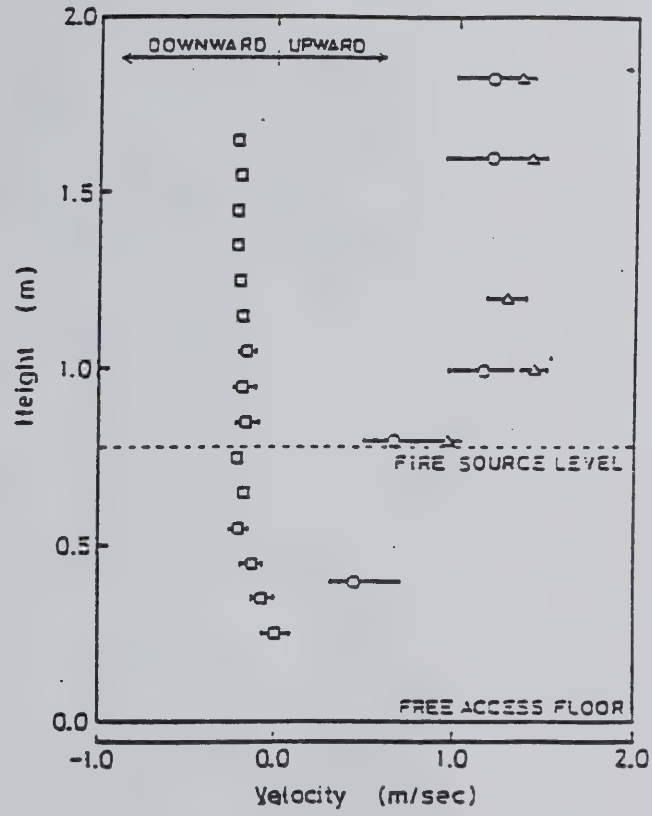

□ without fire source and with down flow
△ with fire source and without down flow
○ with fire source and with down flow

Figure 4 Variation of upward velocity along the center line.

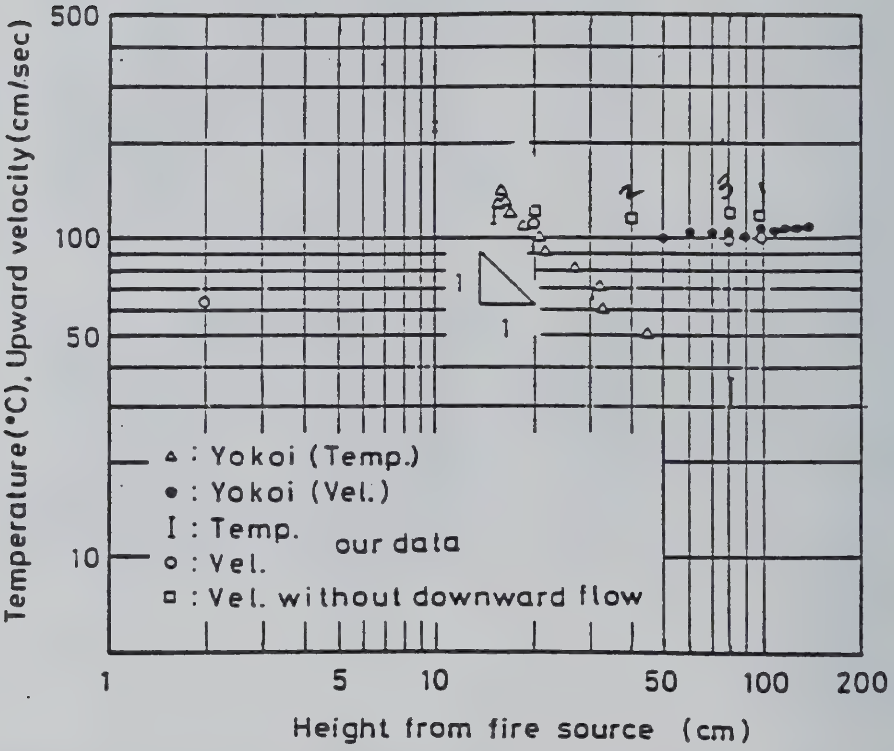

Figure 9 Variations of temperatures and velocities along the center line of the upward flow with and without down flow. Yokoi's data are also plotted.

Flame Height from Rectangular Fire Sources
(Sugawa, Satoh, & Oka)

Flame Height		
L_f/D	Q^*_{rec}	Z^*/D
1.45	0.22	0.364247
1.85	0.3	0.447961
2.25	0.375	0.519851
2.5	0.51	0.638189
3	0.75	0.825403
3.75	1	1
4	1.3	1.191243
6	1.45	1.281246
5	1.8	1.480017
7.5	2	1.587768
7.5	2.5	1.842578
9	3	2.080846
9.25	3.5	2.306181
10.1	4	2.521007
12	4.25	2.625037
11	5	2.925587
14.5	5.5	3.117611
13.5	6	3.3039
15	8.5	4.167949
17	8.25	4.085778
18	8.5	4.167949
18.5	10	4.645153
18.5	11.1	4.980012
22.5	11.1	4.980012
21	12	5.245826
23	14	5.813898
24.5	15	6.087695
30	22.5	7.978215

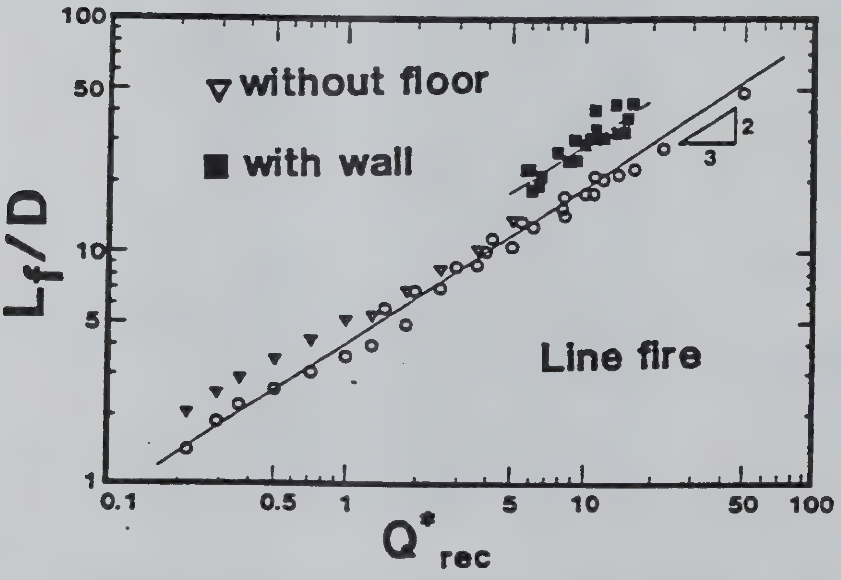

Figure 2 Dependence of flame height in dimensionless form on heat release rate in dimensionless form. Data were obtained from a line fire source using an unconfined rectangular propane gas diffusion burner without wall (○ , ▽) and against wall (■).

Linear Flame Heights for Various Fuels
F. R. Steward

Flame Height (Propane)

log (H/W)	H/W	log (x-axis	x-axis	$(Q_l)^{2/3}/W$	Z*/W
2	100	2	100	4641.589	43.12036
2.02	104.7129	2.05	112.2018	4823.178	44.80733
2.15	141.2538	2.3	199.5262	5843.414	54.28532
2.2	158.4893	2.5	316.2278	6812.921	63.29203
2.24	173.7801	2.65	446.6836	7644.223	71.01483
2.28	190.5461	2.75	562.3413	8254.042	76.68005
2.32	208.9296	2.9	794.3282	9261.187	86.03643
1.95	89.12509	1.8	63.09573	3981.072	36.98416
1.88	75.85776	1.7	50.11872	3686.945	34.25172
1.82	66.06934	1.55	35.48134	3285.993	30.52688
1.79	61.6595	1.45	28.18383	3043.22	28.27151
1.75	56.23413	1.25	17.78279	2610.157	24.24836
1.7	50.11872	1.1	12.58925	2326.305	21.61137
1.64	43.65158	1	10	2154.435	20.0147
1.65	44.66836	0.92	8.317638	2026.127	18.82272
1.6	39.81072	0.75	5.623413	1778.279	16.52022
1.55	35.48134	0.63	4.265795	1621.81	15.06662
1.43	26.91535	0.4	2.511886	1359.356	12.62842
1.41	25.70396	0.2	1.584893	1165.914	10.83134
1.37	23.44229	0.18	1.513561	1148.154	10.66635
1.2	15.84893	-0.2	0.630957	857.6959	7.967995
1.1	12.58925	-0.5	0.316228	681.2921	6.329203
1.05	11.22018	-0.62	0.239883	621.3458	5.772302
1.01	10.23293	-0.75	0.177828	562.3413	5.224151
0.975	9.440609	-0.8	0.158489	541.1695	5.027465
0.9	7.943282	-0.9	0.125893	501.1872	4.656029
0.83	6.76083	-1.2	0.063096	398.1072	3.698416

Flame Height (Methane)

log (H/W)	H/W	log (x-axis	x-axis	$(Q_l)^{2/3}/W$	Z*/W
1.205	16.03245	-0.3	0.501187	783.5111	7.278818
1.19	15.48817	-0.35	0.446684	754.0124	7.004775
1.15	14.12538	-0.43	0.371535	709.1071	6.587605
1.12	13.18257	-0.45	0.354813	698.305	6.487254
1.1	12.58925	-0.55	0.281838	646.7134	6.007967
1.04	10.96478	-0.7	0.199526	576.3839	5.354606
1	10	-0.8	0.158489	533.7999	4.959001
0.94	8.709636	-0.93	0.11749	483.109	4.488083
0.84	6.91831	-1.37	0.042658	344.6502	3.2018

Flame Height (Hydrogen)

log (H/W)	H/W	log (x-axis	x-axis	$(Q_l)^{2/3}/W$	Z*/W
1.23	16.98244	-0.4	0.398107	849.5199	7.89204
1.22	16.59587	-0.25	0.562341	953.177	8.855015
1.33	21.37962	0.2	1.584893	1346.398	12.50804
1.43	26.91535	0.22	1.659587	1367.226	12.70153
1.4	25.11886	0.4	2.511886	1569.785	14.5833
1.47	29.51209	0.55	3.548134	1761.328	16.36274
1.5	31.62278	0.55	3.548134	1761.328	16.36274
1.55	35.48134	0.65	4.466836	1901.838	17.66808
1.61	40.73803	0.9	7.943282	2304.13	21.40536
1.68	47.86301	1.05	11.22018	2585.276	24.01721
1.66	45.70882	1.1	12.58925	2686.418	24.95682
1.79	61.6595	1.3	19.95262	3132.133	29.09752
1.88	75.85776	1.62	41.68694	4004.118	37.19826
1.91	81.28305	1.7	50.11872	4257.685	39.5539
1.97	93.32543	1.85	70.79458	4777.202	44.3802

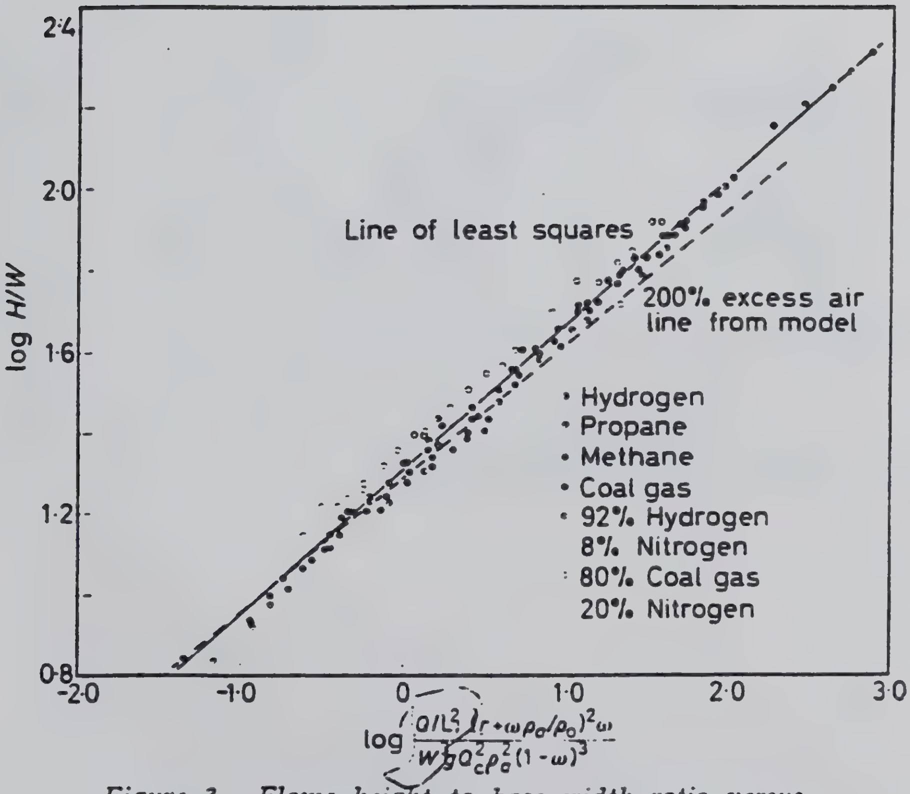

Figure 3. Flame height to base width ratio versus mixing controlled burning rate parameter

The Size of Flames from Natural Fires

P. H. Thomas

Flame Height		
L_f/D	$m''/p_o(gD)^{1/2}$	Z^*/D
1.2	0.009	0.538274
1.6	0.00925	0.548202
1.7	0.0095	0.55804
1.7	0.0115	0.633883
3	0.016	0.790081
3.75	0.0225	0.991812
4	0.03	1.20161
5	0.04	1.455787
5.5	0.045	1.574768
7	0.065	2.012505

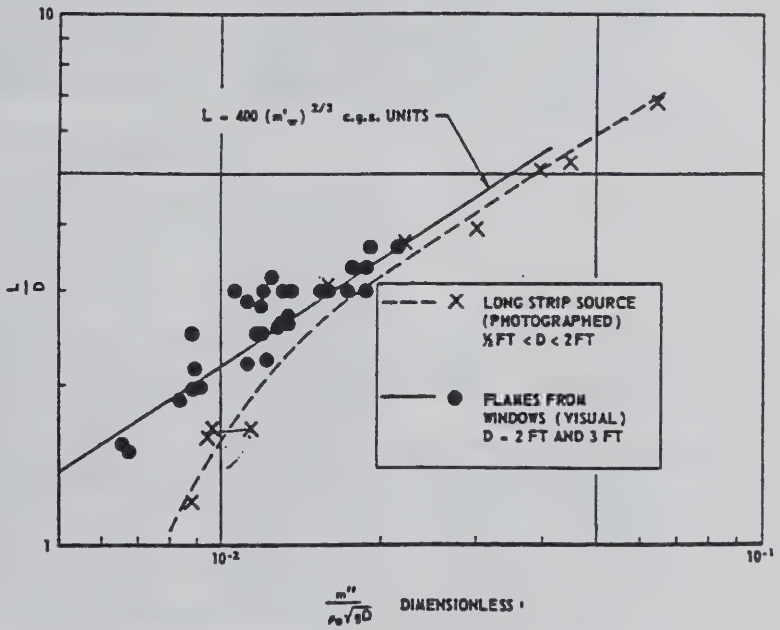

Fig. 7. Flames from long strips and windows.

Velocity

Z (m)	Z/Z*	u (m/s)	$u/(gZ^*)^{1/2}$
0.50	14.97	1.03	1.79
0.60	17.96	1.05	1.83
0.70	20.96	1.05	1.83
0.80	23.95	1.08	1.88
0.90	26.95	1.02	1.77
1.00	29.94	1.07	1.86
1.10	32.93	1.03	1.79
1.20	35.93	1.04	1.81
1.30	38.92	1.06	1.84
1.40	41.92	1.08	1.88

Temperature (6.86 kW)

dT	dT/T_o	Z	Z/Z**
44.00	0.15	0.50	14.84
33.00	0.11	0.60	17.80
32.00	0.11	0.70	20.77
27.00	0.09	0.80	23.74
22.00	0.08	0.90	26.71
21.00	0.07	1.00	29.67
18.50	0.06	1.10	32.64
17.00	0.06	1.20	35.61
16.50	0.06	1.30	38.58
16.00	0.06	1.40	41.54

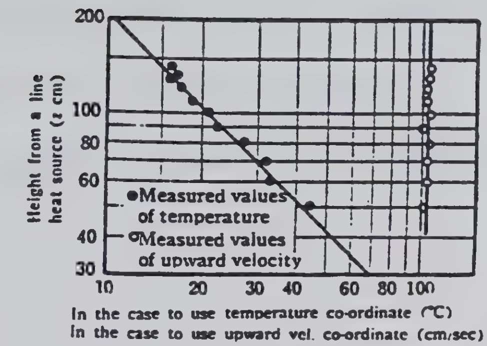

Figure 1.7

Vertical distribution of temperature and upward velocity at the axis of upward current from a line heat source.

Table 1.2 Comparison of the calculated values with the measured values of the temperature at the central axis of the upward current. (in the case of an infininte line heat source)

Height from a heat source, z	Measured values of ascending velocity, w_m	Absolute temperature of the ambient air, θ_0	Values of temperature at the axis of stream, $\Delta\theta_m$	
			calculated	measured
50 cm	103 cm/sec	290 °K	41 °C	44 °C
60 "	105 "	"	34 "	33 "
70 "	105 "	"	29 "	32 "
80 "	108 "	"	26 "	27 "
90 "	102 "	"	23 "	22 "
100 "	107 "	"	20 "	21 "
110 "	103 "	"	18.6 "	18.5 "
120 "	104 "	"	17.1 "	17 "
130 "	106 "	"	15.8 "	16.5 "
140 "	108 "	"	14.6 "	16 "

Appendix C Conversions of Data

Conversions

In order to consolidate the data presented by numerous authors onto one single graph conversions between the data presented in its original form and that used in my graphs were often necessary, as would be expected. Listed below are a summary of the variables used in the plots; definitions of these variables; and generic numerical values used in the variables unless otherwise stated by the individual data sets themselves. Note, the notation used in this appendix may differ from the rest of the thesis.

Numerical Values:

Unless stated other wise ambient values are assigned as follows:

Specific Heat (c_p)	1.01 kJ/kg-K
Ambient Temp (T_o)	293 K
Ambient Density (ρ_o)	1.21 kg/m^3
Gravity (g)	9.81 m/s^2

Variable summary:

$$z^*_{axi} = \left(\frac{\dot{Q}}{\rho_o c_p T_o \sqrt{g}} \right)^{5/2}$$

Plot summary:

Temperature	Velocity:	Flame Length:
Ordinate: $\frac{\Delta T}{T_o}$	Ordinate: $\frac{u}{\sqrt{gz^*}}$	Ordinate: $\frac{L_f}{w}$
Abscissa: $\frac{z}{z^*}$	Abscissa: $\frac{z}{z^*}$	Abscissa: $\frac{z^*}{w}$

Experimental Investigation of Laminar Free-Convection Flow in Air Above Horizontal Wire with Constant Heat Flux

K. Brodowicz and W. T. Kierkus

Temperature Conversion:

Data was taken from "Experimental Investigation of Laminar Free-Convection Flow in Air Above Horizontal Wire with Constant Heat Flux." The values were graphed against T - T_∞ (°C) and y (mm). Only centerline data was extracted therefore there was no use for the x-axis, y (mm), which represents distamce off set from the centerline. Temperature values were taken at arbitrarily chosen levels above the wire including 1, 4, and 8 (cm).

Ordinate: T - T_∞ (°C)

Absissa: y (mm)

(1) Divide T - T_∞ or ΔT by T_o = 19.8 (°C) ≅ 293 K

(2) Determine z*:

$$z^* = \left(\frac{\dot{Q}'}{\rho_o T_o c_p \sqrt{g}}\right)^{2/3} = \left(\frac{9.75\times10^{-3}}{1121.52}\right)^{2/3} = 4.23\times10^{-4}\ (m)$$

(3) Convert arbitrarily chosen z (cm) into z (m) and divide by z* (m).

Velocity Conversion:

Data was taken from "Experimental Investigation of Laminar Free-Convection Flow in Air Above Horizontal Wire with Constant Heat Flux." The values were graphed against u (cm/sec) and y (mm). As before, the x-axis, y (mm), was ignored because only centerline values were used. Velocity values were taken at arbitrarily chosen levels including 1, 2, 4, and 8 (cm). In order to graph these values against $u/\sqrt{gz^*}$ velocity values were divided by 0.0644 and z was divided by z* = 4.23 x 10^{-4}.

(1) Determine z* using the procedure outlined above.

(2) Convert arbitrarily chosen z (cm) into z (m) and divide by z* (m).

(3) Determine $\sqrt{gz^*}$:

$$\sqrt{gz^*} = \sqrt{\left(9.81\frac{m}{s^2}\right)\left(4.23\times10^{-4}\ m\right)} = 0.0644\frac{m}{s}$$

(4) Convert u (cm/sec) to u (m/sec) and divide by $\sqrt{gz^*}$ or 0.0644 m/sec.

An Experimental Study of Some Line Fires
Lin-Ming Yuan, G. Cox

Flame Height Conversion:

Ordinate (Visible Flame Length): L (m)

Absissa: Q_l (kW/m)

(1) Divide flame length L (m) by the burner width, w (m)

$$\frac{L_f\ (m)}{0.015\ (m)}$$

(2) Determine z*:

$$z^* = \left(\frac{\dot{Q}'}{\rho_o T_o c_p \sqrt{g}}\right)^{2/3} = \left(\frac{\dot{Q}'}{1121.52}\right)^{2/3} = 0.0334\ (m)$$

(3) Divide z* by the burner width, w (m):

$$\frac{z^*\ (m)}{0.015\ (m)}$$

Temerpature Conversion:

Ordinate: ΔT (°C)

Absissa: $Z/Q_l^{2/3}$ (m-kW$^{-2/3}$)

(1) Divide ΔT by T_o or 293 K.

(2) Determine z/z*:

$$\frac{z}{Q_l^{2/3}} \times \left(\rho_o T_o c_p \sqrt{g}\right)^{2/3} = \frac{z}{Q_l^{2/3}} \times (1121.52)^{2/3}$$

Velocity Conversion:

Ordinate: $u/Q_l^{1/3}$ (m-s^{-1}-kW$^{-1/3}$)

Absissa: $Z/Q_l^{2/3}$ (m-kW$^{-2/3}$)

(1) Determine $\dfrac{u}{\sqrt{gz^*}}$:

$$\frac{u}{Q_l^{1/3}} \times \left(\rho_o T_o c_p \sqrt{g}\right)^{1/3} \frac{1}{\sqrt{g}} = \frac{u}{Q_l^{1/3}} \times \left(121.52\right)^{1/3} \frac{1}{\sqrt{9.81}} = \frac{u}{\sqrt{gz\,*}}$$

(2) Determine z/z* using the same method outlined above.

Fuel Shape Effect on the Deterministic Properties of Turbulent Diffusion Flames
(Hasemi, Nishihata)

Flame Height Conversion:

Data was taken from "Fuel Shape Effect on the Deterministic Properties of Turbulent Diffusion Flames" page 279, Figure 3. Like Sugawa's data, X-axis values had to be raised to the 2/3 power so that they may be graphed on the z*/w axis.

Ordinate: Q^*_{mod} (dimensionless)

Absisissa: L_f/A (dimensionless)

$$Q^*_{\mathrm{mod}} = \frac{Q}{\rho c T \sqrt{g} A^{3/2} B}$$; where B = burner length and A = burner width.

$$Q^*_{\mathrm{mod}} = \frac{z^{*\,5/2}_{axi}}{w^{3/2} l} = \frac{z^{*3/2}}{w^{3/2}} = \left(\frac{z^*}{w}\right)^{3/2}$$

$$\left(\frac{z^*}{w}\right) = Q^{*\;2/3}_{\mathrm{mod}}$$

Remember: $z^* = \left(\dfrac{z^{*\,5/2}_{axi}}{l}\right)^{2/3}$;B = l; A = w.

Note that the ordinate is already in the correct form and no conversions are necesary.

Temperature Conversion:

Data was taken from "Fuel Shape Effect on the Deterministic Properties of Turbulent Diffusion Flames" page 280, Figure 4 and page 282 Figure 6. The values were graphed against Θ (°C)and $z/Q^{*\;2/3}_{\mathrm{mod}} \bullet A$. After a little manipulation it was apparent that $z/Q^{*\;2/3}_{\mathrm{mod}} \bullet A$ equals z/z*. The only adjustment required to place these values on my graph was to divide the Y-axis by 293 K.

Although Hasemi plotted values for 15 different heat release rates only nine of them were graphed on the regular temperature graph so as not to over shadow the values listed by the other authors. As a general rule the two extreme heat release rates were graphed followed by every other value in between so as to get an unbiased distribution. One additional heat release rate was graphed to fill a hole not covered by the other values.

Ordinate: $z/Q^{*\;2/3}_{\mathrm{mod}} \bullet A$ (dimensionless)

Absisissa: Θ (°C)

$$Q^*_{\mathrm{mod}} = \frac{Q}{\rho c T \sqrt{g} A^{3/2} B}$$; where B = burner length and A = burner width

From above flame height conversion:

$$\dot{Q}^{*\;2/3}_{\text{mod}} = \frac{z^*}{A}$$

$$\frac{z}{\dot{Q}^{*\;2/3}_{\text{mod}} \bullet A} = \frac{z}{\frac{z^*}{A} \bullet A} = \frac{z}{z^*}$$

(1) Divide Θ, which equals ΔT, by T_o.

(2) The x-axis is alreay in the correct format and can be left alone.

Natural Convection Above a Line Fire
Shao-lin Lee

Flame Height Conversion:

Data was taken from "Natural Convection Above a Line Fire" pgs. 5-21 and 5-22. The flame height was given in inches and was therefore divided by the burner width in inches to yield L_f/w. To graph the x-axis values given in terms of a fuel consumption rate, (q), on a z*/w axis requires a little more manipulation. First multiply by the appropriate $\Delta H_{c(chem)}$ for either acetone or methanol, and then multiply by 100 to convert cm into m. $\Delta H_{c(chem)}$ values were taken from Tewarson's chapter pg. 3-78 in the Second Edition of the SFPE Handbook. Next raise $\dot{Q}'$ to the 2/3 power and multiply by .00924 which yields z*. This value is then divided by the width of the burner converted into m or .0143 m.

Ordinate: L (in)

Abscissa: q (gm/s-in)

(1) Divide the flame height, L, by the width of the burner 0.564 in to yield L_f/w.

(2) Find $\dot{Q}'$:

$$\dot{Q}' = q\Delta H_c$$

$$\Delta H_{c_{ace}} = 19.1\frac{kJ}{g}$$

$$\Delta H_{c_{meth}} = 27.9\frac{kJ}{g}$$

A quick example best explains this step.

$$\dot{Q}'_{meth} = q_{meth}\Delta H_{c_{meth}} = \left(0.00155\frac{g}{s-cm}\right)\left(27.9\frac{kJ}{g}\right)\left(\frac{100\ cm}{1\ m}\right) = 4.3\frac{kJ}{s-m}$$

(3) Raise 4.3 kJ/s-m to the 2/3 power.

(4) Multiply the resultant by 0.00924 or-

$$\frac{\dot{Q}'^{2/3}}{\left(\rho_o c_p T_o \sqrt{g}\right)^{2/3}} = \frac{\dot{Q}'^{2/3}}{1121.52^{2/3}} = z*$$

(5) Divide z* by the burner width or 0.564 in converted to 0.0143 m to get z*/w.

Gravitational Convection from a Boundary Source
Hunter Rouse, C. S. Yih, and H.W. Humphreys

Temperature Conversion

$$\frac{-\Delta\gamma}{(\rho(-u/L)^2/x^3)^{1/3}} = \frac{\Delta T/T_o}{\left[\left(\frac{\dot{Q}'}{\rho_o C_p T_o \sqrt{g}}\right)^{2/3} \Big/ x\right]} = \frac{\Delta T/T_o}{Z^*/Z}$$

(1) Convert x(ft) to x(m)

(2) $\dot{Q}/l = C_p T_o (w/L)$ look at eq. 12 & convert to SI units

$$= 1.01\left(\frac{kJ}{kg \bullet K}\right) 293(K) \left(\frac{W}{L}\frac{lb}{s \bullet ft}\right) .4536\left(\frac{kg}{lb}\right)\frac{1ft}{.3048m}$$

$$= 440.34\left(\frac{W}{L}\frac{lb}{s \bullet ft}\right)$$

(3)
Find

$$Z^* = \left(\frac{\dot{Q}/l}{\rho_o C_p T_o \sqrt{g}}\right)^{2/3} = \left(\frac{(2)}{1.21\left(\frac{kg}{m^3}\right) 1.01\left(\frac{kj}{kg \bullet K}\right) 293(K)\sqrt{9.81}\left(\frac{m}{s^2}\right)}\right)^{2/3} = \left(\frac{(2)}{1121.52}\right)^{2/3}$$

(4) $\left(\frac{Z}{Z^*}\right) = \frac{(1)}{(3)}$

Note that the Y-axis can be left as is because it is already in the correct form. Z/Z*, however, was transformed into SI units for ease of operation.

Temperature conversion:

Temperature data came from pages 5-6 and 5-15 of Shao-lin Lee's thesis, "Natural Convection Above a Line Fire."

Ordinate (Reciprocal of Buoyancy): $\frac{\gamma_1}{\Delta\gamma}$ (dimensionless)

$$\frac{\gamma_1}{\Delta\gamma} = \frac{g\rho_o}{g(\rho_o - \rho)} = \frac{\rho_o}{(\rho_o - \rho)} = \frac{T_o}{T - T_o} \text{ because...}$$

$$\frac{\rho_o - \rho}{\rho_o} = 1 - \frac{\rho}{\rho_o} = 1 - \frac{T_o}{T} \cong \frac{T - T_o}{T_o}$$

Absissa (Vertical Distance): $\bar{x}$ (in)

Fuel Flow Rate Variable: q (g/s-cm)

(1) Convert $\bar{x}$ (in) to z in m.

(2) Find z* using the conversions illustrated above for flame height.

(3) To get $\frac{z}{z*}$ divide step one by step two.

(4) $\frac{\Delta T}{T_o}$ is achieved by taking the inverse of the ordinate.

Fire Induced Flow in a Clean Room with Downward Vertical Flow
Sugawa

Temperature Conversion:

Data was taken from "Fire Induced Flow in a Clean Room with Downward Vertical Flow" page 364. The values were graphed against ΔT (°C) & H (cm). In order to graph these values against T/T_∞ and Z/Z^* temperature values were divided by 293 K and Z was divided by Z*=.0334. The value for Q used in Z* was found by taking the average volumetric methanol fuel flow rate for the entire burner length times the density of methanol times the chemical heat of combustion for methanol (ΔH_{chem}). Sugawa never indicated whether the center line temperatures were recorded with or without downward flow. However, in my opinion ignorance of this fact is not detrimental as the flow was not fast enough to significantly alter temperature readings.

Ordinate: ΔT (°C)

Abscissa: H (cm)

(1) Divide temperature by T_o.

(2) Calculate Q':
Sugawa reported a range of fuel flow rates between .37 and .4 ml. Therefore the average of the two flow rates will be used to determine the heat release rate per unit length. In addition, the value used for ΔH_c was found in Tewarsons chapter of the *Second Edition* of the SFPE Handbook on pg. ?

$$\dot{Q} = \frac{\left(.37+.4\dfrac{ml}{s}\right)}{2} \times \left(.793\frac{g}{ml}\right) \times \left(19.1\frac{kJ}{g}\right) = 5.83\ kW$$

$$\dot{Q}' = \frac{5.83\ kW}{.85\ m} = 6.86\frac{kW}{m}$$

(3) Determine z*:

$$z^* = \left(\frac{5.83\dfrac{kW}{m}}{\left(1.21\dfrac{kg}{m^3}\right)(293\ K)\left(1.01\dfrac{kJ}{kg-K}\right)\left(\sqrt{g}\dfrac{m^{1/2}}{s}\right)}\right)^{2/3} = .0334$$

(4) Convert H (cm) into (m) and divide by z*.

Velocity conversion:

Data was taken from "Fire Induced Flow in a Clean Room with Downward Vertical Flow" pages 361 & 364. The values were graphed against u (cm/sec) and H (cm) on page 364 and u (m/sec) and H (m) on page 361. In order to graph these values against $u/(gZ^{**})^{1/2}$ and Z/Z^{**} velocity values were divided by .572 and Z was divided by $Z^{**}=.0334$. To see how either of these values was attained reference Sugawa temperature notes.

Velocity values were recorded from two different graphs off the same paper under the same general conditions. Intuition tells us that these values should be the same, however they are slightly different. Unfortunately, I have no understanding of the discrepancy.

Ordinate: u (cm/sec) or (m/sec)

Abscissa: H (cm) or (m)

(1) Convert both axis to meter based values if necesary.

(2) z* has already been computed above under temperature conversions.

(3) Divide z (m) by z* (m) or .0334 to get z/z*.

(4) Find $\sqrt{gz^*}$:

$$\sqrt{gz^*} = \sqrt{\left(9.81\frac{m}{s^2}\right)(0.0334\, m)} = 0.572\,\frac{m}{s}$$

(5) Divide u (m/sec) by $\sqrt{gz^*}$ (m/sec) to get $\frac{u}{\sqrt{gz^*}}$.

Flame Height from Rectangular Fire Sources Considering Mixing Factor
(Sugawa, Satoh, Oka)

Data was taken from "Flame Height from Rectangular Fire Sources Considering Mixing Factor" page 438. The values were graphed against L_f/D vs. Q*rec. In order to graph these values against z*/w the Q*rec values had to be raised to the 2/3 power.

Ordinate: L_f/D (dimensionless)

Absisssa: Q^{*}_{rec} (dimensionless)

$$Q^{*}_{rec} = \frac{\dot{Q}}{\rho_o c_p T_o \sqrt{g} W D^{3/2}}$$; where W = burner length and D = burner width.

$$Q^{*}_{rec} = \frac{z^{*\,5/2}_{axi}}{w^{3/2} l} = \frac{z^{*3/2}}{w^{3/2}} = \left(\frac{z^{*}}{w}\right)^{3/2}$$

$$\left(\frac{z^{*}}{w}\right) = Q^{*\,2/3}_{rec}$$

Remember: $z^{*} = \left(\frac{z^{*\,5/2}_{axi}}{l}\right)^{2/3}$;W = l; D = w.

Note that the ordinate is already in the correct form and no conversions are necesary.

Linear Flame Heights for Various Fuels

F. R. Steward

Flame Height Converson:

Data was taken from, "Linear Flame Heights for Various Fuels" on page 177, Figure 3. Neither the ordinate nor the absissa were plotted on a logarithmic scale, however, data on both axis was plotted as a logarithmic function. The y-axis need only be converted out of its logarithmic function and it is then ready to be plotted. The x-axis also needs to be converted however it rquires the removal of many terms found in its equation before it is in a suitable form for plotting.
Values for heat release rate and stoichiometric ratio were found in Archibald Tewarson's chapter of the SFPE Handbook, Second Edition, on pages .... with exception of the heat release rate for hydrogen. This value was not reported by Tewarson and ~~had to~~ be calculated.

Ordinate: $\log \dfrac{(Q/L^2)(r+\omega\rho_a/\rho_o)^2\omega}{W^3 g Q_c^2 \rho_a^2 (1-\omega)^3}$

Absissa: log H/W

Fuel	Stoichiometric mass of air/mass of fuel req'd for combustion	Heat of combustion	$\rho'_o = \dfrac{\rho_{fuel@source}}{\rho_{air}}$
Methane	17.2	50,200	0.553
Propane	15.7	46,000	1.52
Hydrogen	34.7	120,900	0.0348

ρ'_o was developed through manipulation of the Ideal Gas Law as follows:

$$P = \rho RT = \rho\left(\frac{R}{M}\right)T \Rightarrow \rho = \frac{PM}{RT}$$

$\dfrac{\rho_{air}}{\rho_{fuel}} = \dfrac{M_{air}}{M_{fuel}}$; thus:

$$\rho'_{o_H} = \frac{1.0080}{28.95} = 0.0348; \rho'_{oC_3H_8} = \frac{44}{28.95}; \rho'_{oCH_4} = \frac{16}{28.95} = 0.553$$

Calcualtion of the heat of combustion for hydrogen:

$$H_2 + \frac{1}{2}O_2 \rightarrow H_2O + Q$$

$$Q = H_2 - H_1 = 241.83\frac{kJ}{mole\ H_2O} - 0$$

$$\Delta H_c = \frac{Q_{lost}}{m_{fuel}} = \frac{241.83\,kJ/mole\ H_2O}{1\,mole H_2/mole\ H_2O} = 241.83\frac{kJ}{mole\ H_2} \times \frac{1\,mole\ H_2}{2\,g} = 120.9\frac{kJ}{g}H_2$$

Note the best way to illustrate this conversion is through an example. Therefore the methane point

$\log \dfrac{(Q/L^2)(r+\omega\rho_a/\rho_o)^2\omega}{W^3 g Q_c^2 \rho_a^2 (1-\omega)^3} = -0.030$ and log H/W = 1.205 will be examined.

(1) Determine Lf/D:

log H/W = 1.205 $\Rightarrow H/W = 10^{1.205} = 16.03$

(2) $\omega = \dfrac{1}{1+\dfrac{\Delta H_c}{c_p T_o r}} = \dfrac{1}{1+\dfrac{50{,}200\dfrac{kJ}{kg}}{\left(1.01\dfrac{kJ}{kg-K}\right)(293\ K)(17.2)}} = 0.0921$;(from manipulation of eq. 11)

$$\frac{\left(r+\omega/\rho_o'\right)^2\omega}{gQ_c^2\rho_a^2(1-\omega)^3} = \frac{\left(17.2+\frac{0.0921}{0.553}\right)^2 0.0921}{\left(9.81\frac{m}{s^2}\right)\left(50{,}200\frac{kJ}{kg}\right)^2\left(1.21\frac{kg}{m^3}\right)(1-0.0921)^3} = 1.042\times 10^{-9}\left(\frac{kJ^2}{kg-s-m^2}\right)^{-1}$$

Note - $\rho_o' = \rho_o/\rho_a$

log (x-axis) = -0.030 $\Rightarrow (x-axis) = 10^{-0.030} = 0.933$

$$0.933\left(\frac{1}{1.042\times 10^{-9}}\right) = 8.95\times 10^{8} = \frac{(Q/l)^2}{W^3}$$

$$\frac{(Q/l)^{2/3}}{W} = (8.95\times 10^{8})^{1/3}$$

$$\frac{(Q/l)^{2/3}}{W}\left(\frac{1}{\rho_o c_p T_o\sqrt{g}}\right)^{2/3} = \frac{z^*}{w} = (8.95\times 10^{8})^{1/3}\left(\frac{1}{1.21\times 1.01\times 293\times\sqrt{9.81}}\right)^{2/3} = 8.947$$

$\dfrac{z^*}{W} = 8.947;$ *where* $W = w$

The Size of Flames from Natural Fires
P.H. Thomas

Flame Height Conversion

Data can be found in "The Size of Flames from Natural Fires" on page 850. The experiment was referenced from a paper conducted by Thomas, Pickard, and Wraight "for wood fires on effectively infinite strips of width D." In order to graph Thomas' data on a Z**/D axis his X-axis values were multiplied by 43.9 and then the total was raised to the 2/3 power. 43.9 was attained from ΔHc/(To*Cp). 13.0 kj/g was used for the heat of combustion. According to Thomas his first four values do not follow the same slope of his latter due to the discrepancy at small values of L/D which arise from the difference in geometry between the two situations.

Ordinate: L/D

Absisca: $\frac{\dot{m}''}{\rho_o \sqrt{gD}}$ (dimensionless)

$$\frac{\dot{m}''}{\rho_o \sqrt{gD}} \Rightarrow \frac{\dot{m}}{\rho \sqrt{gl} D^{3/2}} \times \left(\frac{\Delta H_c T_o c_p}{\Delta H_c T_o c_p} \right)$$

Note - $\dot{Q} = \dot{m} \Delta H_c$

$$\frac{\dot{Q}}{\rho_o T_o c_p \sqrt{gl}} \times \frac{T_o c_p}{D^{3/2} l \Delta H_c} = \left(\frac{z*}{D} \right)^{3/2} \times \left(\frac{c_p T_o}{\Delta H_c} \right)$$

Thus:

$$\left(\frac{z*}{D} \right) = \left[\left(\frac{\dot{m}''}{\rho_o \sqrt{gD}} \right) \times \left(\frac{\Delta H_c}{c_p T_o} \right) \right]^{2/3}$$

Where a value of 13.0 kj/g was used for ΔH_c because the specie of wood used during the test was not reported.

$$\frac{\Delta H_c}{c_p T_o} = \frac{13 \times 10^3 \, {}^{kj}\!/\!{}_{kg}}{\left(1.01 \, {}^{kj}\!/\!{}_{kg - K} \right) (293K)} = 43.9$$

Therefore:

$$\frac{z*}{D} = \left(43.9 (x - axis) \right)^{2/3}$$

The ordinate is already in the correct form and no changes are required.

Report of the Building Research Institute
"Study on the Prevention of Fire Spread Caused by Hot Upward Current"
Yokoi

Yokoi never reported a heat release rate, therefore it was assumed that the heat release rate per unit length for his burner was equivalent to that used by Sugawa in his paper, "Fire Induced Flow in a Clean Room with Downward Vertical Laminar Flow," because both burners had the same width and used similar fuels, aclcohol and Methnol respectively. The value calcualted for Yokoi's burner was compared to heat release rates he reported for axisymmetric burners using an "equal area concept." The two values are relatively close to each other.

Calculation of heat releae rate using Sugawa's burner:

$$\dot{Q} = \frac{\left(.37+.4\,\frac{ml}{s}\right)}{2} \times \left(.793\,\frac{g}{ml}\right) \times \left(19.1\,\frac{kJ}{g}\right) = 5.83\ kW$$

$$\dot{Q}' = \frac{5.83\ kW}{1\,m} = 5.83\,\frac{kW}{m}$$

Note - For more detailed information reference Sugawa's paper.

Calculation of heat release rate using equal area concept:

Area of line burner = 1 cm x 100 cm = 100 cm^2

Interpolating from

Temperature Conversion:

Data was taken from "Upward Current from an Infinite Line Fire Source" page 11, Figure 1.7 and page 25, Table 1.2. The values were graphed against ΔT (°C) & H (cm). In order to graph these values against T/T_∞ and Z/Z^{**} temperature values were divided by 290 K and z was divided by $z^* = .0337$.

Ordinate: ΔT (°C)

Absissa: H (cm)

(1) Convert H (cm) to z (m).

(2) Divide temperature by 290 K.

(3) Determine z*:

$$z^* = \left(\frac{\dot{Q}'}{\rho_o T_o c_p \sqrt{g}}\right)^{2/3} = \left(\frac{6.86}{1110.04}\right)^{2/3} = 0.0337\ (m)$$

(4) Divide z (m) by z* (m) or 0.0337 (m).

Velocity Conversion:

Data was taken from "Upward Current from an Infinite Line Fire Source" page 11, Figure 1.7 and page 25, Table 1.2. The values were graphed against u (cm/sec) and H (cm). In order to graph these values against $u/\sqrt{gz^*}$ and z/z* velocity values were divided by .575 and Z was divided by z* = 0.0337.

Ordinate: u (cm/sec)

Absissa: H (cm)

(1) Convert H (cm) to z (m).

(2) Divide z (m) by z* (m) or 0.0337 (m) as previously determined in the temperature conversin section.

(3) Determine $\sqrt{gz^*}$

$$\sqrt{gz^*} = \sqrt{\left(9.81\frac{m}{s^2}\right)(0.0337\ m)} = 0.575\frac{m}{s}$$

(4) Convert u (cm/sec) to u (m/sec).

(5) Divide u (m/sec) by $\sqrt{gz^*}$ (m/sec) or 0.575 (m/sec).

PAGE 1 OF 2

NIST-114
(REV. 11-94)
ADMAN 4.09

U.S. DEPARTMENT OF COMMERCE
NATIONAL INSTITUTE OF STANDARDS AND TECHNOLOGY

MANUSCRIPT REVIEW AND APPROVAL

INSTRUCTIONS: ATTACH ORIGINAL OF THIS FORM TO ONE (1) COPY OF MANUSCRIPT AND SEND TO THE SECRETARY, APPROPRIATE EDITORIAL REVIEW BOARD.

(ERB USE ONLY)

ERB CONTROL NUMBER	DIVISION
PUBLICATION REPORT NUMBER NIST-GCR-98-744	CATEGORY CODE
PUBLICATION DATE March 1998	NUMBER PRINTED PAGES

TITLE AND SUBTITLE (CITE IN FULL)
Correlations for Fire Plumes

CONTRACT OR GRANT NUMBER

TYPE OF REPORT AND/OR PERIOD COVERED
February 1998

AUTHOR(S) (LAST NAME, FIRST INITIAL, SECOND INITIAL)
Quintiere, J.G and Grove, B.S.
University of Maryland
Department of Fire Protection Engineering
College Park, MD 20742

PERFORMING ORGANIZATION (CHECK (X) ONE BLOCK)
☒ NIST/GAITHERSBURG
☐ NIST/BOULDER
☐ JILA/BOULDER

LABORATORY AND DIVISION NAMES (FIRST NIST AUTHOR ONLY)

SPONSORING ORGANIZATION NAME AND COMPLETE ADDRESS (STREET, CITY, STATE, ZIP)
U.S. Department of Commerce
National Insitute of Standards and Technology
Gaithersburg, MD 20899

PROPOSED FOR NIST PUBLICATION
☐ JOURNAL OF RESEARCH (NIST JRES)
☐ J. PHYS. & CHEM. REF. DATA (JPCRD)
☐ HANDBOOK (NIST HB)
☐ SPECIAL PUBLICATION (NIST SP)
☐ TECHNICAL NOTE (NIST TN)
☐ MONOGRAPH (NIST MN)
☐ NATL. STD. REF. DATA SERIES (NIST NSRDS)
☐ FEDERAL INF. PROCESS. STDS. (NIST FIPS)
☐ LIST OF PUBLICATIONS (NIST LP)
☐ NIST INTERAGENCY/INTERNAL REPORT (NISTIR)
☐ LETTER CIRCULAR
☐ BUILDING SCIENCE SERIES
☐ PRODUCT STANDARDS
☐ OTHER ____

PROPOSED FOR NON-NIST PUBLICATION (CITE FULLY) ☐ U.S. ☐ FOREIGN

PUBLISHING MEDIUM
☐ PAPER
☐ CD-ROM
☐ DISKETTE (SPECIFY) ____
☐ OTHER (SPECIFY)

SUPPLEMENTARY NOTES

ABSTRACT (A 2000-CHARACTER OR LESS FACTUAL SUMMARY OF MOST SIGNIFICANT INFORMATION. IF DOCUMENT INCLUDES A SIGNIFICANT BIBLIOGRAPHY OR LITERATURE SURVEY, CITE IT HERE. SPELL OUT ACRONYMS ON FIRST REFERENCE.) (CONTINUE ON SEPARATE PAGE, IF NECESSARY.)

This study began as a review of data and correlations for line plumes. In its attempt to develop a consistent set of correlations for that data set, it developed an analysis to account for the base geometry of the fuel source. Although point source models were used, the diameter or rectangular source dimensions were included in improved solutions for flame height and entrainment rate. The analysis also explicitly includes the effect of flame radiation. The entraiment coefficients determined for Gaussian velocity and temperature profiles and for constant density were found to be 0.098 and 0.091 for the axisymmetric and line far field values, respectively. The entrainment coefficients in the near field were found to be 0.22 and 0.59 for the axisymmetric and line cases, respectively. Theoretically developed equations for near field entrainment and flame height with empirical lead coefficients were found to fit a wide range of data including fuel base diameters of up to 0.5m. Results are also presented for rectangular fires, and the theoretical basis for the correlation developed unifies data over a wide range of base dimensions ranging from a square to a line.

KEY WORDS (MAXIMUM OF 9; 28 CHARACTERS AND SPACES EACH; SEPARATE WITH SEMICOLONS; ALPHABETIC ORDER; CAPITALIZE ONLY PROPER NAMES)

entrainment; fire plumes; flame height; flame radiation

AVAILABILITY
☒ UNLIMITED ☐ FOR OFFICIAL DISTRIBUTION - DO NOT RELEASE TO NTIS
☐ ORDER FROM SUPERINTENDENT OF DOCUMENTS, U.S. GPO, WASHINGTON, DC 20402
☒ ORDER FROM NTIS, SPRINGFIELD, VA 22161

NOTE TO AUTHOR(S): IF YOU DO NOT WISH THIS MANUSCRIPT ANNOUNCED BEFORE PUBLICATION, PLEASE CHECK HERE. ☐

ELECTRONIC INFORMS